Journal of Engineering

A Scientific Refereed Journal
Published by College of
Engineering University of
Baghdad

April

201 3
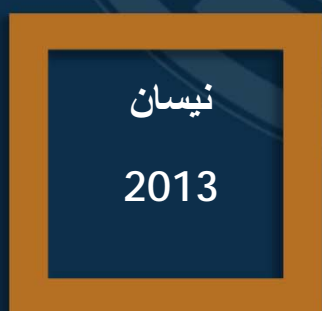
Number 4

Volume 19

قائمة المحتويات

:

Performance Evaluation of Al-RustamiyaWastewater Treatment Plant

AbdulKarim Muneer AbdulRazzak

E-mail: abd_almokhtar59@yahoo.com

Assistant Lecture

Baghdad University /Director Of The University President Office

ABSTRACT

Al-Rustamiya sewage treatment plant (WWTP) serves the east side of Baghdad city (Rusafa) and is considered one of the largest projects.It consists of three parts (old project F0, first extension F1, and second extension F2) that treat wastewater and the effluent is discharged into Diyala river and thus into the Tigris River. These plants are designed and constructed with an aim to manage wastewater to reachIraqi effluent standard for BOD_5, COD, TSS and chloride concentrations of 40, 100, 60 and 600 mg/L respectively. The data recordedfrom March till December 2011 provided from Al-RustamiyaWWTP, were considered in this study to evaluate the performance of the plant. The results indicated that the strength of the wastewater entering the plant varied from medium to high. The average concentrations of the effluent of BOD_5, COD, TSS and chloride were within Iraqi effluent standards. The overall efficiency removalswere:

For BOD_5: 92.1, 90.31, and 92.96% for F0, F1, and F2 respectively

COD: 88.23, 87.9, and 87.95% for F0, F1, and F2 respectively

TSS: 86.98, 80.72, and 89% for F0, F1, and F2 respectively

Chloride: 14.79, 15.37, and 15.31% for F0, F1, and F2

The mean value of BOD_5/COD ratio of the raw wastewater was 0.67 as for typical untreated domestic wastes. The mean BOD/COD ratios of the treated sewage from F0 was 0.48, from F1 0.50 and from F2 0.38. These ratios did not confirm with the typical ratios indicating that the wastewaterneeds more treatment.

KEYWORDS: Al-RustamiyaWWTP, domestic wastewater characteristics, chemical oxygen demand,biochemical oxygen demand, total suspended solids, pH, chloride.

<div dir="rtl">

تقييم اداء محطة الرستمية لمعالجة مياه الصرف الصحي

م.م عبدالكريم منيرعبدالرزاق

مدرس مساعد

جامعة بغداد-مدير مكتب رئيس الجامعة

الخلاصة

تخدم محطة معالجة مياه الصرف بالرستمية الجانب الشرقي لمدينة بغداد الرصافة ويعتبر واحد من اكبر المشاريع ويتالف من ثلاثة اجزاء (المشروع القديم F0والتوسعة الاولىF1 والتوسعة الثانية F2) ويقوم المشروع بمعالجة مياه الصرف الصحي ورمي المياه بعد المعالجة الى نهر ديالى وهكذا الى نهر دجلة بعد المرور بمجموعة من العمليات. وهذه المحطة مصممة لمعالجة مياه الصرف الصحي يموجب المواصفة العراقية 40لتراكير BOD5,COD والمواد العلقة والكلوريد

</div>

المساوية الى 40 و100و60و 600 ملغم/لتر على التوالي.القراءات اليومية للفترةمن بداية شهر اذار ولغاية نهاية كانون الاول عام 2011 لقياسات خصائص مياه الصرف الصحي في مداخل ومخارج المحطة زودت من ادارة محطة معالجة الرستميةلتقييم اداء المحطة.النتائج اظهرت ان قوة مياه الصرف الصحي تتفاوت من الوسط الى المستوى العالي وان المياه المعالجة ذات تراكيز لل BOD_5 و COD والمواد العالقة والكلوريدكانت ضمن المواصفة العراقية لرمي المياه المعالجة الى المصادر المائية. والاداء العام لمحطة الرستمية بمراحله المشار لها يكون جيد .وكانت كفاءة الازالة العامة هي:

1-قيم ال $BOD_5$92.1 و 90.31 و 92.96% على التوالي للرستمية F_oوF_1 و F_2

2-قيم الCOD87.23 و 87.9و 87.95 %على التوالي للرستمية F_oوF_1 و F_2

3-قيم ال SS 86.98 و 80.72و 89%على التوالي للرستمية F_oوF_1 و F_2

4-قيم الكلورايد 14.79 و 15.37و 15.31% على التوالي للرستمية F_oوF_1 و F_2.

ان متوسط قيمة نسبة (BOD_5/COD) لمياه الصرف الخام كانت 0.67 وكما هي لمياه الصرف المنزلية غير المعالجة. واماللمياه الصرف المعالجة فان معدل نسبة BOD_5/COD في الرستمية القديم F0هي 0.48 وبالنسبة للتوسع الاولففكانت0.50 والبالنسبة للتوسع الثاني Fكانت النسبة 0.38 . وهذه النسب من (BOD_5/COD) لم تكن مطابقة للنسب المثالية للمياه المعالجة.و هذه المياه تحتاج الى معالجة اكثر .

الكلمات الرئيسة: الرستمية(محطة معالجة مياه الصرف)، خصائص مياه الصرف المنزلية، الحاجة الكيميائية للاوكسجين، الحاجة البايوكيميائية للاوكسجين، المواد العالقة الكلية ، الدالة الحامضية PH، الكلورايد.

INTRODUCTION

Sewage is created by residences, institutions, commercial and industrial establishments. It can be treated close to where it is created (in septic tanks, onsite package plants or other aerobic treatment systems), or collected and transported via a network of pipes and pumping stations to a treatment plant. Industrial sources of wastewater often require specialized treatment processes. Wastewater treatment is the process of removing the contaminants from itby physical, chemical and biological processes. Its objective is to produce a treated effluent and a solid waste or sludge suitable for discharge. This sludge may also be reused. The sludge is often inadvertently contaminated with toxic organic and inorganic compounds. Typically, sewage treatment involves three stages, called primary, secondary and tertiary treatment.

Surface water bodies in developing countries are under serious threat as a result of indiscriminate discharge of polluted effluents from industrial, agricultural, and domestic/sewage activities (Kambole, 2003). Water pollution is the most serious environmental issue due to the disposal of solid and liquid waste on land and into surface water. Among them the most significant are domestic wastewater, industrial effluent and agriculture residues and chemicals (Poudyal, 2000). Moreover continued discharge of domestic and industrial wastewater directly into the rivers is one of the main cause'sriver pollution.

Wastewater treatment plantsare designed and operated to reduce pollutant loads to a level that nature can handle. In this regard, special attention is necessary to assess the environmental impacts of existing wastewater treatment facilities (Jamrah,1999). As such urban drainage system should also be considered as an important infrastructure in removing both wastewater and rainwater from the city to prevent unhygienic conditions and to avoid damage from flooding (Karrman, 2001 and Erbe*et al*., 2002).

The reduction of BOD_5 and COD in different treatment units of a plant can be used to measure the efficiency of each unit in wastewater treatment. The ratio of BOD_5/COD indicates the biodegradability of wastewater and the higher the ratio thehigher biodegradability of the wastewater (Metcalf and Eddy, 2003).

Ratio values depend on the nature of the wastewater namely; whether it is municipal or industrial oriented andvaryconsiderably with the degree of treatment the wastewater has undergone (Metcalf and Eddy, 2003). The COD/BOD_5 ratio value for municipal raw wastewater is in the range of 1.25 to 2.5,

whereas for industrial wastewater up to 10 or more (Markantonatos,1990).Therefore, municipal wastewater is able to be biologically degraded more than industrial wastewater. COD/BOD_5 ratios in the range from 3 to 7, indicates that the wastewater is moderately biodegradable. However, there is no official COD/BOD_5 ratio index for different types of wastewater. In the case of extremely low biodegradable wastewater, ($COD/BOD_5 > 10$), a treatment process that will reduce the chemically oxidized organic part is required so the ratio will reach the 'biodegradable' range ($COD/BOD_5 < 3$). Such a significant change in COD/BOD_5 improves the efficiency of subsequent biological treatment (Pak and Wonseok, 1999, Hsieh et al., 2000).

Several researches studied the performance of Al-Rustamiya wastewater treatment plant.

Palmer, (2004)carried out a description field study on the performance of the Al-Rustamiya plant, 3rd extension for the benefit of the American International Development Agency (USIDA) and CPA (Coalition Provisional Authority). The study was done in order to carry out a rehabilitation work on the plant which was later executed. The aim of the rehabilitation program was to achieve a secondary (biological) treatment compatible with thedesign aim as stated previously by Haist and Parteners in 1981. His study presented a description for the treatment process (physical, biological and chemical) and an assessment of the quality of effluents as stated by the original designer Haist and Partners in1981. The effluent quality which was employed by the designer was based on the Iraqi standards of effluent discharges into receiving waters.

AL-Samawi, H., (2008) studied the efficiency performance of Al-Rustamiyah WWTP before and after rehabilitation, to check the efficiency of the rehabilitated work. Data from the different treatment units within the plant for year 2006 were statistically analyzed and compared with the original design parameters and the Iraq standards of effluent discharges into the receiving water. The results indicated that the effluent discharged from Al-RustamiyaWWTPinto DiyalaRiver was not in complete agreement with the Iraqi effluent standards. However, the results of the biological processes;aeration tanks and final clarifiers showed that there was a clear chronic biological upset. The results indicated clearly that the rehabilitated program had no significant effect on improving its state of dereliction.

Alzuhary, (2008) evaluated the efficiency of the sewage treatment plants at Al-Risafa and Al-Karkh sides of Baghdad city. The calculations were executed according to the average and peak capacity of each plant depending on three values of population growth rates in Baghdad for the period 2005-2025. The study reveals that the deficit ratio in treatment efficiency will reach 273% at 2025 in Al-Rustamiyah WWTP. The situation will be more critical at Al-Karkh sewage treatment plant where the deficit in efficiency will approach 700%.

Knowledge of mean concentrations, ratios and variation range of chemical parameters used to describe wastewater quality is crucial for ensuring suited design and sizing of treatment facilities. This paper describes the performance of Al-Rustamiya wastewater treatment (WWTP), in Baghdad, in terms of wastewater characterization of the influent and effluent.The performance evaluation is to derive a comparative account between the pollution load before and after the treatment processes, besides, discerning their efficiency. The main objective of the study is to study the concentrations; ratios and variation range of wastewatercharacterized by BOD_5, COD, TSS, pH and chloride as well toexamine the BOD_5/COD ratio fluctuation based on BOD_5 and COD variations.

MATERIAL AND METHODS:

Study Area Description

Baghdad city is about 900 km^2 and the approximation number of population for the year 2010 was 7.6 million people. It is a very largecity and almost flat divided by the Tigris River to two main parts: the east side (Rusafa) and the western side (Karkh). The city includes 457 sectors where about 82% of the sectors are served by sewerage systems.

Baghdad city has three projects for wastewater treatment. These projects are Al-RustamiyaSouth Station,Al-Rustamiya North Station and Al-Karkh.These stations suffer in the recent years of weakness in the arrival of spare parts and a deficit in the maintenance of mechanical and electrical equipment. Karkh sewage treatment project serves the western side of Baghdad (Karkh) at a design capacity of205,000m^3/day, while the current incoming flow is 625,000 m^3/day.

Al-Rustamiya wastewater treatment plant serves the eastern side of Baghdad (Rusafa) it is considered one of the largest projects that treats wastewater.The effluent is discharged into Diyala river and thus into the Tigris River. Al-Rustamiya wastewater treatment plants are illustrated in Fig. (1).

Al-Rustamiya (WWTP) is the oldest project in Iraq,it consists of**:**

a) The old project, Al-RustamiyaSouth station working since1963and consists of threeintegratedprojects which are zero (F0)andexpansionI(F1), with a designed capacity of175,000m^3/daywhere theactual flow reaches300,000m^3/day.This plant serves 1,500,000 inhabitants on the eastern side of Baghdad.

b) Al-RustamiyaNorth station,Expansion II (F2) working since 1984with a design capacity of 300,000m^3/dayandtheactual influent

450,000 m^3/day from1.5 millionpeopleserved in theeasternside of Baghdad. Thefinal disposalof the plantis into the Diyala River.

DATA COLLECTION AND ANALYSIS

The collection and experimental data used in this paper were provided by Al-Rustamiya STP's office-Mayoralty of Baghdad.

The data collected were biochemical oxygen demand (BOD$_5$), chemical oxygen demand (COD), total suspended solids (TSS), pH and chloride of the influent and effluent of the Al-RustamiyaWWTPthrough the study period from March till December 2011 and represented as daily and monthly average values for each parameter.

RESULTS AND DISCUSSION

One of the commonly found environmental problems in developing countries is water pollution caused by direct disposal of untreated wastewater. In Iraq, most of the wastewater treatment plants are not functioning due to high cost of spare parts, chemical additives, utility bills and lack off trained human resources. These financial and managerial problems are common in every developing country.

1. Characteristics of the influent Wastewater

The average monthly concentrations of BOD$_5$, COD, TSS, pH and chloride in the influent ranged from 221.43 to 252.11 mg/L with an average of 235.39 mg/L for BOD$_5$.As for COD it ranged from 258 to 443 mg/L with an average of 361.09 mg/L.The TSS ranged from 203.59 to 355.3 mg/L with an average of 245.16 mg/L and 288.55 to 342.21 mg/L with an average of 324.25 mg/L for chloride. The pH varied from 7.07 to 7.39 with an average value of 7.18 as shown in Table 1. The strength of the wastewater entering the plant varied from medium to high according to Table 2.

2. Characteristics of the effluent Wastewater

The average monthly concentrations of BOD_5, COD, TSS, pH and chloride of the effluentare shown in Table 1, from F0,F1 and F2 in Al-RustamiyaWWTP.The effluent concentrations of BOD_5, COD, TSS and chloride were within Iraqi effluent standards of 40, 100, 60 and 600 mg/L respectively. Considering the effluent of F1 in November, the BOD (44.3mg/L) and TSS (162.19mg/L) concentrations exceeded the effluent standards also the COD value was high regarding the overall effluent characteristics over the period of the study. This may be due to operational problems in the biological treatment of F1.

3. Overall Efficiency of Al-Rustamiya Treatment Plant

The overall efficiency of the Al-RustamiyaWWTPis shown in Table 3. The average BOD_5reduction at F0, F1and F2 was 92.1%, 90.31%, and 92.96% respectively. The average reduction of COD was88.23%, 87.95%, and 87.95% in F0, F1 and F2 respectively. As for the average reduction at F0, F1 and F2 for TSS was 86.98%, 80.72%, and 89% respectively.
As for F1 the lowest percentages removal for BOD, COD and TSS were observed in November. Low chloride reductionswere observed at F0,F1 and F2 that reached 14.79%, 15.73%, and 15.31% respectively as this plant is designed for the biological treatment of the organic matter represented by BOD or COD reduction and not for dissolved matter.

4. BOD_5/COD RATIO

Typical values ofBOD_5/COD ratio for untreated municipal wastewater are in the range of 0.3 to 0.8 as shown in Table 4. If the ratio is 0.5 and greater the waste is considered to be easily treatable by biological means. If the ratio is below 0.3,

either the waste may have some toxic components or acclimated microorganisms may be required for degradation. This ratio decreases to 0.1-0.3 for the treated sewage.For the influent raw sewage the BOD_5/COD ratios,shown in Table 5 ranged from a minimum of 0.54 to a maximum value of 0.89 with an average of 0.67, these values confirm with the typical ratios for the untreated sewage.For the effluent sewage from F0, the BOD_5/COD ratios range from a minimum value of 0.28 and maximum of 1.12 with an average of 0.48.The effluent from thefirst extension F1 had BOD_5/COD ratios ranging from 0.32 to 0.82 with an average of 0.50. As for the second extension F2the BOD_5/COD ratios ranged from 0.24 to 0.54 with an average value of 0.38. The high concentrations of BOD_5 and COD in the effluent gave highBOD_5 /COD ratios that did not confirm with the typical values for the treated sewage (Table 5). These results indicate that the wastewaterneeds more treatment.

The BOD_5/CODratio remains practically constant, after the wastewater has been treated anaerobically. This type of treatment plays a very important role in the performance of the whole treatment system, since it efficiently removes chemical and biological material maintaining.There is usually no correlation between BOD_5 and COD in wastewater with slowly biodegradable organic suspended solids and in complex waste effluents containing refractory substances (Eckenfelder, 1989). Hence, treated effluents may exert virtually no BOD_5 and yet exhibit a substantial COD. Since, the COD represents virtually all organic matter, either partially degradable or non-biodegradable where BOD_5represents the biodegradable matter only.

433

CONCLUSION

This study aimed to evaluate the BOD_5, COD, TSS and chloride removal efficiencies as well as itexamined the BOD_5/CODratio fluctuation inAl-Rastumiya municipal wastewater treatment plant comprising of its three stages.

The strength of the wastewater entering the plant varied from medium to high.

The concentrations of BOD_5, COD, TSS and chloride in the effluent were within the Iraqi effluent standards of 40, 100, 60 and 600 mg/L respectively.

The mean BOD_5/CODratio of the influent raw sewage to Al-RustamiyaWWTP was 0.67. andthe waste is considered to be easily treatable by biological means.

The mean BOD_5/CODratios of the effluent from Al-RustamiyaWWTP were, for F0 0.48, F1 0.5 and F2 0.38. The BOD_5/COD ratios varied considerably with the degree Of treatment the wastewater had undergone.

The performance ofAl-Rustamiya WWTP is determined fromthe overall efficiency removal in:

1. $BOD_5$was 92.1, 90.31, and 92.96% for F0, F1, andF2 respectively.
2. COD was 88.23, 87.9, and 87.95% for F0, F1, and F2 respectively.
3. SS was 86.98, 80.72, and 89% for F0, F1, and F2 respectively.
4. Chloride was 14.79, 15.37, and 15.31% for F0, F1, and F2 respectively.

REFERENCES:

Al-Samawi, H. A., (2008). "Evaluation of Al- Rustamiya 3rd extension wastewater treatment plant's efficiency and its environmental effect using remote sensing data" M.Sc Thesis-Building And Construction Engineering Department University Of Technology.

Alzuhary,M., (2008). "Evaluation for future Baghdad wastewater treatments plants efficiency" J. Technical Vol. 21 No. 1.

Eckenfelder, W. (1989) "Industrial Water Pollution Control", McGraw-Hill Company,New York.

Erbe, V., Risholt, L.P., Schilling, W. and Londong, J. (2002). "Integrated modeling for analysis and optimization of wastewater systems - the Odenthal case" Urban Water, 4(1): 63–71

Hsieh, Y.H., Wang, K.H., KO, RC &.,Chang, CY. (2000). "Photocatalytic degradation of wastewater from manufacturing fiber by titanium dioxide suspensions in aqueous solution in a feasibility study" Water Science & Technology 42 (5-6), 95-99.

Jamrah, A.I. (1999). "Assessment of characteristics and biological treatment technologies of Jordanian wastewater" Bioprocess Engineering, 21: 331-340.

Kambole, (2003). "Managing the water quality of the Kafue river" M. Sc. Physics and Chemistry of the Earth, parts A/B/C. 28(20-27): 1105-1109.

Karrman E. (2001). "Strategies towards sustainable wastewater management" Urban Water, 3(1–2): 63–72

Markantonatos G, (1990). "Treatment and disposal of wastewater (in Greek)" Athens.

Metcalf and Eddy Inc., (2003), "Wastewater Engineering - Treatment, Disposal and Reuse", 4th Edition, Tata McGraw Hill Publishing Co. Ltd.,

Pak, D. andWonseok, C., (1999) "Decolorizing dye wastewater with low temperature catalytic oxidation" Water Science & Technology 40 (4-5), 115-121.

PalmerSteve,J.,(2004), "Rehabilitation of Al-Rustamiya Sewage Treatment Plant Works-3rd Extension", 1st Edition, Bechtel International United Company, Project No. 617-24910, USA

Poudyal, S.R., (2000). "Country paper presented in Asian Productivity Organization (APO) International Symposium on Management of Industrial Estate through Green Productivity, Penang, Malaysia.

Fig(1) Al-Rustamiya wastewater treatment plant.

Table 1 Average monthly variation of BOD$_5$, COD, TSS, pH and chloride of Al-Rustamiya WWTP

Month	BOD ppm				COD ppm				TSS ppm				pH				Chloride ppm			
	Influent	F0	F1	F2	Influent	F0	F1	F2	Influent	F0	F1	F2	Influent	F0	F1	F2	Influent	F0	F1	F2
Effluent Standard		40				100				60				6.5 - 8.5				600		
Mar.	228.64	37.33	22.36	11.73	258.00	33.33	27.33	43.86	233.36	46.91	38.68	23.27	7.22	7.27	7.35	7.33	337.59	289.18	290.45	286.09
Apr.	241.58	11.53	16.95	16.26	397.00	41.67	41.00	54.50	355.30	24.35	28.55	23.80	7.07	7.33	7.33	7.35	334.45	283.45	288.85	289.75
May.	234.55	20.41	16.36	16.23	432.67	54.00	51.33	54.83	279.00	25.41	26.82	21.23	7.12	7.33	7.35	7.31	334.00	286.64	279.68	275.50
Jun.	242.38	17.05	18.19	19.67	443.00	39.38	39.38	42.38	235.86	21.29	26.48	20.19	7.07	7.25	7.25	7.26	325.33	281.33	274.10	277.71
Jul.	252.11	22.42	20.39	19.50	342.83	46.00	37.33	44.17	214.32	23.00	26.79	29.53	7.07	7.27	7.28	7.26	342.21	286.74	293.05	294.63
Aug.	240.50	18.55	20.30	18.30	341.70	40.00	38.40	33.90	203.59	28.45	28.95	22.59	7.15	7.32	7.34	7.30	318.77	278.32	273.91	274.00
Sep.	221.43	12.86	14.00	15.90	343.38	26.13	26.13	33.63	220.18	23.27	23.86	21.55	7.39	7.54	7.51	7.51	288.55	243.95	234.36	242.82
Oct.	226.09	18.48	15.04	13.17	331.21	38.21	38.50	38.75	235.92	29.96	24.42	21.79	7.28	7.43	7.44	7.45	317.29	267.13	267.71	264.67
Nov.	226.00	17.30	44.30	15.30	398.31	42.19	77.81	36.19	228.63	34.63	162.19	32.19	7.24	7.45	7.48	7.43	324.00	271.25	272.50	270.13
Dec.	240.59	14.76	21.82	11.65	322.76	49.00	51.32	48.47	245.45	22.55	29.90	20.60	7.22	7.43	7.47	7.46	320.30	264.75	262.60	262.30
Average	235.39	19.07	20.97	15.77	361.09	40.99	42.85	43.07	245.16	27.98	41.66	23.67	7.18	7.36	7.38	7.37	324.25	275.27	273.72	273.76
STDEV	9.64	7.21	8.67	2.91	56.29	7.83	14.80	7.74	43.67	7.80	42.55	4.00	0.11	0.09	0.09	0.09	15.16	13.91	17.09	15.08
MIN.	221.43	11.53	14.00	11.65	258.00	26.13	26.13	33.63	203.59	21.29	23.86	20.19	7.07	7.25	7.25	7.26	288.55	243.95	234.36	242.82
MAX.	252.11	37.33	44.30	19.67	443.00	54.00	77.81	54.83	355.30	46.91	162.19	32.19	7.39	7.54	7.51	7.51	342.21	289.18	293.05	294.63

Table 2 Strength classification of Untreated Sewage (Metcalf and Eddy, 2003).

Parameter	Strength		
	Low	Medium	High
BOD_5 mg/L	100	200	400
COD mg/L	175	300	600
TOC mg/L	100	200	400

Table 3 Average monthly overall of BOD, COD, TSS and chloride

removal in Al-Rustamiya WWTP

Month	BOD_5 Removal%			COD Removal%			TSS Removal%			Chloride Removal%		
	F0	F1	F2	F0	F1	F2	F0	F1	F2	F0	F1	F2
Mar.	88.87	89.88	94.52	86.82	89.22	85.87	78.46	80.32	88.34	13.87	13.75	15.07
Apr.	94.98	92.80	92.64	89.56	89.52	86.27	92.04	91.04	92.16	14.97	13.45	13.19
May.	90.71	92.40	92.86	86.84	87.81	86.90	89.72	89.20	91.40	13.95	16.22	17.17
Jun.	92.72	92.41	91.39	90.33	90.07	90.03	89.34	87.87	90.39	12.91	15.16	13.98
Jul.	91.05	92.22	92.64	86.34	89.03	87.19	87.86	85.80	84.43	16.10	14.05	13.76
Aug.	92.01	91.26	92.19	87.86	88.41	89.59	84.44	83.89	87.97	12.05	13.52	13.29
Sep.	93.55	93.23	91.89	92.27	92.13	89.47	88.04	87.88	89.09	15.51	18.53	15.93
Oct.	91.48	93.02	93.81	87.84	88.24	87.90	85.85	88.71	90.13	15.72	15.70	16.62
Nov.	91.80	75.80	92.64	89.23	80.49	90.86	84.05	25.77	84.86	15.83	15.72	16.51
Dec.	93.83	90.06	95.03	85.17	84.11	85.46	90.01	86.70	91.20	16.99	17.60	17.61
Average	92.10	90.31	92.96	88.23	87.90	87.95	86.98	80.72	89.00	14.79	15.37	15.31
STDEV	1.75	5.23	1.15	2.13	3.30	1.91	3.93	19.54	2.65	1.55	1.75	1.67
MIN.	88.87	75.80	91.39	85.17	80.49	85.46	78.46	25.77	84.43	12.05	13.45	13.19
MAX.	94.98	93.23	95.03	92.27	92.13	90.86	92.04	91.04	92.16	16.99	18.53	17.61

Table 4 Comparison of ratios of various parameters used to characterize wastewater.

Type of wastewater	BOD_5/COD	BOD_5/TOC
Untreated	0.3-0.8	1.2-2.0
After primary settlement	0.4-0.6	0.8-1.2
Final effluent	0.1-0.3	0.2-0.5

Table 5 Average monthly values of BOD_5/COD ratio of Al-RastumiyaSTP.

Month	BOD_5-COD RATIO			
	C	F0	F1	F2
Mar.	0.89	1.12	0.82	0.27
Apr.	0.61	0.28	0.41	0.30
May.	0.54	0.38	0.32	0.30
Jun.	0.55	0.43	0.46	0.46
Jul.	0.74	0.49	0.55	0.44
Aug.	0.70	0.46	0.53	0.54
Sep.	0.64	0.49	0.54	0.47
Oct.	0.68	0.48	0.39	0.34
Nov.	0.57	0.41	0.57	0.42
Dec.	0.75	0.30	0.43	0.24
Average	0.67	0.48	0.50	0.38
STDEV	0.11	0.24	0.14	0.10
MIN.	0.54	0.28	0.32	0.24
MAX.	0.89	1.12	0.82	0.54

Effect of Metakaolin on Properties of Lightweight Porcelinate Aggregate Concrete

Prof. Nada M. Fawzi

Civil Eng. Dept.
College of Engineering
University of Baghdad

Asst.Prof. Kalil I. Aziz

Civil Eng. Dept.
College of Engineering
University of Al-Anbar

Asst.Let. Sheelan M. Hama

Civil Eng. Dept.
College of Engineering
University of Baghdad

ABSTRACT

Research in Iraq has expanded in the field of material technology involving the properties of the lightweight concrete using natural aggregate. The use of the porcelinate aggregate in the production of structural light concrete has a wide objective and requires a lot of research to become suitable for practical application. In this work metakaolin was used to improve compressive strength of lightweight porcelinate concrete which usually have a low compressive strength about 17 MPa . The effect of metakaolin on compressive, splitting tensile, flexure strengths and modulus of elasticity of lightweight porcelinate concrete have been investigated. Many experiments were carried out by replacing cement with different percentages of metakaolin. The metakaolin was replaced by 5%, 10%, 15% and 20%. A control reference mix without metakaolin was made for comparison purpose. For all mixes, compressive, splitting tensile, flexure strengths and modulus of elasticity were determined at 28-day. The results showed that the using of metakaolin improve the compressive, splitting tensile, flexure strengths and modulus of elasticity of lightweight porcelinate concrete. The higher compressive, splitting tensile, flexure strengths and modulus of elasticity were found for 15% metakaolin.

Keywords: Lightweight concrete, porcelinate, metakaolin

الخلاصة

توسـعت البحـوث فـي العـراق فـي حقـل تكلنوجيـا المـواد مـن ضـمنها دراسـة خـواص الخرسـانة خفيفـة الـوزن باستخدام ركـام طبيعـي. استخدام البورسلينايت كركـام خفيـف الـوزن فـي انتـاج خرسـانة انشائية يتطلب العديد من الدراسات لفهم وتحسين خواصها لتصبح مناسبة للتطبيقات العملية.

في هذه الدراسة استخدمت مادة ميتاكاؤلين كنسبة مئوية مِنْ وزن سمنت، لتحسين خـواص خرسـانة البورسلينايت الخفيفـة الـوزن التـي تمتاز عادة بمقاومة انضغاط واطئة حـوالي 17 ميكاباسكال. تم دراسـة تـاثير اضـافة ميتاكاؤلين علـى كـل مـن مقاومـة الانضغاط، مقاومـة الانفلاق، معامـل التصدع، و معامـل المرونـة للخرسـانة البورسلينايت الخفيفـة الـوزن. وقد استبدل جـزء مـن السمنت بالنسب التالية مـن ميتاكـاؤلين: 5%، 10%، 15%، و 20% مـن وزن السمنت، بالاضافة الى الخلطـة المرجعية بدون اضـافات لغرض المقارنـة. لكل الخلطـات تم قياس كل من مقاومـة الانضغاط، مقاومـة الانفلاق، معامـل التصدع، و معامـل المرونة بعمر 28 يوم. وقد وجد بان استبدال نسبة 15% من سمنت بميتاكاؤلين تحسن مقاومـة الانضغاط، مقاومـة الانفلاق، معامـل التصدع، و معامـل المرونة.

Prof. Nada M. Fawzi
 Asst.Prof. Kalil I. Aziz
 Asst.Led. Sheelan M. Hama

Effect of Metakaolin on Properties of Lightweight
Porcelinate Aggregate Concrete

INTRODUCTION

Structural Lightweight Concrete: ACI committee 213 defined structural lightweight aggregate concrete as a concrete with an air-dried density at 28-day in the range of 1120 and 1920 kg/m^3 and a compressive strength above 17.2 MPa. The same committee defined high strength lightweight concrete as concrete with a 28-day compressive strength of 41.4 MPa or greater. Structural lightweight aggregate concrete is an important and versatile material in modern construction. It has many and varied applications including multistory building frames and floors, bridges, offshore oil platforms, and prestressed or precast elements of all types.

Many architects, engineers, and contractors recognize the inherent economies and advantages offered by this material, as evidenced by the many impressive lightweight concrete structures found today throughout the world. Structural lightweight concrete offers design flexibility and substantial cost savings by providing: less dead load, improved seismic structural response, longer spans, better fire ratings, and thinner sections, decreased story height, smaller size structural members, less reinforcing steel, and lower foundation costs. Lightweight concrete precast elements offer reduced transportation and placement costs (Sylva et al. 2002). There are many types of aggregates available that are classified as lightweight and their properties cover wide ranges. In 1986 the State Company of Survey and Mining discovered Porcelinate rocks in Traifawi in the Iraqi Western Desert, near Rutba (Bassam et al. 1986). Preliminary studies were made to find its mineral and chemical properties, as well as estimating reserve of this rocks. According to these studies the

Company recommended the use of porcelinate as a coarse aggregate in the production of lightweight aggregate concrete (Bassam et al. 1986) and (خـــــضير محمـــد و عبـــود افنــان1993). Lightweight porcelinate concrete (LWPC) usually have low compressive strength about 17 MPa. Most efforts have concentrated on improving the properties of concrete and studying the factors that influence on these properties. Since the compressive strength is considered a valuable property and is invariably a vital element of the structural design, especially high early strength development which can be provide more benefits in concrete production, such as reducing construction time and labor and saving the formwork and energy. To improve the strength of lightweight concrete the using of supplementary cementitious materials like fly ash, ground granulated blast – furnace slag, silica fume, and natural pozzolans, such as calcined shale, calcined clay or metakaolin, which contribute to the strength gain of concrete, is necessary. Al–Musawi used porcelinate as lightweight aggregate. The cementitious materials considered type I Portland cement with 4% superplasticizer (% weight of cement) and maximum size of aggregate (MSA) 9.5 mm were used, 28-day compressive strengths were found between 13.2 and 21.9 MPa, with a density between 1761 and 1975 kg/m3 (Al–Musawi 2004). Al–Mohamady found 28-day compressive strength of lightweight porcelinate concrete between 20.9 and 29.03 MPa (The highest values were obtained for the 9.5 mm lightweight aggregate mixture with 650 kg/m3 of type I Portland cement with 2% superplasticizer), with a density between 17645 and 1815 kg/m3 (Al–Mohamady 2007).

EXPERIMENTAL INVESTIGATIONS AND SPECIFICATIONS

Properties of Materials

Cement; one type of Portland cement; ordinary portland cement (OPC) was applied. Total percentages for its oxides, compound composition and some properties were fulfilled to the requirement of Iraqi specification No.5/1984 as denoted in Table 1and 2 .

Aggregate; the fine aggregate used was local sand, it met the requirements of Iraqi specification No.45/1984 with respect the sieve analysis and physical properties as denoted in Table (3) and (4). While the coarse aggregate used was crushed porcelinate with maximum size 9.5 mm, it met the requirements of ASTM C330-05. Sieve analysis, chemical analysis and physical properties as denoted in Table (5,6 and 7), respectively.

Water; Normal tap water was used as mixing water.

Superplasticizer (SP);

The superplasticizer used in this research is Sikament −163 (high range water– reducing agent and superplasticizer); which complies with ASTM C494–05, type F. Table (8) shows the technical description for it.

Metakaolin (MK); metakaolin , which used in this research , is obtained by calcination of kaolinitic clay at temperatures from 700 °C for one hour. It has strength activity index 102% $\geq$ 75%, which is complying with the strength activity index for Portland cement requirements of ASTM C311–05. Chemical analysis of metakaolin is complying with ASTM C618–05 requirements as denoted in Table (9).

CONCRETE MIXES PROPORTION

The basic objective of this present research is to investigated the influence of metakolin on some properties of lightweight porcelinate concrete. Accordingly, other mix design variables were considered constant such as mix proportions, the aggregate-binder, coarse-medium-fine aggregate ratio, dosage of SP, curing conditions and testing procedure. The total binder content was fixed at 500 kg/m^3, total sand content was 500 kg/m^3, 0.33 w/c ratio and total porcelinate content was 520 kg/m^3 . The dosage of SP was fixed 3.5% (% weight of cement) and kept constant for all the mixes. The metakaolin was replaced by 5%, 10%, 15% and 20%. In additional to the reference mix w/o metakaolin for comparison purpose. In order to minimize variations in workability, the compaction energy was varied for obtaining proper compaction and the mixing procedure and time were kept constant for all the concrete mixes investigated.

PREPARATION OF SPECIMENS AND CURING

The cylindrical molds of size 150 *300 mm and 150*150*500 prism lightly oiled were filled with fresh concrete and compacted by using vibrating table. For each concrete mix, fifteen specimens were used, three cylindrical specimens for density test, three for compressive strength test, three for splitting tensile strength test and three for modulus of elasticity test and three prism for modulus of rupture test. The molds after casting were covered with polyethylene sheet and kept in the laboratory environment for a period of 24-hr. After that, the specimens were demoulded and placed in the water curing tanks up to the wanted age for test (28-day).

HARDENED CONCRETE TESTS

Compressive   Strength; Concrete compressive strength is measured by using   (300x150mm)   cylinder specimens for 28–day age according to ASTM C39–01. The average of three specimens for each mix was adopted.

Prof. Nada M. Fawzi
Asst.Prof. Kalil I. Aziz
Asst.Led. Sheelan M. Hama

Effect of Metakaolin on Properties of Lightweight
Porcelinate Aggregate Concrete

Splitting Tensile Strength; The splitting tensile test is carried out on (150x300mm) concrete cylinders for 28–day age according to the ASTM C496–05. The average of three specimens for each mix was adopted.

Modulus of Rupture; The modulus of rupture test was carried out by using (100x100x500mm) prisms, loaded at 450mm span with one points loading hydraulic machine. The test is carried out according to ASTM C78–05, using three concrete prisms and the average of three results is adopted.

Static Modulus of Elasticity;
Measurement of modulus of elasticity are made according to ASTM C469–02 at 40% of ultimate load. The average of three specimens for each mix was adopted.

Unit Weight (Density); An average of three cylinders (300x150mm) was used to determine fresh density and hardened unit weight according to ASTM C567–00.

TEST RESULTS AND DISCUSSION
Compressive Strength
Test results are shown in Table (9). The compressive strength of concrete is usually measured for the purpose of quality control. The isolated effect of MK on the compressive strength are investigated. Fig. (1). shows the variation of compressive strength with MK replacement percentages in addition to the control mix (0% MK). The percentages of gaining strength with respect to the control at 5%, 10%, 15% and 20% MK replacements are 40.0%, 104%, 135.5% and 80.0%, respectively. The results indicate that the highest compressive strength was 47.1 MPa at 15% MK replacement. These results show that the optimum MK replacement percentages for

obtaining maximum 28-day compressive strength of lightweight porcelinate concrete > 40 MPa ranges from 10% to 15%. This can explained by particle packing, micro–filling, and chemical reaction of MK with calcium hydroxide (CH) released from cement hydrates (hydration of C_3S) to form additional strong calcium silicate hydrate i.e cement gel (CSH) providing higher strength, additionally to the CSH, it produces other cementitious compounds as hydrogarnet or hydrogrossular phases (Taylor 1997, and Frías and Cabrera 2002),and the one can see that for all mixing the one contain metakaolin gave the higher compressive strength than reference control mix.

SPLITTING TENSILE STRENGTH
Fig. (2) shows the variation of splitting tensile strength with the MK replacement percentages. The trend in the strength gain is almost similar to that in compressive strength. The percentages of gaining strength with respect to the control mix at 5%, 10%, 15% and 20% MK replacements are 29.5%, 66.7%, 80.5% and 42.9%, respectively. The results indicate that the highest splitting tensile strength was 3.79 MPa at 15% MK replacement. Metakaolin particles increase the packing of the solid materials by filling the spaces between cement grains thereby increasing of bond strength leading to a significant increase in splitting tensile strength (Taylor 1997 and ASTM: C642–06). Fig. (3) shows the relationship between the 28-day splitting tensile and compressive strength for MK replacement percentages 0%, 5%, 10%, 15% and 20%, respectively. The splitting tensile strength increase with the increasing of compressive strength, and results show that the optimum MK replacement percentages for obtaining maximum 28-day splitting tensile

strength of lightweight porcelinate concrete is 15% which gave higher compressive strength as mentioned before.

MODULUS OF RUPTURE

Fig. (4) shows the variation of modulus of rupture with the MK replacement percentages. The percentages of gaining strength with respect to the control mix at 5%, 10%, 15% and 20% MK replacements are 24.5%, 78.5%, 97.4% and 50.2%, respectively. This increasing percentages in flexural strength attributed to improving properties of concrete by using metakaolin (Taylor 1997 and ASTM: C642–06). Fig.   (5) show the relationship between the 28-day modulus of rupture and compressive strength for MK replacement percentages 0%, 5%, 10%, 15% and 20%, respectively. The modulus of rupture increase with the increasing of compressive strength and the results indicate that the highest modulus of rupture was 4.6 MPa at 15% MK replacement.

MODULUS OF ELASTICITY

Fig. (6) shows the variation of modulus of elasticity with the MK replacement percentages. The percentages increase in modulus elasticity of with respect to the control mix at 5%, 10%, 15% and 20% MK replacements are 33.6%, 77.3%, 99.2% and 50.4%, respectively. Fig. (7) show the relationship between the 28-day modulus of elasticity and compressive strength for MK replacement percentages 0%, 5%, 10%, 15% and 20%, respectively. The modulus of elasticity increase with the increasing of compressive strength and the results indicate that the highest compressive strength was 23.7 GPa at 15% MK replacement. Lightweight aggregates are weaker than normal weight aggregates, this decrease in stiffness can be seen in modulus of

elasticity measurements of lightweight concretes. So higher cement contents are needed to get a required strength for a mixture (Nawy 2001).

UNIT WEIGHT (DENSITY)

Based on the experimental results one can see that the both fresh and dry density of lightweight Porcelinate concrete contain metakaolin were higher then reference control mix, and the density increase with increasing of compressive strength. The reaction between MK with CH as mentioned above provide a dense impermeable pore structure. The percentages of increasing of density with respect to the control mix at 5%, 10%, 15% and 20% MK replacements are 8.4%, 14.0%, 15.3% and 10.8%, respectively.

CONCLUSIONS

The following conclusions have been reached in this study;

1.   The isolated effect of MK increases the compressive, splitting tensile strengths, modulus of rupture and modulus of elasticity. The highest increase has been found in the compressive strength.

2.   The trend in the strength gain due to MK replacement in modulus of rupture is almost similar to that in splitting tensile strength for lightweight porcelinate concrete.

3.   The optimum MK replacement percentages for obtaining maximum 28-day compressive strength of lightweight porcelinate concrete ranges from 10% to 15%.

4.   The optimum MK replacement percentages for obtaining maximum splitting tensile strengths, modulus of rupture and modulus of elasticity of at 28-day for lightweight porcelinate concrete was 15%.

5.   Splitting tensile strengths, modulus of rupture, modulus of elasticity and density of lightweight

Prof. Nada M. Fawzi
 Asst.Prof. Kalil I. Aziz
 Asst.Led. Sheelan M. Hama

**Effect of Metakaolin on Properties of Lightweight
Porcelinate Aggregate Concrete**

porcelinate concrete were increasing with increasing of compressive strength.

REFERENCE

ACI Committee 213, "Guide for Structural Lightweight–Aggregate Concrete", in ACI Manual of Concrete Practice. American Concrete Institute: Farmington Hills, MI., 2003, 38pp.

Al-Musawi, J.;" Flexural Behavior of Porcelinite Reinforced Concrete Beams", A Thesis Submitted to The Civil Engineering Department College of Engineering / University of Technology in Partial Fulfillment of the Requirements for the Degree of Doctor of Philosophy in Structural Engineering, November 2004.

Al-Mohamady, A. F.; " Shear Strength of Porcelinite Aggregate Reinforced Concrete Beams", A Thesis Submitted to The Civil Engineering Department College of Engineering /Al–Anbar University in Partial Fulfillment of the Requirements for the Degree of Master of Science in Structural Engineering, February 2007.

ASTM: C29–97, "Standard Test Method for Unit Weight and Voids in Aggregate", American Society of Testing and Material International, 1997.

ASTM: C39–01, "Compressive Strength of Cylindrical Concrete Specimens", American Society of Testing and Material International, 2005.

ASTM: C127–84, "Standard Test Method for Specific Gravity and Absorption of Coarse Aggregate", Annual Book of ASTM: Standards, Vol.04–02, 1988, pp. 64–68.

ASTM: C293–05, "Flexural Strength of Concrete (Using Simple Beam with Center–Point Loading", American Society of Testing and Material International, 2005.

ASTM: C311–05 , "Standard Test Methods for Sampling and Testing Fly Ash or Natural Pozzolans for Use in Portland–Cement Concrete", American Society of Testing and Material International, 2005.

ASTM: C330–05, "Standard Specification for Lightweight Aggregates for Structural Concrete", Annual Book of ASTM: Standards, Vol. 04–02, 2005, pp. 187–189.

ASTM: C494–05, "Chemical Admixtures for Concrete", American Society of Testing and Material International, 2005.

ASTM: C469–02, "Standard Test Method for Static Modulus of Elasticity and Poisson's Ratio of Concrete in Compression", American Society of Testing and Material International, 2002.

ASTM: C496–05, "Splitting Tensile Strength of Cylindrical Concrete Specimens", American Society of Testing and Material International, 2005.

ASTM: C567–00, "Standard Test Method for Unit Weight of Structural Lightweight Concrete", American Society of Testing and Material International, 2000.

ASTM: C618–05, " Coal Fly Ash and Raw or Calcined Natural Pozzolan for Use in Concrete",

American Society of Testing and Material International, 2005. 75. 76.

ASTM: C642–06   "Density, Absorption, and Voids in Hardened Concrete", American Society for Testing and Material International, 2006.

Bassam, K.S., Hagopian D., and Al–Sadi N. " Geological investigation of Traifawi Montmorillon Clay – Stone Deposit, West Desert", Geosuv. Internal report, Sep. 1986.

B.S.1881, Part 116, "Method for Determination of Compressive Strength Concrete Cubes", British Standard Institution, 1989, 3pp.

Frías, Rojas M., Cabrera J., "The effect of temperature on the hydration rate and stability of the hydration phases of metakaolin – lime– water systems", In: Cement and Concrete Research, Volume 32, Issue 1, January 2002, pp. 133– 138.

خضير، محمد و عبود افنان، " التحري المعدني عـن ترسـبات البورسـلينايت – الـدانبان (الطبقـة الوسـطى) فـي منطقـة الطريفـاوي الـصحراء الغربيـة"، تقريـر داخلـي للمـسح الجيولـوجي و التعدين، ايلول 1993.

Nawy, E.G., "Fundamentals of High–Performance Concrete", John Wiley & Sons, Inc., New York, 2nd ed., 2001

Neville, A.M., "Properties of Concrete", Fourth And Final Edition, England, 1995.

Sylva, G., Breen, J., Burns, N., "Feasibility of Utilizing High–Performance Lightweight Concrete in Pretensioned Bridge Girders and Panels". Research report 1852–2, Center for Transportation Research Bureau of Engineering Research of the University of Texas at Austin, January 2002.

Taylor, H.F.W., "Cement Chemistry", 2nd edition. Tomas Telford, 1997.

Table (1) Chemical oxide composition and components of
Ordinary Portland cement

Chemical analysis	Test results % By weight	Limits of Iraqi specification No.5/1984
CaO	62.07	–
SiO$_2$	21.60	
MgO	1.93	5% (maximum)
SO$_3$	2.19	2.8(maximum)
Fe$_2$O$_3$	3.18	–
Al$_2$O$_3$	5.30	–
Loss of Ignition (L.O.I)	1.78	4%(maximum)
Insoluble Residue	0.5	1.5%(maximum)
Lime saturation factor (L.S.F)	0.89	0.66–1.02
Main compounds (Bogue's equation)		
C$_3$S	47.16	–
C$_2$S	26.62	–
C$_3$A	6.43	–
C$_4$AF	9.97	–

#Tests are carried out by the stat company of geological survey and mining (SCGSM).

Table (2) Physical properties of cement used

Physical properties	Test results	Limits of Iraqi specification No.5/1984
Fineness by Blaine method m^2/kg	350	230 (minimum)
Setting time (Vicat apparatus)		
Initial setting (min.)	140	45 (minimum)
Final setting (hr.)	4.083	10 (maximum)
Compressive strength for cement–mortar cube at:		
3 days (MPa)	24.7	15 (minimum)
7 days (MPa)	33.3	23 (minimum)

#Tests are carried out by the stat company of geological survey and mining (SCGSM).

Table (3) Grading of sand according to Iraqi specification No.45/1984

Sieve size (mm)	%Passing	Limits of Iraqi specification No.45/1984 % passing (Zone No. 1)
10	100	100
4.75	90	90– 00
2.36	75	60– 95
1.18	56	30–70
0.6	30	15–34
0.3	13	5–20
0.15	6	0–10

- Fineness modulus = 3.27

Table (4) Chemical and Physical properties of sand

Property	Results	Limit of Iraqi specification No.45/1984
Bulk specific gravity	2.5	–
Absorption %	2.2	–
Dry loose unit weight (kg/m^3)	1600	–
Sulphate content (SO$_3$)%	0.25	0.5 (max.)
Material finer than 0.075 mm sieve %	2.3	5.0 (max.)

- The test was carried out at the laboratory of Baghdad University/Civil Engineering.

Table (5) Grading of coarse porcelinate aggregate

Sieve size (mm)	Coarse aggregate % passing	ASTM C330–05 % Passing
12.5	100	100
9.5	83	80–100
4.75	36	5–40
2.36	10	0–20
1.18	0.7	0–10

Table (6) Chemical analysis of porcelinate aggregate

Oxides	By weight %
SiO$_2$	71.15
Fe$_2$O$_3$	0.92
Al$_2$O$_3$	3.2
TiO$_2$	7.31
CaO	5.5
MgO	0.16
SO$_3$	0.08
L.O.I	9.65

#Tests are carried out by the SCGSM.

Table (7) Physical properties of porcelinate aggregate

Property	Results	Specification
Specific gravity	2.0316	ASTM C127–84
Absorption %	46.249	ASTM C127–84
Dry loose unit weight (kg/m^3)	802*	ASTM C29–97

*Within the limit of ASTM C330 (880kg/m^3).
#Tests are carried out by the stat Company Of Geological Survey and Mining (SCGSM).

Prof. Nada M. Fawzi
Asst.Prof. Kalil I. Aziz
Asst.Led. Sheelan M. Hama

Effect of Metakaolin on Properties of Lightweight
Porcelinate Aggregate Concrete

Table (8) Properties of superplasticizer

Properties	Description
Main action	Highly effective water–reducing agent and superplasticizier for the production of high quality concrete in hot climates
Dosage	0.6% – 2.5% by weight of cement
Type	Polymer type dispersion
Appearance	Liquid
Color	Brown
Specific gravity	1.2 kg/l
PH value	10 ± 1.0.

Supply by manufacture

Table (9) Chemical analysis of metakaolin

Oxides	% By weight	ASTM C618–03 [67]
SiO_2	52.38	Silicon dioxide (SiO_2) plus aluminum oxide (Al_2O_3) plus iron oxide (Fe_2O_3)=70% (Min.)
Al_2O_3	37.31	
Fe_2O_3	1.21	
CaO	1.68	–
MgO	0.3	–
K_2O	0.44	–

#Tests are carried out by the stat company of geological survey and mining (SCGSM).

Table (9) Properties of lightweight concrete

No. of mix	MK % of cement weight	Compressive strength (MPa)	Splitting tensile strength (MPa)	Modulus of rupture (MPa)	Modulus of elasticity (GPa)	Unite weight (Density) kg/m^3	
						Fresh unit weight	Dry unit weight
1.	5%–MK	28.0	2.72	2.90	15.9	1773	1698
2.	10%–MK	40.8	3.50	4.16	21.1	1868	1787
3.	15%–MK	47.1	3.79	4.60	23.7	1898	1806
4.	20%–MK	36.0	3.00	3.50	17.9	1806	1736
5.	0%–RC	20.0	2.10	2.33	11.9	1620	1567
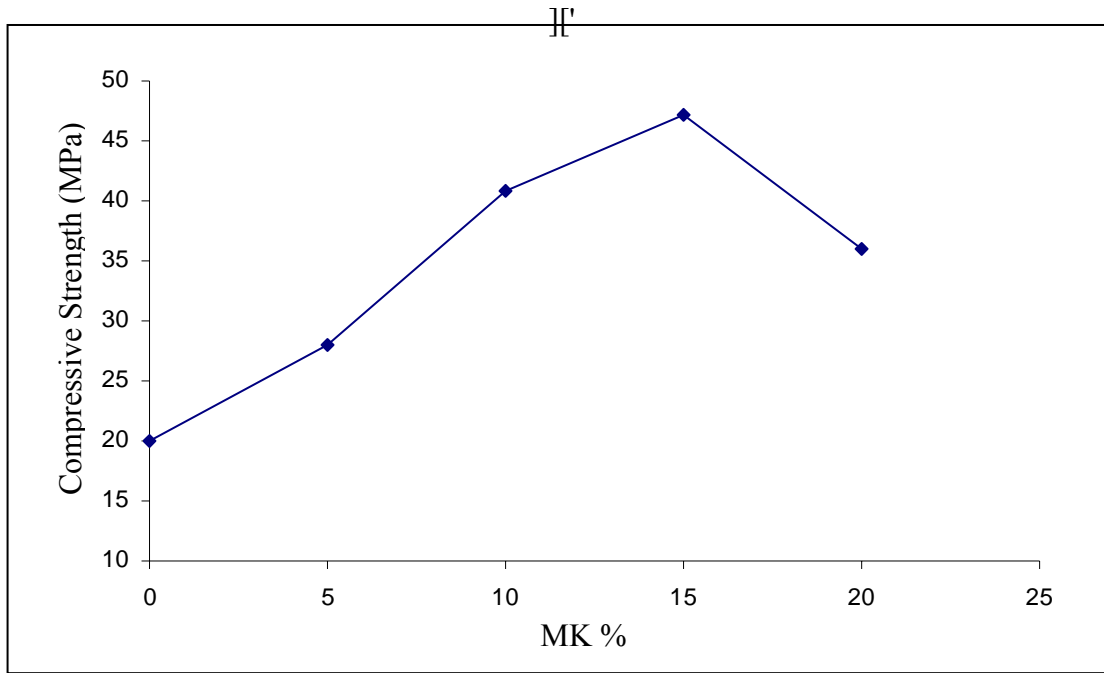
Fig. 1 Relationship between 28 day compressive strength and percentage replacement of Metakaolin
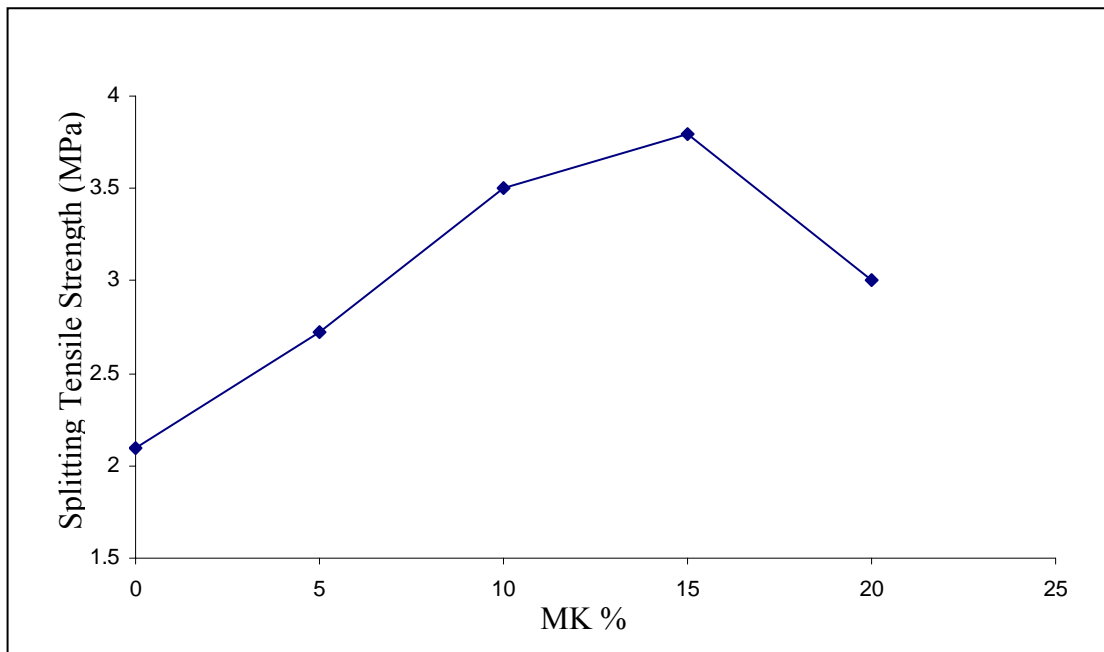
Fig. 2 Relationship between 28 day splitting tensile strength and percentage replacement of Metakaolin

Prof. Nada M. Fawzi
 Asst.Prof. Kalil I. Aziz
Asst.Led. Sheelan M. Hama

Effect of Metakaolin on Properties of Lightweight
 Porcelinate Aggregate Concrete
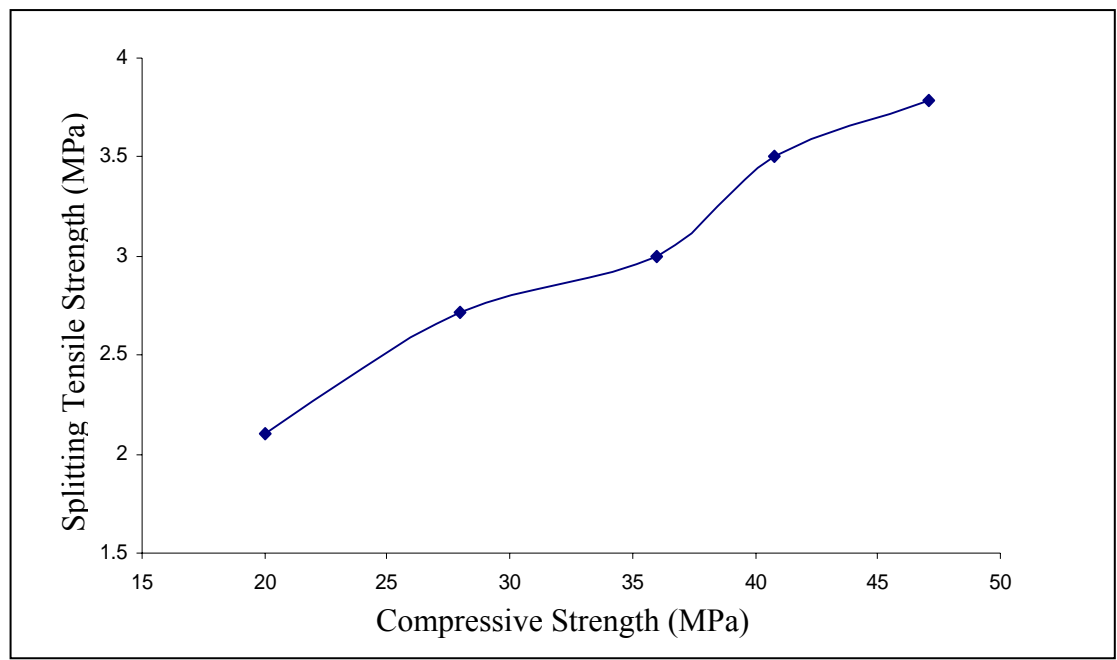
Fig. 3 Relationship between 28-day splitting tensile strength and compressive strength
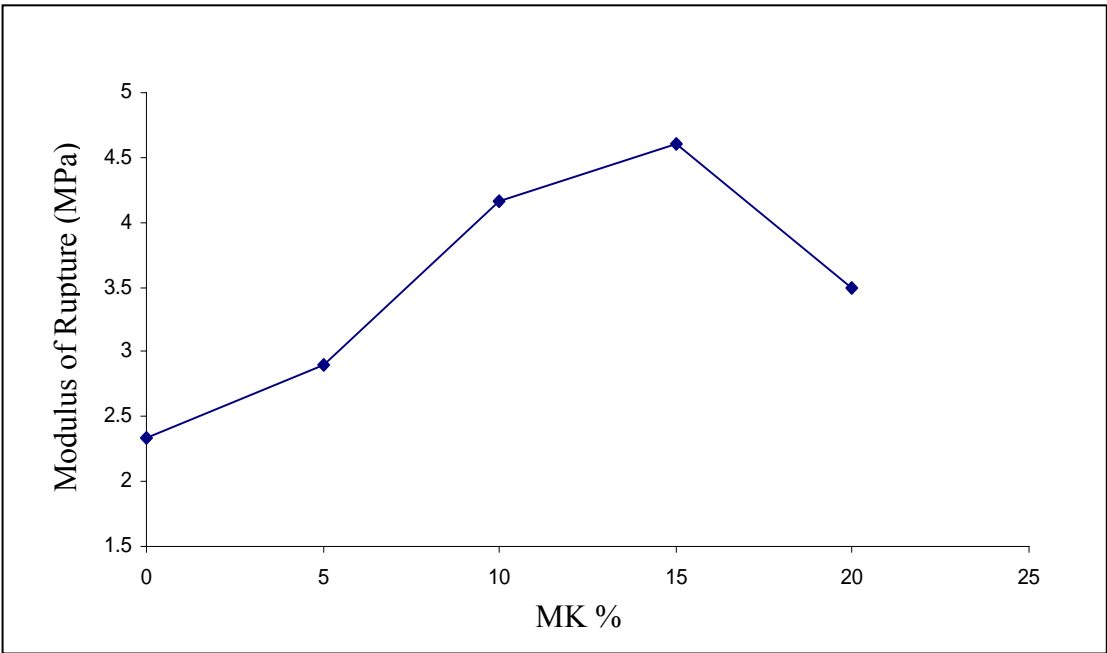
Fig. 4 Relationship between 28 -day modulus of rupture and percentage replacement of Metakaolin
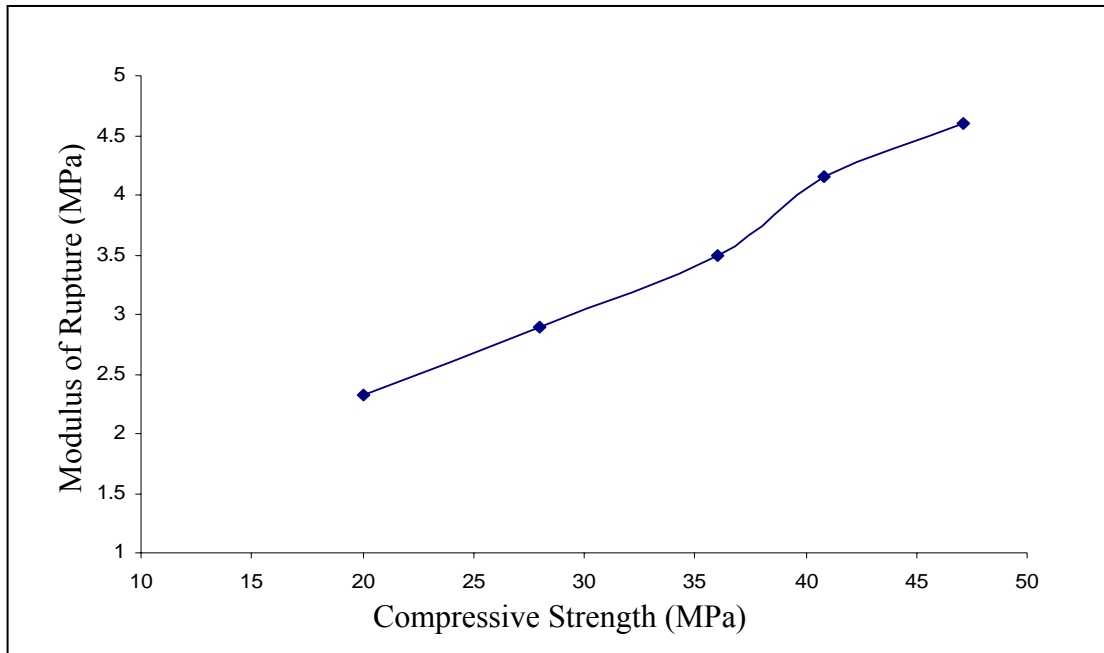
Fig. 5 Relationship between 28-day modulus of rupture and compressive strength
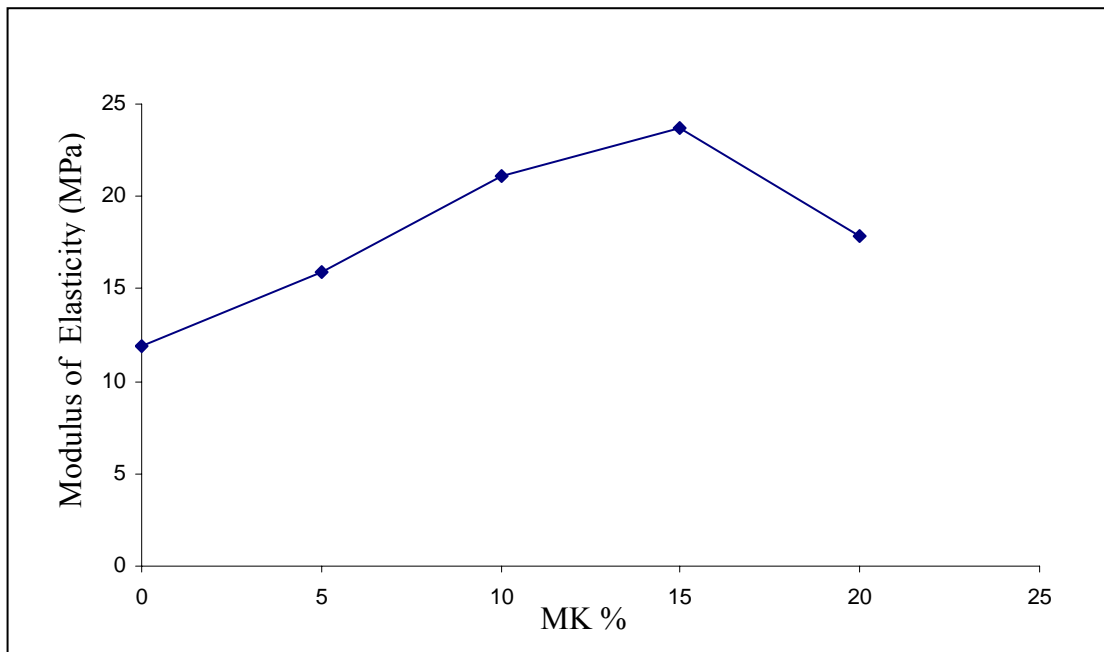
Fig. 6 Relationship between 28 -day modulus of elasticity and percentage replacement of Metakaolin

Prof. Nada M. Fawzi
Asst.Prof. Kalil I. Aziz
Asst.Led. Sheelan M. Hama

Effect of Metakaolin on Properties of Lightweight
Porcelinate Aggregate Concrete
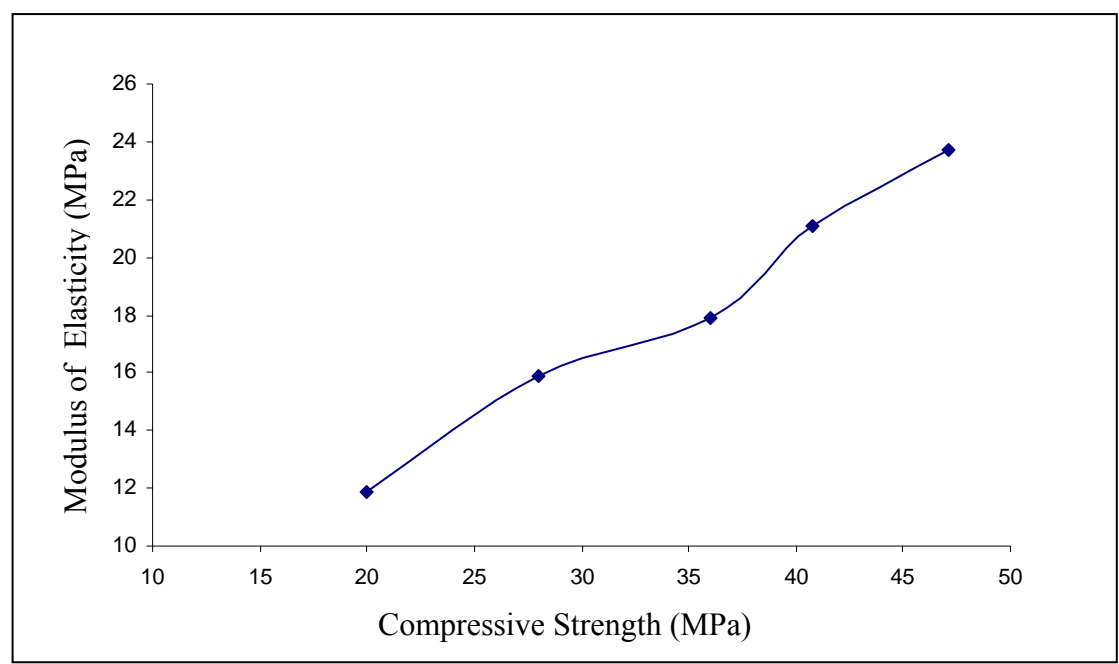
Fig. 7 Relationship between 28-day modulus of elasticity and compressive strength

Equilibrium Moisture Sorption Isotherms of Aspirin

Maha M Alwan

Chemical Engineering Department- College of Engineering- University of

Baghdad-Iraq

ABSTRACT:

Equilibrium Moisture sorption isotherms are very important in drying and storage analysis. Experimental moisture equilibrium data (adsorption and desorption) of Aspirin were determined using the static method of saturated salt solutions and that by exposing the material to different conditions of temperatures and water activities. Three different temperatures (25, 30, 40C°) and water activities in the range of (6.3- 83.6%) were used.

The results showed that the equilibrium moisture content increased with the increase in water activity at any temperature and decreased with temperature increase at constant water activity. The water activity increases with increasing in temperature when moisture content was kept constant. The sorption isotherm curves are of type II according to Brunauer`s classification. The hysteresis effect was not distinctly expressed only for equilibrium sorption values of Aspirin at 25ºC. The experimental results were fitted to two sorption models (GAB and Henderson).The average relative deviation between the experimental and calculated data were obtained to select the best model. The GAB and Henderson models, obtaining values of 3.54 and 1.42 % average relative deviation and coefficient of regression of 0.98 and 0.977 respectively. The Henderson model was found to be the best fit out of the two models to predict the sorption behavior of Aspirin.

Keywords: Equilibrium moisture content, Water activity, sorption isotherms, Mathematical modeling, pharmaceutical, Aspirin.

الخلاصة :

ان دراسة منحنيات محتوى الرطوبة عند الاتزان لكل من حالتي الامتزاز والأد-امتزاز مهمة في تحليل ودراسة الظروف المناسبة للخزن واختيار ظروف وطريقة تجفيف المواد خاصة المواد الحساسة مثل الاسبرين.

تم الحصول على النتائج العملية باستعمال طريقة المحاليل الملحية المشبعة وذلك بتعريض المادة الى ظروف مختلفة من درجة الحرارة وفعالية الماء (الرطوبة النسبية عند الاتزان) . تم استعمال ثلاث درجات حرارية مختلفة (40,30,25) درجة سيليزية وفعالية الماء في المدى (6.3- 83.6%) .

اوضحت النتائج العملية ان محتوى الرطوبة عند الاتزان يزداد مع زيادة فعالية الماء عند اي درجة حرارية، ويقل مع زيادة درجة الحرارة بثبوت فعالية الماء. والأخيرة تزداد مع زيادة درجة الحرارة بثبوت محتوى الرطوبة .الهسترة لم تكن واضحة فقط عند درجة حرارة 25. إن المنحنيات في الحالتين هي من النوع الثاني حسب تصنيف العالم برونير. تم تحليل النتائج العملية ومطابقتها مع موديلين رياضيين هما (كوكنهام- أندرسون ودي – بور) وهندرسون . نسبة الانحراف النسبية للموديلين 3.54 و 1.42 % ومعامل التطابق 0.98 و 0.977 % ، حيث وجد ان موديل هندرسون أفضل في تمثيل الايزوثيرم للاسبرين.

INTRODUCTION

The knowledge of equilibrium moisture isotherm is very important in storage and drying processes analysis. During the storage and drying of products, physical and chemical changes occur; these changes are particularly influenced by moisture content of a material, relative humidity and the storage and drying conditions. (Motta L., et al., 2004)

The water sorption isotherm of a material shows the equilibrium relationship between the relative humidity and the moisture content of a material (expressed as mass of water per unit mass of dry material) at constant temperature and pressure (Maria L. et al., 1993). Thus with the knowledge of the moisture isotherm it is possible to predict the maximum moisture that the material can be allowed to gain or loss during storage. The adsorption isotherms data can be used for a storage method determination and while the desorption data can be used for drying analysis. (Daniel S. et al., 2004)

Water is an important component of nearly all materials and plays a decisive role in dictating the degradation of a material. For most materials, much of the water content is freely available to behave physically as pure water with properties such as vapor pressure equal to pure water; As moisture content is lowered, a point will be reached at which the water becomes less active, in that it can not act physically or chemically as pure water, in this state, it is considered to be bound water .Thus, the amount of free water rather than the amount of total water is critical to the chemical and physical stability of a dry substance that is moisture sensitive (Bags K. et al.2009).

When a sample comes into equilibrium with the atmosphere surrounding it, the water activity in the sample becomes equal to the relative humidity of the atmosphere surrounding it or in which it is stored. Once this equilibrium is reached, the sample neither gains nor loses moisture over time. The moisture uptake/loss rate depends on the relative humidity of the environment and the time (Mark J. et al., 2006).So the water activity a measure of the free water in a pharmaceutical dosage form (Bell L.,2000).

The relationship between water content and water activity is complex. An increase in water activity is almost always accompanied by an increase in the water content, but in a non-linear relationship. These isotherm curves are determined experimentally (Bell L., 2000), and they are important to determine

the stability criteria for pharmaceuticals which their properties are critically dependent on the presence of moisture (Mark J.et al., 2006). Water in pharmaceutical products either as the residual water from processing or as the result of exposure to high relative humidity may affect the chemical and physical stability of moisture sensitive products (Yanxia L. et al.,2003). The stability is a critical quality of pharmaceutical products and it varies with time under the influence of a variety of environment factors; such as; temperature, humidity, light, and others. So these curves can be used to help predict product stability over time in different storage conditions or drying processes (Kim H., 2001). The free water content and therefore degree of water activity provides more valuable information than the total moisture content when considering the stability of moisture sensitive products (Cunningham C. et al., 2001).

Water activity, is unitless and the values of unity indicates pure water where as zero indicates the total absence of water molecules ($0 < a_w < 1$), is defined as the ratio of vapor pressure of water in the material to the vapor pressure of pure water at the same temperature (Bob S. et al., 2007):

$$a_w = \frac{p}{p_o} \qquad (1)$$

Equilibrium relative humidity is water activity expressed as a percentage:

$$ERH = a_w \times 100 \qquad (2)$$

Since the vapor pressure of water is strongly dependent upon temperature, then the water activity is temperature dependent, it follows that temperature has a significant effect on sorption isotherms. so when a material is subjected to an upward temperature shift, at any moisture content, water activity increases with increasing temperature .Thus both temperature and relative humidity must be specified to determine the total amount of water available during the sorption process(Yihong Q. et al.,2009).

The study of whether water will adsorb or desorb from a particular component is essential to prevent degradation, especially if the substance is moisture sensitive. For example, two separate materials (initially at different water contents and

water activities) stored at 25% relative humidity, will reach a water activity of 0.25, although the final water content of the two materials will be different. If the materials are moved to a higher or lower relative humidity then the water will increase or decrease, respectively until equilibrium is reached. Likewise, if two materials of differing water activities and the same water content are mixed together, then the water will adjust between the materials until equilibrium water activity is obtained. Therefore, water activity over water content provides useful information for formulation design, manufacturing conditions and packing requirements. Many disciplines use water content calculations to regulate product quality, however, water content measurement can be inaccurate and time-consuming, especially for pharmaceuticals, a particular compound has a water content of 0.05% and measuring water content in this range is difficult and requires a precision balance. For this compound, changes as small as 0.02% in water content corresponded with a 0.2 change in water activity, clearly, the water activity measurement permits much tighter control of the products specifications (Martin C.,2009) . The drying equipment is designed to remove moisture, and only moisture content can be measured and controlled on the factory floor (not water activity). The sorption isotherm becomes the fundamental tool by which it is possible to specify the moisture content needed that will assure the required water activity of a pharmaceutical solid with optimal properties. (Anthony J. et al. , 1999). Many researches have developed to study and model the equilibrium moisture content of food but very few of pharmaceuticals (Daniel S. et al., 2004).

Aspirin, some times known as acetylsalicylic acid, is the salicylate ester of acetic acid, is the most widely used drug in the world, no other drug in the history of medicine has exhibited such an array of multifaceted therapeutic properties (Alexander G., 1998). Aspirin is moisture sensitive and considered as a hygroscopic material (Hygroscopicity is a term used to describe how readily a material will take up moisture when subjected to a given change in relative humidity). (Charles R. et al.2004).

The compound is a white, crystalline powder or tabular or needle like crystals. It is a weak acid. Aspirin tablets should be stored in tight, moisture resistant containers. It is stable in dry air, but readily hydrolyzes to acetate and salicylate when exposed to moisture air, the addition of heat will speed the rate of hydrolysis (Susan K. et al., 2003). The deterioration may take several forms: It can be physical deterioration in which aspirin compositions become completely unmanageable, wet, gummy, sticky masses, or chemical decomposition in which Aspirin loses its molecular structure, or may degrade to a toxic substance (Sumie Y.et al., 2008). In both cases, such composition becomes unsuitable for all practical commercial and medicinal purposes (Alexander G., 1998).

The experimental equilibrium data were obtained by using the classical methodology of exposing the solid material to different conditions of temperature and relative humidity (Motta L. et al., 2004). This method is called the static method or the gravimetric technique, in which, the sample brought in to equilibrium in a closed system of known constant relative humidity. All classical methods require either temperature stability and uniformity or accurate measurement of the temperature (Wolf W. et al., 1985).

The relative humidity was controlled by saturated salt solutions. The value of the relative humidity depends on the salt used. The salts were chosen to obtain a large range of relative humidity (6.3- 83.6 %). The method is widespread as humidity generators because of the ease of handling, low cost of salts and the ease of maintenance of the humidity conditions with high accuracy, but it is labor-intensive and time - consuming until equilibrium is reached between the material and water vapor (Jiri B. et al., 2008).

The objective of this study is the determination of the adsorption and desorption isotherms of Aspirin, at water activities ranging from 6.3- 83.6 and temperatures of 25, 30 and 40 ºC. Two models: GAB and Henderson were fitted to the experimental data in order to describe the equilibrium moisture sorption isotherms of Aspirin.

EXPERIMENTAL PROCEDURE

Material:

Aspirin, produced by Samarah Drug Industry (SDI) was used. For adsorption process the material was with a final moisture content of 1.5%, and for the desorption process a wet material was used with an initial moisture content of 19%.

Method:

The method of preparation of saturated salt solutions was as follows:

Pure salts and distilled hot water in the proportions shown in table (1) were mixed with stirring, excess salt should then be added. The final solution was cooled and allowed to stand a few days at the desired temperature in closed conditions. The solution should be stirred once a day using magnetic stirrer to assure the right formation of the saturated salt solutions. Solutions are made at a higher temperature than equilibration to ensure that they are saturated when cooled. (Shyam S. et al., 2001).

Table 1: preparations of saturated salt solutions at 25ºC (Greenspan, 1977)

Salt kind	Relative Humidity (%)	Distilled Water (ml)	Salt (gm)
LiCl	11.3 ± 0.27	75	42.5
NaOH	8.9 ± 0.7	100	36
MgCl$_2$	33.07 ± 0.18	100	12.5
K$_2$CO$_3$	43.16 ± 0.18	100	45.0
Mg(NO$_3$)$_2$	54.4 ± 0.23	100	15.0
NaBr	59.1	100	40.0
KI	69.9	100	25.0
NaCl	75.47 ± 0.14	100	30.0
KCl	84.34 ± 0.48	100	40
kBr	80.9	100	32

The temperature might affect the relative humidity promoted by the saturated solutions; this effect was considered in the correction of the solutions relative humidity values used in the construction of the isotherms curves (Motta L. et al, 2004).The correction is shown in table (2).

Table 2: correction of relative humidity with temperature (Greenspan, 1977)

Salt Solution	Temperature ºC		
	25	30	40
	Relative Humidity		
NaOH	8.9	7.6	6.3
LiCl	11.3	11.3	11.2
MgCl$_2$	33.1	32.5	31.6
K$_2$CO$_3$	43.2	43.1	43.0
Mg(NO$_3$)$_2$	54.4	51.4	48.4
NaBr	59.1	56	53.2
KI	69.9	67.9	66.1
NaCl	75.5	75.1	74.7
KCl	84.82	83.6	82.3
kBr	80.9	80.6	79.9

A glass desiccators, containing the salt solutions, were tightly sealed from the outside atmosphere, their covers are designed in such away that can by easily opened and re-closed quickly for removal of the samples during the few minutes required for periodic weighing. The desiccators were kept in a temperature controlled chamber, in an air circulation oven, to ensure that the temperature was constant. The experiments were carried out at three different temperatures (25, 30, and 40 ºC).

The equilibrium moisture contents were determined by a gravimetric technique: Samples of known initial moisture content (of 3g each) were weighted just prior to storage using a standard balance of sensitivity ± 0.0001g (model Sartorius). The samples placed in uncovered crucibles placed over the support inside the tightly closed desiccators, so that they do not enter in contact with the salt solutions. It is important to note that the sample size has a great effect on time required to reach equilibrium because of time needed for diffusion of molecules though the interior structure of the sample, so small sizes are recommended. The sorption process is strongly temperature dependent and the temperature must be kept constant and controlled while all experiments are being carried out, thus, each desiccator with the sample inside it was placed in an electric oven at the desired temperature ± 0.2 ºC and allowed to equilibrate with the environment inside the containers. The samples were weighted and recorded periodically until the percentage of changes between two successive readings was less than 1% to ensure that the equilibrium was reached. The sample had a water activity equal to the controlled constant relative humidity regenerated by the salt solutions. The moisture content of the sample was determined

by the oven method (LOD method) at 105 ºC for 24hr (Ludger O. et al., 2003).

To obtain sorption isotherm experimental curves ,moisture content values were measured at provided relative humidity conditions in increasing order ,for the desorption , the same saturated salt solutions were used but in this case in decreasing relative humidity order.

RESULTS AND DISCUSSION

The results of the experimental measurement of the equilibrium moisture content and the respective water activity (equilibrium relative humidity)   at three temperatures 25, 30, 40 ºC are presented in Fig. 1, 2, 3. (Some experimental values were not considered).

Fig. 2 Experimental moisture sorption isotherms of Aspirin at 30 ºC
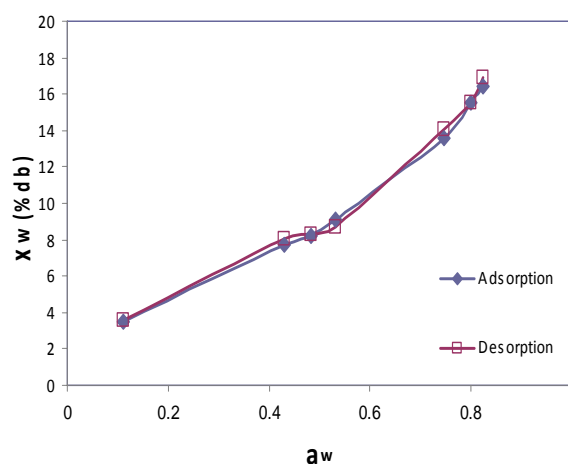
Fig. 3 Experimental moisture sorption isotherms of Aspirin at 40 ºC

Fig. 1 Experimental moisture sorption isotherms of Aspirin at 25 ºC

There was an increase in equilibrium moisture content values with increase in the water activity at constant temperature, this behavior was observed for both adsorption and desorption curves. (Bell L. , 2000) , (Joseph A., 2009).

The curves can be described by isotherms type II according to Brunauer`s classification (Mark D., 2001), they have sigmoid shape (S-shaped), which is common for many hydroscopic products (Ethman C. et al., 2008), and this can be explained by the changes in equilibrium moisture content are due to an inability of the substance to maintain vapor pressure at unity with decreasing moisture content. As moisture content decrease, moisture in the

material tends to show a lower vapor pressure, acting as if in a solution, changing with atmospheric humidity. It is these changes in vapor pressure in the pharmaceutical with atmospheric humidity which result in the characteristic S-shape of water sorption isotherms (Caurie M., 1970).The resulted curves are caused by the combination of effects (physical properties of solution ,capillary effects and surface-water interactions) .A distinct "knee" usually indicates a formation of a well-defined monolayer (Bell L.,2000).

The equilibrium moisture content values for the adsorption process is lower than that of the desorption process at constant water activity, this behavior was analogous to other pharmaceutical (Jhoany A. et al, 2010).

The hysteresis effect was not distinctly expressed only for equilibrium sorption values of Aspirin at 25°C. By increasing the temperature the hysteresis effect was undergo a reduction in size (Rouquerol F. et al.,1999).Also the shape and width of sorption hysteresis loops were dependent on temperature and type of material (Thommes M. et al.2002). This hysteresis is due to non- reversible structural changes and non- equilibrium effects. (Martin C.,2009); and this can be explained that the principle factors affecting hysteresis are the composition of product, isotherm temperature ,storage time before isotherm measurement ,pretreatments , drying temperature and the number of successive adsorption and desorption cycles. It should be noted that the occurrence of hysteresis indicates either the adsorption or the desorption curve is not at true equilibrium or that some material in the product changed state in the process. (Rahman M. et al., 2000).
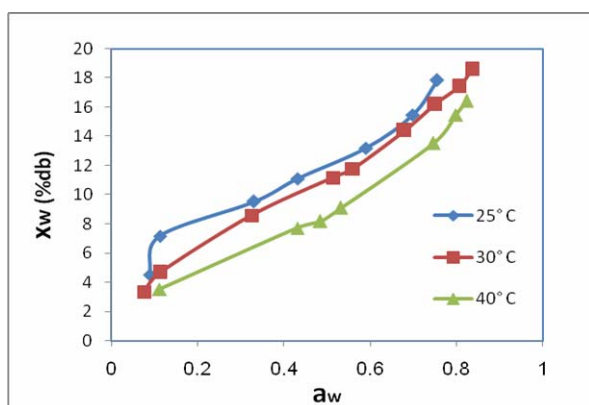
Fig. 4 Adsorption isotherms of Aspirin at different temperatures.
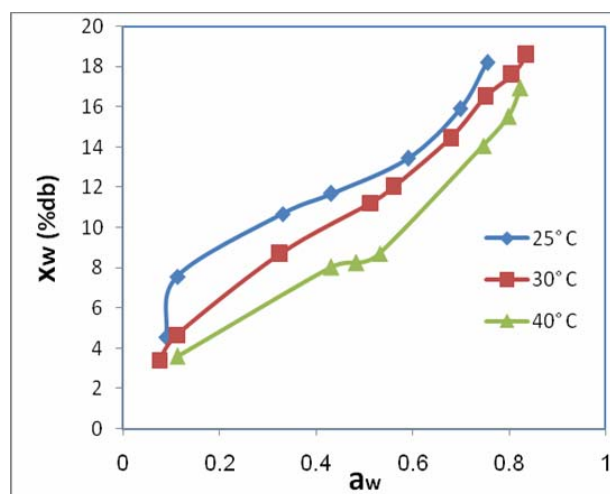
Fig. 5 Desorption isotherms of Aspirin at different temperatures.

As shown in Fig. 4 and 5, temperature has a significant effect on sorption isotherms. The equilibrium moisture content values decreased with an increase in the temperature at constant water activity (Milton C. et al., 2004).This behavior indicates that the material becomes less hygroscopic at higher temperatures (Daniel S. et al.,2004) and this result may be explained that at higher temperatures, the kinetic energy of the water molecules was high and that mean the molecules are in an increased state de excitation, thus increasing their distance apart and decreasing their attractive forces between them, this leads to a decreased in the degree of water sorption at given water activity (Bags K. et al., 2009).This behavior is typical for pharmaceuticals(Acosta J. et al.,2010).

An increase in temperature causes an increase of water activity at the same moisture content, and this is mainly due to the change in the enthalpy of water binding, dissociation of water, physical state of water or increase in solubility of solute in water as temperature increases, which causes of the reaction rates leading to quality deterioration. So the relative humidity had the greater influence compared to other variables (Shyam S. et al., 2001).

At constant moisture content, an increase in temperature caused lowering of isotherm curves making Aspirin more susceptible to degradation (Joseph A., 2009).

The points at low values of water activity (a_w < 0.55) represent the sorption bound water and so isotherm has only a gentle upward slop. As the water

activity increases, the equilibrium moisture content increases sharply with water activity due to capillarity. This moisture content can be chosen as a guarantee that the product will be adequately preserved because the water activity is low enough to prevent degradation and also to maintain the moisture content of the product with the desired range of values (Aroldo A. et al., 2004).

FITTING OF SORPTION MODELS TO EXPERIMENTAL DATA

The experimental equilibrium moisture content data at 25, 30, 40 ºC were fitted using two isotherm models namely: Guggenhein , Anderson and de Boer (GAB) and Henderson models. The parameter values were derived from the regression curves of the two models.

The goodness of fit of both models was evaluate and expressed as mean relative percentage deviation (%E) using the equation with value below 5% indicative of a good fit for practical purposes (Menkov D. et al., 2004).

$$\% \ E \ = \ \frac{100}{N} \sum_{i=1}^{N} \left| \frac{x_w - x_w^\wedge}{x_w} \right| \qquad (3)$$

THE GAB MODEL:

The GAB model (Guggenhein , Anderson and de Boer) is a multi molecular sorption model intended for use over a wide range of water activity (up to 0.9) and it is one of the most widely accepted models for sorption isotherms (Jiri B. et al., 2008), and can be written as a three parameter as follows:

$$x_w = \frac{x_m \ c \ k \ a_w}{(1 - k \ a_w)(1 + (c - 1))k \ a_w} \qquad (4)$$

The monolayer moisture content x_m represents the moisture of the material when its entire surface is covered with a unimolecular moisture layer. It is the moisture content for the maximum stability, and it is generally decreased with temperature (Joseph A., 2009).

The parameter k is a factor correcting the properties of the multilayer in the GAB sorption

equation varies from unity to zero ($0 < k \leq 1$) (Jorge C. et al., 1992).

The third parameter C should be higher than zero. For c ≥ 2, the GAB equation gives a sigmoid shape curve (type II of Brunauer`s classification) (Mark D., 2001).

The parameters x_m, c, k are temperature dependent.

The GAB constant obtained by transforming eq. (4) to the quadratic form (Jiri B. et al., 2008):

$$\frac{a_w}{x_w} \ = \ \alpha \ a_w^2 \ + \ \beta \ a_w \ + \ \gamma \qquad (5)$$

The coefficients of the polynomial can be determined by plotting a_w / x_w versus aw and by a non-linear regression fitting procedure using a polynomial of second degree, the coefficients can be determined and then the GAB constants calculated:

$$\alpha \ = \ \frac{k}{x_m} \left(\frac{1}{c} - 1 \right) \qquad (6)$$

$$\beta \ = \ \frac{1}{x_m} \left(1 - \frac{2}{c} \right) \qquad (7)$$

$$\gamma \ = \ \frac{1}{x_m \ . c \ . k} \qquad (8)$$

The results of the fitting of the GAB model to the experimental data are shown in Fig. 6,7, and 8 and the constants, the regression coefficient (R^2) and the mean relative percent deviation (%E) are presented in Tables (3) and (4).
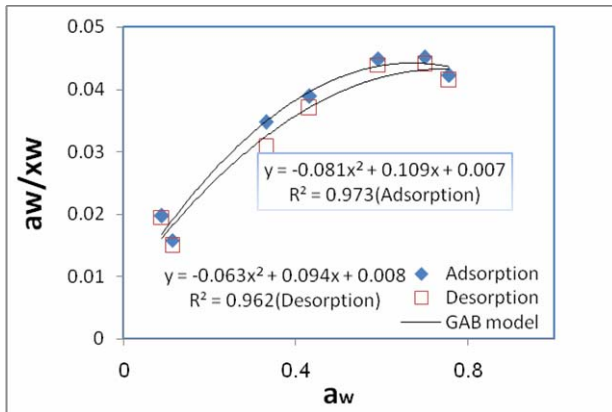
459

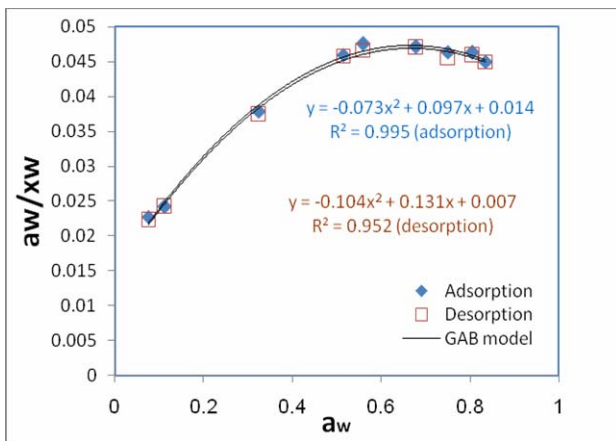**Fig. 6 GAB model isotherm curves for Aspirin at 25 ºC**

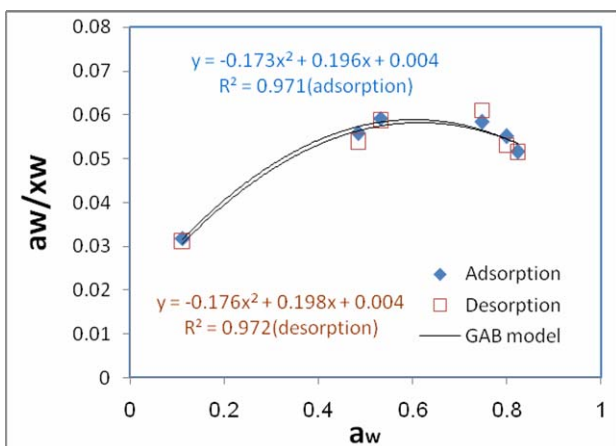**Fig. 7 GAB model isotherm curves for Aspirin at 30 ºC**

Fig. 8 GAB model isotherm curves for Aspirin at 40 ºC

From the results presented in tables 3 and 4, the GAB parameters are temperature dependent. As the temperature increased from 25 to 40 ºC, the monolayer moisture content x_m decreased from 8.03 to 4.93 for adsorption and from 7.28 to 4.88 for desorption and this behavior was an indication that the adsorbed molecules gained kinetic energy making the attractive forces to be loosened and this allowed some water molecules to breakaway from their sorption sites thus decreasing the equilibrium moisture content value (Aroldo A. et al., 2004).The decrease in the monolayer moisture values (x_m) with increase in temperature was an indication on that the multilayer has properties between these of the monolayer and bulk liquid(Menkov D. et al.,2004).

The range of k values, less than unity, was in agreement with the GAB model assumptions. The constant k increased with temperature from 0.79 to 0.88 for adsorption, and 0.79 to 0.87 for desorption while C decreased from 49.5 to 11.46 for adsorption and 58.25 to 9.72 for desorption , increase in K values was an indication that at higher temperature ,the multilayer molecules became more entropic while a decrease of C was an indication of more enthalpy and a gain in kinetic energy resulting in loss of more moisture at higher temperature(Joseph A.,2009).

The C values are greater than 2 and that with agreement that the isotherm sorption curves of type II of Brunauer`s classification (Mark D., 2001).

The mean relative percent deviation (%E) values were, in all cases, less than 5%, is an indication that the model is well suited for describing sorption isotherm of Aspirin(Menkov D. et al., 2004).

The Henderson Model
It is predicts greater changes in equilibrium moisture content for a given temperature change at high water activity. The model fits the lower part of the sorption isotherm curve (Ludger O. et al., 2003).

The Henderson model is:

$$1 - a_w = \exp \left[- a \left(x_w \right)^b \right] \quad (9)$$

This may be written as follows:

$$\ln\left[- \ln\left(1 - a_w\right) \right] = b \ln x_w + \ln a \quad (10)$$

By linear regression of eq. 10 using the experimental data, the constants of the model can be

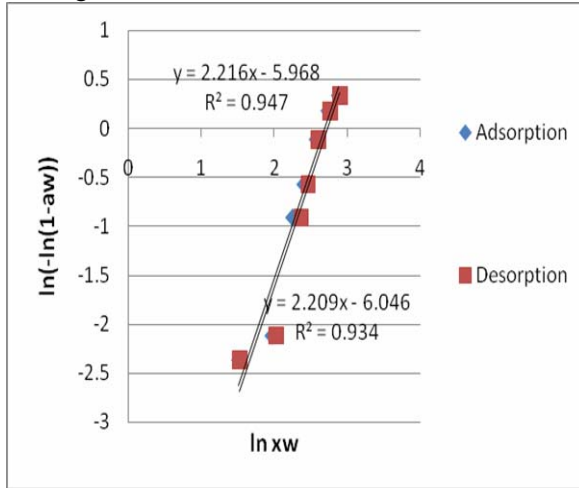calculated. The results are shown in Tables 3 and 4, and Figs. 9, 10, and 11.

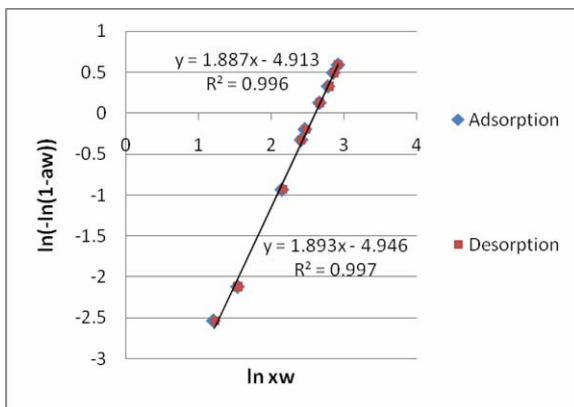**Fig. 9 Henderson model isotherm curves for Aspirin at 25 ºC**

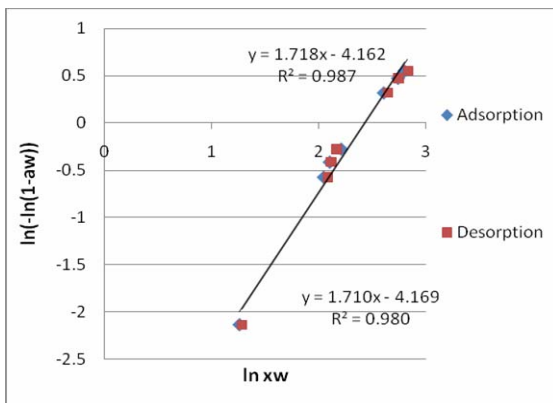**Fig. 10 Henderson model isotherm curves for Aspirin at 30 ºC**

Fig. 11 Henderson model isotherm curves for Aspirin at 40 ºC

From the results, the regression coefficients were high and the mean percent relative deviation was lower than 5%.

Table 3: GAB and Henderson parameters of adsorption isotherms for Aspirin

Model	Constants	25 ºC	30 ºC	40 ºC
GAB	X_m	8.03	8.6	4.93
	C	49.5	12.06	11.46
	K	0.75	0.69	0.88
	R^2	0.973	0.995	0.972
	E%	4.1	3.32	3.14
Henderson	a	0.003	0.0075	0.0156
	b	2.218	1.887	1.718
	R^2	0.947	0.996	0.987
	E%	0.57	0.19	3.5

Table 4: GAB and Henderson parameters of desorption isotherms for Aspirin

Model	Constants	25 ºC	30 ºC	40 ºC
GAB	X_m	7.28	7.06	4.88
	C	58.25	26.6	9.72
	K	0.79	0.76	0.87
	R^2	0.962	0.952	0.972
	E%	0.84	4.04	4.3
Henderson	a	0.0024	0.007	0.0155
	b	2.21	1.893	1.71
	R^2	0.934	0.997	0.980
	E%	0.66	0.19	1.84

Comparing the results of the two models; the Henderson model fits the experimental data better than the GAB model.

CONCLUSIONS

The following conclusions are drawn from the above discussed results:-

1- The equilibrium moisture content increases with the water activity increase at any temperature, and decreases with an increase in temperature at constant water activity.

2- The water activity increases with increased temperature when moisture content was kept constant.

3- The sorption isotherm curves have an S-shape profile.

4- The monolayer moisture content and the sorption capacity decreased with an increase in temperature at constant water activity.

5- The hysterias effect was not distinctly expressed only for isotherms at 25 ºC.

6-The Henderson model is suitable for describing the sorption isotherms for Aspirin   .

NOMENCLATURE

a_w Water activity   (dimensionless)
a ,b Constants of Henderson model
c ,k Characteristic constants of GAB model
d .b.   Dry basis
E   Mean relative deviation   (%)
ERH   Equilibrium relative humidity   (gH_2O/g dry solid)
P   Vapor pressure   (N/m^2)
P_0 Vapor pressure of pure water   (N/m^2)
R^2 Coefficient of regression
X_w Equilibrium moisture content   (%g H_2O /g dry solid)
$x_w^\wedge$ Predicted (calculated) moisture content (%g H_2O /g dry solid)
X_m GAB monolayer moisture content (%g H_2O /g dry solid)
LOD   Loss on Drying
Greek Letters
α, β, γ Constants of GAB model (in quadratic form).

REFRENCES

Acosta J., Nuevas L., Rodriguez I.," The Moisture Isotherms of Cefotaxime Sodium Salt", Drying Tech., V.18, 1-2, 2010.

Alexander G.," Water –Soluble Aspirin Composition", Patent 5776431, July, 1998.

Anthony J., Fontana Jr."Pharmaceutical Applications for Water Activity "Pharmaceutical on Line, April, 29, 1999.

Aroldo A. P., Abraham D.G. –Z., Fernando L. D.," Sorption Isotherms Experimental Data and Mathematical Models For Murici Pulp ", IDS, V. A , PP. 634-639 , 2004.

Bags K., Srivastav P. , Mishra H.," Desorption and Adsorption Characteristics of Bael Pulp and Powder ",International Food Research J.,16, PP.561-569,2009.

Bell L. N., Labuza T. P.," Practical Aspects of Moisture Sorption Isotherm and Use "2nd Edition AACC Egan Press., 2000.

Bob S. , Peihong L., Neil P.," Implementation of Water Activity Testing to Replace Karl Fischer Water Testing, " Pharmaceutical Tech. ,Feb., PP.56-71,2007.

Caurie M. A.," Practical Approach to Water Sorption Isotherms and the Basis for the Determination of Optimum Moisture Levels of Hydrated Foods ", J. Food Tech.., V.6, PP.85-93, 1970.

Charles R. Cunningham K.," The Effect of Starch on the Stability of Aspirin Tablets", American Association of Pharm. Scientists, Oct., 2004.

Cunningham C.," Formulations of Acetyl Salicylic Acid Tablets for Aqueous Enteric Film Coating", Pharm. Tech. Europe, May, 2001.

Daniel S. C., Wanderley P. O.,"Drying of Medicinal Plants : equilibrium Moisture Content and Mathematical Modeling of Maytenus Ilicifolia Leaves ", IDS , V.C,PP.1712-1719,2004.

Ethane C.S., Kahila M. , Lamharrer A.," Moisture Sorption Isotherms and Thermodynamic Properties of two Mints", Revue des Energies Renouvelables, V.11, No.2, PP. 181-195, 2008.

Greenspan L." Humidity Fixed Points of Saturated Aqueous Solutions", J. of Research of the National Bureau of Standards, V.81 A , No.1, pp.89-96, Jan-Feb, 1977.

Jhoany A. E., Vlisea J.H. and Galo C.R.," Behavior and Modeling of Humidity Isotherms of Mangifera Medical (Vimang) Powder ", J. World Applied Science, 11(12), PP.1504-1509, 2010.

Jiri B., Stavrosy Y."GAB Generalized Equation for Sorption Phenomena", Food Bioprocess Tech., No.1, PP. 82-90 , 2008.

Jorge C. , Ernsto O. Timmermann H. , A. Iglesias " Some Features of the Parameter k of the GAB Equation as Applied to Sorption Isotherms of Selected Materials ",J. of Food Engineering ,V.15 ,pp.75-82 ,1992.

Joseph A. , Simon V., Adesola S.," Moisture Adsorption Characteristic of Giner Slices ", Sienc. Technol. Aliment, 29(1), 155-164, Jan.-Mar., 2009.

Kim Huynh-Ba ,"Hand Book of Stability Testing in Pharmaceutical Development",Springer,2009.

Ludger O. F., Arther A. Teixeira "Food Physics: physical Properties –Measurement and Applications", Springer, 2003.

Maria L., Panagiotis G. D. ,"Equilibrium Moisture Characteristics of Food –Hysterias Effects and Isotherm Models ",Lebensmilel-Technologie ,26 ,No.4 ,1993.

Mark J. K., James J. C.," Water sorption of Drugs and Dosage Forms", Encyclopedia of pharmaceutical Tech., 2006.

Martin Chaplin, "Water structure and Science", 2009

Menkov D., Durakova G. ,"Moisture Sorption Isotherms of Walnut Flour at Several Temperatures",Biotechnol and Biotechnol.Eq.,2004.

Milton C., Afonso M., Paulo C.,"Drying Curves and Water Activity Evaluation of Dried Banana" , IDS, 22-25,Aug.,V.C,PP.2013-2020,2000.

Motta L. O. , Guilherme D. M., Roberta M.L.," Moisture Equilibrium Isotherms for A Handmade Kraft Paper ", IDS, V.B, PP.1241-1248, 2004.

Motta L. O., Carlos E.S., Nehemias C.," Moisture Equilibrium Isotherms for Pinnus Long Fiber Cellulose", Acta Scientiurum Tech., No.1,V.26, PP.27-32,2004.

Rahman m. s., Shyams S.S., Labuza T.P.," Measurement of Water Activity Using Isopiestic Method, "Current Protocols in Food Analytical Chemistry, 2000 Rouquerol F., Rouquerrol J., Sing K.," Adsorption by Powders and Porous Solids", Academic Press , London ,1999.

Susan K., Donald C. P.," Aspirin", http://elephant cares org., 2003

Shyam S. S., Rahman P. L. ,Theodol P. L.," Measurement of Water Activity using Isopiestic Method ", Food Analytical Chemistry ,A 2.3.1.-A 2.3.10,2001.

Thommes M., Kohn R., Froba M.," Sorption and Pore Condensation Behavior of Pure Fluids", Appl. Surface Sci. 196, PP.239-249, 2002.

Sumie Y.,Valeatimo J.," Stability of Drugs and Dosages Forms",2008.

Wolf W. , Spiess W. E., Jung G.," Standardization of Isotherm Measurement", (COST-90 and 90 BIS), Properties of Water in Foods, PP.661-678 , 1985.

Yanxia L., Yeshwaut D., Sanzgiri Y.C.,"A Study on Moisture Sorption Isotherms of Formulations" , AAPS Pharm. Sci. Tech. , 4(4), 59, 2003.
Yihong Q., Yisheng C., Liroug L.,Geoff G.," Developing Solid Oral Dosage Form: Pharmaceutical Theory and Practice ,Academic Press.,2009.

Design of a Differential Chaotic on-off keying communication system

Dr. Hikmat Najem Abdullah
Assistant Professor
Al-Mustansiryah University
Electrical Engineering Department
E-mail: hikmat_04@yahoo.com

ABSTRACT

Among the available chaotic modulation schemes, differential chaos shift keying (DSCK) offers the perfect noise performance. The power consumption of DCSK is high since it sends chaotic signal in both of 1 and 0 transmission, so it does not represent the optimal choice for some applications like indoor wireless sensing where power consumption is a critical issue. In this paper a novel noncoherent chaotic communication scheme called differential chaos on-off keying (DCOOK) is proposed as a solution of this problem. With the proposed scheme, the DCOOK signal have a structure similar to chaos on-off keying (COOK) scheme with improved performance in noisy and multipath channels by introducing the concept of differential coherency used in DCSK. The simulation results show that the proposed scheme have achieved more than 3 dB gain in signal-to-noise ratio for AWGN and Rayleigh multipath fading channels at BER=10^{-3} over COOK scheme.

Keywords: chaotic communication; noncoherent; modulation; chaos on-off keying; differential chaos keying

تصميم منظومة اتصالات فوضوية ذات قدح ارتفاع تفاضلي

د. حكمت نجم عبدالله
أستاذ مساعد
الجامعه المستنصريه- قسم هندسة الكهرباء

تعد طريقة تضمين قدح التزحيف التفاضلي الفوضوي (DCSK) ذات اداء ممتاز في الاوساط الضوضائية مقارنة بطرق التضمين الاخرى المستخدمة في الاتصالات الفوضوية. ان الطريقة المذكورة آنفا تستهلك قدرة ارسال عالية كونها ترسل اشارة فوضوية في كلتا حالتي قيمة البيانات 0 و 1 لذلك فهي لا تمثل الخيار الامثل لبعض التطبيقات مثل منظومات التحسس ذات الارسال اللاسلكي داخل الابنية والتي يكون فيها موضوع استهلاك القدرة قضية حساسة. في هذا البحث تم اقتراح طريقة تضمين لاتشاكهية فوضوية تم تسميتها طريقة قدح الارتفاع التفاضلي (DCOOK) لحل هذه المشكلة. إن الطريقة المقترحة ذو تركيب مادي مشابه لطريقة قدح الارتفاع (COOK) الا انها تمتلك اداء محسن في القنوات الضوضائية وقنوات الخفوت وذلك من خلال استخدام مفهوم التفاضل التشاكهي المستخدم في طريقة DCSK. ولقد اوضحت نتائج المحاكاة ان الطريقة المقترحة حققت ربحا يزيد عن 3 dB في نسبة الاشارة الى الضوضاء مقارنة بطريقة COOK عند اختبارها في قناة الضوضاء نوع AWGN وقناة الخفوت نوع Rayleigh عند قيمة معدل خطأ المعلومة الثنائية (BER) مساوي لـ 10^{-3}.

الكلمات الرئيسية: الاتصالات الفوضوية ، لاتشاكهي ، تضمين ، قدح الارتفاع الفوضوي ، القدح التفاضلي الفوضوي

INTRODUCTION

Chaos communications has been an active research area in the last few years. Chaotic signals possess some unique properties such as pseudorandomness, noise-like wide bandwidth and long term unpredictability. They satisfy special requirements of some communication systems. It makes chaos attractive to wideband and security communications (M. Xu and Henry Leung 2010).

At present, the studying of the chaos systems mainly focuses on chaotic digital communications which include chaos digital keying modulation like chaos shift keying (CSK)(H. Dedieu, M. P. Kennedy and M. Hasler 1993), chaotic on-off keying (COOK)(G. Kolumbàn, M. P. Kennedy and G. Kis 1997), differential chaos shift keying (DCSK)(G. Kolumbàn, G. K. Vizvari and W. Schwarz 1996), correlation delay shift keying(CDSK)(M. Sushchik, L. S. Tsimring and A. R. Volkovskii 2000), etc. Because of the sensitivity to initial conditions, it is difficult that chaotic signals realize reliably synchronization in both two sides of transmitter and receiver. Therefore, noncoherent chaos communication systems which don't need chaos-synchronization are the most preferred ones. Among several noncoherent systems proposed, one of the best bit-error rate (BER) performances has been achieved by the DCSK and its variation utilizing frequency modulation, FM-DCSK (G. Kolumbán, G. Kis, Z. Jákó, and M. P. Kennedy 1998).

In DCSK scheme, a reference chaotic waveform c(t) is transmitted during the first half of each data bit. If the bit is a "1", c(t) is transmitted again during the second half. If the bit is a "0", -c(t) is transmitted. Modified versions of DCSK like quadrature chaos shift keying (QCSK)(Z. Galias, and G. M. Maggio 2001), quadrature amplitude chaos shift keying (QACSK)(J. Pan and H. Zhang 2009) and quadrature differential chaotic phase shift keying (QDCPSK)(S. Zhu, Yinlin Xu and Kuixi Yin 2009) were proposed to improve the band usage and transmission speed. In COOK, the chaotic signal is multiplied directly by the bit sequence to be transmitted, i.e. radiation of a chaotic signal is disabled for data bit "0" and enabled for data bit "1".

Although the performance of COOK chaotic modulation lags behind the DCSK, the COOK have an advantage of that it consumes less power since it sends chaotic signal only in case of sending the data bit "1" while no power is sent for case of data bit "0". In this paper, a novel scheme that combines the features of DSCK and COOK, i.e. good BER performance with less power consumption has been proposed. The proposed system is called Differential Chaotic On-Off Keying (DCOOK). The rest of the paper is organized as fellows: In the next section the proposed modulation scheme is introduced. Then, the performance of the proposed scheme is analyzed and compared with some existing schemes. Finally, some conclusions drawn from the work are given at the end of the paper.

DIFFERENTIAL CHAOTIC ON-OFF KEYING (DCOOK) SCHEME

Fig.1 shows the structure of the proposed DCOOK system. At the transmitter, when the data bit is "1" a reference chaotic waveform c(t) is transmitted during the first half of data bit duration T, while a delayed version of c(t) by T/2 is transmitted during the second half (like DCSK). If the bit is a "0", the transmission is disabled (like COOK). Therefore, signal transmitted by DCOOK can be expressed in a symbol period T as:

$$S_{DCOOK}(t) = \begin{cases} \sqrt{E_b}\,c(t) & when\ d(t)=1\ and\ 0 \le t < \dfrac{T}{2} \\ \sqrt{E_b}\,c\left(t-\dfrac{T}{2}\right) & when\ d(t)=1\ and\ \dfrac{T}{2} \le t < T \\ 0 & when\ d(t)=0 \end{cases} \quad (1)$$

where d(t) is the transmitted data and E_b is the energy per bit. To get maximum noise performance E_b should have constant value which is possible by applying the chaotic signal to a frequency modulator[6]. At the receiver, the signal is delayed by half a bit period and correlated with the undelayed signal to get the decision variable for producing the output data stream. **Fig.2** shows the signal structure of DCOOK scheme as compared with DCSK and COOK schemes where C_i represents the chaotic signal part (a set of chaotic symbols) corresponds to ith half a bit to be transmitted (chip). It can be seen in this figure that both the principles of differential representation used in DCSK and the on-off representation used in COOK are combined together and depending on the data bit value.

The major advantage of DCOOK scheme as compared with COOK is that it increases the signal space of the decision variable, i.e. increases the separation between the amplitude levels upon which the data is declared to be "0" or "1" after threshold comparison. This can be explained as fellows: In traditional COOK scheme, the detection operation includes performing correlation between the received signal and itself along the data bit duration. This means the received noise in case of "0" transmission would be correlated with itself (i.e. with exactly the same replica) which will produce a nonzero correlation result with always positive value which increases as SNR increases. While in the proposed DCOOK scheme, the detection operation includes performing correlation between the received signal and a delayed version of it along half

data bit duration. This means the received noise in case of "0" transmission would be correlated with another noise replica which will produce a correlation result might be positive (lower than that of COOK case) or negative or zero value with almost independency on SNR value. The relation between the correlation results in both cases can be understood mathematically by the following inequality:

$$\int_0^T n^2(t)dt > \int_0^{T/2} n(t)n(t-\frac{T}{2})dt \qquad (2)$$

where n(t) is the received AWGN noise. The correlation result in case of "0" transmission for DCOOK scheme; the right hand of eq.2, is less than the corresponding correlation result for COOK; the left hand of eq.2. This is because the some point-to-point multiplication results of noise samples in DCOOK case have negative values which are not the case of COOK scheme. Given that the correlation between the received signal plus noise results in always high positive results in both schemes, the signal space of the decision variable is increased in DCOOK scheme which as a result would improve the noise performance. It is worth noted that the number of chaos symbol per data symbol should be large enough to ensure good noise performance. In DCSK the signal space of the decision variable is bigger than that of DCOOK and the sign is used for decision purpose with zero threshold value independent on noise level. However, the advantage of DCOOK over DCSK is the less power consumption in the transmission side.

SIMULATION RESULTS

A simulation model has been implemented for DCOOK system, as well as COOK and DCSK for performance comparison purpose. Hennon mapping given by:

$$x_{n+1} = 1 + bx_n + ax_n^2 \qquad (3)$$

where a and b are constants and a=-1.4 and b=0.3 is used to generate the chaotic signal. The values of a and b are selected such that the chaotic signal have good randomness properties (C. Y. Li, J. S. Chen, and T. Y. Chang 2006). According to the article by (M. A. B. Faran, A. Kachouri and M. Samet 2006), we define the chip rate equals 0.05 μs and T=4 μsec. **Fig.3** shows the integrator outputs for DCOOK as compared with COOK and DCSK systems in relation to the transmitted data values

at E_b/N_o=6 dB. It can seen in this figure that the integrator output at decision points for d(t)=0 in DCOOK system is changing between low positive and negative values while it is always positive in COOK system (its amplitude depend on signal-to-noise ratio value). Hence the signal space of the decision variable is increased in DCOOK system as compared with COOK system (but less than DCSK system) and a successful decision about data value can be achieved with a little positive threshold.

Fig.4 shows a very important feature in DCOOK system which is the threshold level is almost constant and has very little dependency on signal-to-noise ratio change. Oppositely, the optimum threshold in COOK system is very sensitive to the signal-to-noise ratio change. The DCSK detector has constant threshold value which is zero due to bipolar nature of integrator results as explained in the previous section. **Fig.5** shows the performance of DCOOK as compared with COOK and DCSK in AWGN channel. It is clear in the figure that the noise performance of the proposed DCOOK is superior as compared with COOK for all signal-to-noise ratio values. At P_e=10^{-3}, a 3.6 dB gain in signal-to-noise ratio has been obtained. However, this performance lags behind DCSK system by less than 2 dB at the significant BER values. **Fig.6** shows the corresponding performance in Rayleigh fading channel. In this case we used in our simulations two paths; the second path delay was 75 ns with attenuation of -3 dB which simulates the multipath environment inside office buildings. Here the performance of DCOOK is once again better than COOK for all signal-to-noise ratio values. At P_e=10^{-3}, a 3 dB gain in signal-to-noise ratio has been obtained. This performance lags behind DCSK system by about 1.5 dB at the significant BER values.

CONCLUSIONS

The proposed DCOOK scheme represents a model of chaotic modulation scheme with which the compromise between the noise performance and power consumption can be achieved. The proposed scheme increases the signal space of the decision variable by using the concept of differential correlation instead of self correlation. The optimum threshold value of the proposed scheme detector is found to be almost constant and independent on signal-to-noise ratio value.

ACKNOWLEDGEMENTS

REFERENCES

C. Y. Li, J. S. Chen, and T. Y. Chang, "Chaos based pseudo random number generator using timing-based reseeding method", IEEE proceedings of ISCAS, pp. 21-24, 2006

G. Kolumbán, G. Kis, Z. Jákó, and M. P. Kennedy, "FM-DCSK: A Robust Modulation Scheme for Chaotic Communications," IEICE Transactions on the Fundamentals, vol. E81-A, October 1998, pp. 1798–1802.

G. Kolumbàn, G. K. Vizvari and W. Schwarz, "Differential chaos shift keying: a robust coding for chaos communication," Proceedings of International Workshop on Nonlinear Dynamics of Electronic Systems, 1996, pp. 92-97.

G. Kolumbàn, M. P. Kennedy and G. Kis, "Performance improvement of chaotic communications systems," Proceedings of European Conference on Circuit Theory and Design, 1997, pp. 84-89.

H. Dedieu, M. P. Kennedy and M. Hasler, "Chaos shift keying: modulation and demodulation of a chaotic carrier using self-synchronizing Chua's circuits," IEEE Transactions on Circuits and Systems II, Vol. 40, No.10, 1993, pp. 634-643.

J. Pan and H. Zhang, "Design of FM-QACSK Chaotic Communication System", International Conference on Wireless Communications and Signal Processing, Nanjing, 13-15 November 2009, pp.1184-1187.

M. A. B. Faran, A. Kachouri and M. Samet, "Design of Secure Digital Communication Systems using DCSK Chaotic Modulation," DTIS 2006 International Conference on Design and Test of Integrated Systems in Nanoscale Technology, Tunis, 5-7 September 2006, pp. 200-204.

M. Sushchik, L. S. Tsimring and A. R. Volkovskii, "Performance Analysis of Correlation-Based Communication Schemes Utilizing Chaos," IEEE Transactions on Circuits and Systems I, Vol. 47, No.12, 2000, pp. 1684-1691.

M. Xu and Henry Leung, "A Novel high data rate modulationscheme based on chaotic signal seperation," IEEE Transactions on Communications, Vol. 58, No. 10, October 2010, pp. 2855-2860.

S. Zhu, Yinlin Xu and Kuixi Yin, "Design of a Quadrature Differential Chaotic Phase Shift Keying Communication System, " International Conference on Networks security, Wireless Communications and Trusted Computings, 2009, pp. 518-521.

Z. Galias, and G. M. Maggio, "Quadrature chaos-shift keying: theory and performance analysis," IEEE Transactions on Circuit and Systems. I, Vol.48, No.12, December 2001, pp.1510-1518.

LIST OF SYMBOLS

AWGN: Additive White Gaussian Noise
a: constant used in Hennon mapping
b: constant used in Hennon mapping
BER: Bit Error Rate
$c(t)$: chaotic waveform
C_i: set of chaotic symbols
CDSK: Correlation Delay Shift Keying
COOK: Chaotic On-Off Keying
CSK: Chaos Shift Keying
DCOOK: Differential Chaos On-Off Keying
DCSK: Differential Chaos Shift Keying
$d(t)$: transmitted data
E_b: energy per bit
FM-DCSK: Frequency Modulated DCSK
QCSK: Quadrature Chaos Shift Keying
QACSK: Quadrature Amplitude Chaos Shift Keying
$n(t)$: noise signal
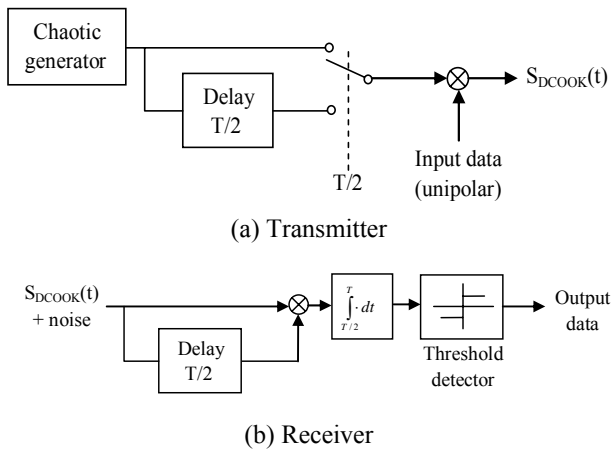T: bit duration
x_n: nth Hennon-mapped chaotic symbol

(a) Transmitter

(b) Receiver

Fig.1 Block diagram of the DCOOK system
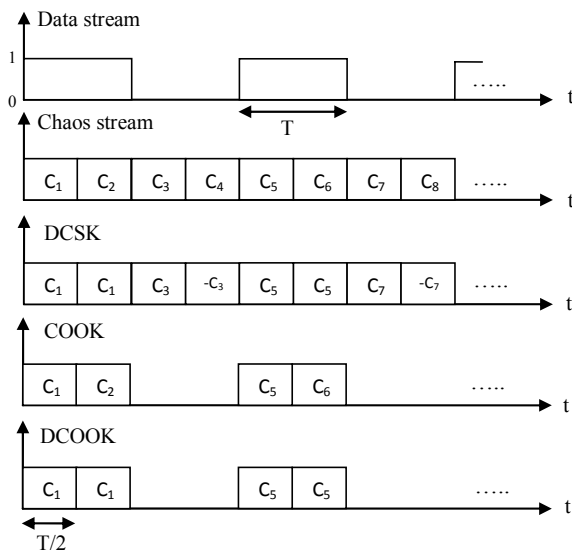

Fig.2 Signal structure of DCOOK scheme as compared with COOK and DCSK schemes.
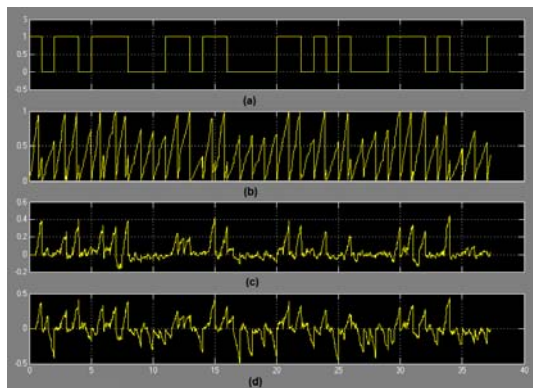

Fig.3 (a) Transmitted data
    (b) COOK integrator output
    (c) DCOOK integrator output
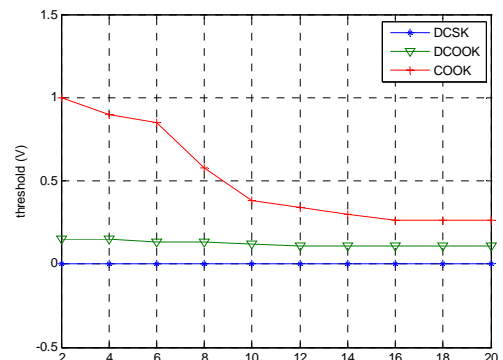   **(d) DCSK integrator output**

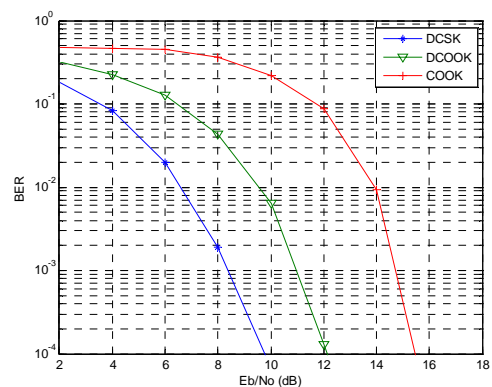**Fig.4 The sensitivity of optimum threshold to signal-to-noise ratio change in DCOOK as compared with COOK and DCSK.**
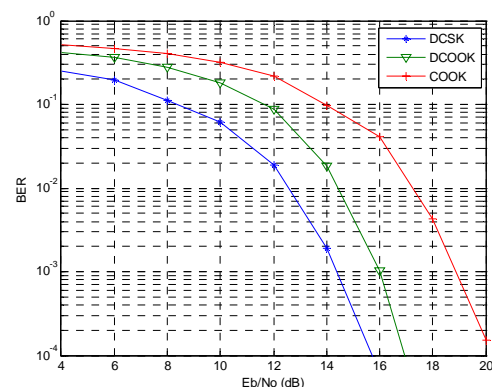

Fig.5 Performance of DCOOK as compared with COOK and DCSK in AWGN channel.

Fig.6 Performance of DCOOK as compared with COOK and DCSK in Rayleigh fading channel.

Multicomponent Biosorption of Heavy Metals Using Fluidized Bed of Algal Biomass

Abbas Hameed Sulaymon	**Ahmed Abed Mohammed**	**Tariq Jwad Al-Musawi**
Professor	Asst. Professor	Lecturer
Baghdad University/College of Eng.	Baghdad University/College of Eng.	Baghdad University/College of Eng.
Energy Engineering Dept.	Environmental Engineering Dept.	Environmental Engineering Dept.
inas_abbas@yahoo.com	ahmed.abedm@yahoo.com	tariqjwad@yahoo.com

ABSTRACT:

This paper aims to study the biosorption for removal of lead, cadmium, copper and arsenic ions using algae as a biosorbent. A series of experiments were carried out to obtain the breakthrough data in a fluidized bed reactor. The minimum fluidization velocities of beds were found to be 2.27 and 3.64 mm/s for mish sizes of 0.4-0.6 and 0.6-1 mm diameters, respectively. An ideal plug flow model has been adopted to characterize the fluidized bed reactor. This model has been solved numerically using MATLAB version 6.5. The results showed a well fitting with the experimental data. Different operating conditions were varied: static bed height, superficial velocity and particle diameter. The breakthrough curves were plotted for each metal. Pb^{2+} showed the largest breakthrough time compared with others, while Cd^{2+} had the lowest value.

Keywords: Algae; Heavy metals; Fluidized bed; Breakthrough curve.

/   /   /

:

.

3.64   2.27   .

.   1-0.6   0.6-0.4   /

.   .MATLAB

.

.

.   :

1.   INTRODUCTION

One of the most challenging environmental problems is the removal of heavy metals and other toxic contaminants from industrial wastewater. Many aquatic environments face metal concentrations that exceed water quality criteria designed to protect humans, environment, animals and (**Gin et al., 2002**). Metals can be distinguished from other toxic pollutants, since are non-biodegradable and can accumulate in the living tissues, thus becoming concentrated throughout the food chain (**Williams et al., 1998**). The metals hazardous to humans include lead, cadmium, mercury, arsenic, copper, zinc, and chromium. Arsenic and cadmium can cause cancer. Mercury can cause mutations and genetic damage, while copper, lead, chromium can cause brain and bone damage (**Wang and Chen, 2009**). Biosorption is an innovative technology that employs inactive and dead biomass for the removal and recovery of metals from aqueous solutions (**Romera et al., 2007; Cui and Grace, 2007**). Various biomasses such as bacteria (**Ridha, 2011**), sludge (**Ali, 2011**), yeast (**Sulaymon et al., 2010**), algae (**Kratochvil, 1997**), fungi (**Brady et al., 1999**) and plants (**Melcakova and Ruzovic, 2010**) have been used to adsorb metal ions from the environment. Among the most promising types of biosorbents studied are algal biomass (**Romera et al., 2006; Figueria et al., 2000**), algal biomass have been reported to have high metal binding capacities due to their containing of functional groups on the cell wall. These functional groups are carboxyl, hydroxyl and sulphate, which can act as binding sites for metals (**Crist et al., 1994**). The term algae refers to a large and diverse assemblage of organisms that contain chlorophyll and carry out oxygenic photosynthesis. Although most algae are microscopic in size and are thus considered to be microorganisms, several forms are macroscopic in morphology (**Davis et al., 2003**). The algae are included in the plant kingdom and are distinguished from other Chlorophyllous plants on the basis of sexual reproduction. There are seven divisions of algae, divisions which include the larger visible algae are: Cyanophyta (blue-green algae), Chlorophyta (green algae), Rhodphyta (red algae) and Phaeophyta (brown algae). These divisions are subdivided into orders, which are

subsequently divided into families and then into genus and species. Differences between these types of algae are mainly in the cell wall, where sorption takes place (**Romera et al., 2007**). The annual production of algae in the world lately reached to 5.9 million ton (**Sunduqgee, 2006**). Green and blue green algae in Iraq are available in huge quantities, approximately in all surface water resources and marshes (**Al-Hassany, 2003; Kassim, 2007**). Fixed and fluidized beds have been used widely by chemical industry, pharmaceutical industry, food industry, wastewater treatment and recovery of different substance (**Park et al., 1999**). Fluidized beds are common and important reactors in process engineering because of the good mass and heat transfer rate between the fluid and the particles, and between the particles and the side wall of the column (**Fu and Liu, 2007**). The term fluidization is used to describe the condition of fully suspended particles. Liquids or gases are passed at certain velocity up through a bed of solid particles, at this velocity the pressure drop across the bed counter balances the force of gravity on the particles and further increase in velocity achieve fluidization at a minimum fluidization velocity. Fluidization quality is closely related to the intrinsic properties of particles, e.g. particle density, particle size and size distribution, and also their surface characteristics (**Richardson, et al., 2002). Diniz et al., (2008**) studied the fixed bed biosorption of lanthanum (La^{3+}) and europium (Eu^{3+}) using protonated Sargassum polycystum biomass (brown algae). The sorption mechanism was based on the ion exchange mechanism. The experimental results were fitted with an ion exchange model, good matching and high regression coefficient were obtained. The calculated affinity constants were 2.7 and 4.7 for La^{3+} and Eu^{3+} respectively, demonstrating a higher affinity of biomass towards Eu^{3+}. Column experiments were carried out in fixed bed system to estimate the mass transfer coefficient for each metal. A series of consecutive sorption/desorption runs demonstrated that the two metals could be recovered. **Rathinam et al., (2010)** studied the batch **biosorption** of cadmium onto Hypnea valentiae biomass (red algae). The results showed that the biosorption capacity was low at pH 3.0, but increased considerably from 4.30 to 14.54 mg/g as

the pH solution increased to 5.0. On further increase in pH to 6.0 and 7.0 the biosorption capacity remained almost stable at 16.89 and 17.02 mg/g, respectively. **Wang et al., (2011)** studied the removal of emulsified oil from water by inverse fluidization of hydrophobic silica aerogels (Nanogel). The hydrodynamics characteristics of the Nanogel granules of different size ranges are studied by measuring the pressure drop and bed expansion as a function of superficial water velocity. The minimum fluidization velocity was measured experimentally by plotting the pressure drop against the superficial fluid velocity. The results showed that the major factors which affect the oil removal efficiency and capacity are the size of Nanogel granules, bed height, and fluid superficial velocity.. Also the experimental data showed that the Nanogel particles can absorb as much as 2.8 times their weight of oil by the inverse fluidization process.

From the previous literature related to the biosorption of heavy metal using algae, it can be concluded the following points:

- In recent years, there have been a significant increase in the studies concerning algae as biosorbents for removal of heavy metal due to their binding ability, availability and low cost.
- It was found that there is lack in literature of using algal biomass as a biosorbent in Iraq
- Several studies concluded that the biosorption mechanisms involving algae are an ion exchange reaction type between light metals already bound to the algae and other metals present in the aqueous solution. Also, the optimum pH for removal was around 3 to 5.

This work aims to study some parameters that influenced the behavior of liquid fluidized bed for removal of Pb^{2+}, Cd^{2+}, Cu^{2+} and As^{3+} from wastewater using algal biomass.

2.   FLUIDIZED BED MODELS

Breakthrough curves serve two purposes (a) to decide whether the adsorbate is efficient for the required separation and (b) to establish break point (process interpretation), based on some criterion, either technical, economic or legal (**Knaebel, 1999**).

In the fluidized bed, the aqueous solution with influent concentration flows from the bottom to the top. The variation of the pollutant concentration in the liquid phase with time at different bed lengths can be measured. In the present work, a fluidized bed reactor was adopted for the continuous removal of metal. **Fig.1** shows a model of fluidized bed reactor.

The first assumption considers that the concentration is uniform in the radial direction. Secondly, there is no material product in the reactor (no chemical reaction between the fluid and bed). Finally, the fluid stream is plug flow and mixed solid flow. Based on the above assumptions, the governing equation can be obtained from differential mass balance of the bulk-fluid phase. The following equations can also be derived from equations of continuity (**Park et al., 1999**):

$$\begin{pmatrix} \text{Rate of input conc. by} \\ \text{convective flow} \end{pmatrix} + \begin{pmatrix} \text{Rate of input conc. by} \\ \text{dispersion} \end{pmatrix} - \begin{pmatrix} \text{Rate of output conc. by} \\ \text{convective flow} \end{pmatrix} - \begin{pmatrix} \text{Rate of output conc. by} \\ \text{dispersion} \end{pmatrix} - \begin{pmatrix} \text{Solute lost by} \\ \text{sorption} \end{pmatrix} = \frac{\partial C}{\partial t}. \varepsilon. dz \quad (1)$$

Then:

$$\frac{U}{\varepsilon}.C + E_z.\frac{\partial C}{\partial z} - \frac{U}{\varepsilon}\left[C + \frac{\partial C}{\partial z}dz\right] - E_z.\left[\frac{\partial C}{\partial z} - \frac{\partial}{\partial z}\left(\frac{\partial C}{\partial z}\right)dz\right] - \frac{(1-\varepsilon)}{\varepsilon}\rho_p\frac{\partial q}{\partial t}dz = \frac{\partial C}{\partial t}.dz \quad (2)$$

Then, equation (2) can be written as follows:

$$\frac{U}{\varepsilon}.C + E_z.\frac{\partial C}{\partial z} - \frac{U}{\varepsilon}.C - \frac{U}{\varepsilon}.\frac{\partial C}{\partial z}dz - E_z.\frac{\partial C}{\partial z} + E_z.\frac{\partial^2 C}{\partial z^2}dz - \frac{(1-\varepsilon)}{\varepsilon}\rho_p\frac{\partial q}{\partial t}dz = \frac{\partial C}{\partial t}.dz \quad (3)$$

Simplified equation (3) to the following:

$$\frac{\partial C}{\partial t} = E_z\frac{\partial^2 C}{\partial z^2} - \frac{U}{\varepsilon}\frac{\partial C}{\partial z} - \frac{1-\varepsilon}{\varepsilon}\rho_p\frac{\partial q}{\partial t} \quad (4)$$

The mass balance for the solid phase is expressed as:

$$(1-\varepsilon)\rho_p \frac{\partial q}{\partial t} = K_L.a.(C-C^*) \qquad (5)$$

Substituting Eq.(5) into Eq.(4), the following equation can be obtained:

$$\frac{\partial C}{\partial t} = E_z \frac{\partial^2 C}{\partial z^2} - \frac{U}{\varepsilon}\frac{\partial C}{\partial z} - \frac{K_L.a}{\varepsilon}(C-C^*) \qquad (6)$$

The initial and boundary conditions are:

$$0 < z < L, t = 0; C = C^* = 0 \qquad (7)$$

$$z = 0, t \geq 0; C = C_i \qquad (8)$$

$$z = L, t > 0; \frac{\partial C}{\partial z} = 0 \qquad (9)$$

The partial differential equation (eq. 6) was solved numerically using Matlab software Version 6.5.

3. EXPERIMENTS AND MATERIALS
3.1 Biomass and Solutions Preparation
Mixture of green (Chlorophyta) and blue-green (Cyanophyta) algae were used in this study as the biosorbent of heavy metal. Large quantities of algae have been observed their spreading along the artificial irrigation canal in Baghdad University. This canal feed by water from the Tigris River. For this study, algae were collected from the selected location of this canal in April and September 2011. Approximately greater than 5 kg of fresh algae was collected at each month. Sample of 0.5 kg of collected algae at each month were analyses for their genus and species and percentage weight by using microscope. These analyses were achieved according to the standard methods (**APHA, 2005**) in laboratories of Iraqi Ministry of Sciences and Technology/ Water Treatment Directory. The results showed that there are five species were dominated in these two samples, Oscillatoria princeps alga was the highest percentage, these results were listed in **Table 1.**

The collected algae were washed several times with tap water and deionized water to remove impurities and salts. The algal biomass was sun-dried and then dried in oven at 50 °C for 48 h. The dried algal biomass was shredded, ground in a mortar and sieved. Average size of 0.4-0.6 and 0.6-1 mm particle diameters was used for biosorption experiments in system. he biomass particle size distribution was determined using a set of standard sieves. Since the algal biomass could swell in water, therefore the biomass was initially soaked in water and then wet sieved. Particles density, surface area and voidage were measured and listed in **Table 2.**

$Pb^{2+}, Cd^{2+}, Cu^{2+}$ and As^{3+} ions solutions were prepared by dissolving $Pb(NO_3)_2.2H_2O$, $Cd(NO_3)_2$, $Cu(NO_3)_2.3H_2O$ and As_2O_3 in distilled water. These solutions were kept at 25 °C. The pH was adjusted at 4 for all heavy metals solution using $0.1M$ HNO_3 and $0.1M$ NaOH solutions. A pH meter type WTW/ inoLab series was used for pH value reading. All chemicals used in this work were analytical reagent grade and were used without further purification. The solubility of $Pb(NO_3)_2.2H_2O$, $Cd(NO_3)_2$, $Cu(NO_3)_2.3H_2O$ and As_2O_3 in water are 54.3, 136, 125 and 1.8 g/100g H_2O, respectively.

3.2 Column Experiments
Fig.2 shows a schematic diagram of fluidized bed reactor used in the experiments. Experiments were carried out in a 7.5 cm inner diameter and 1 m high glass column, 0.5 mm stainless steel distributer was installed at the bottom of the reactor to distribute an influent flow smoothly. A U-tube manometer was connected to the reactor to read the pressure of water at each flow meter reading, the manometer has an inside diameter of 5 mm and length is 50 cm. The manometer liquid is Carbon Tetrachloride (CCl_4) with ρ_f=1590 kg/m³. The feed containing 50 ppm for each element was pumped upward through the column at selected velocities ($1.1U_{mf}$ and $1.5 U_{mf}$) for each particle size. The samples were taken from an effluent of the reactor at time intervals 1, 2, 5, 10, 20, 30, 40, 50, 60, 70, 80, 90 min. During the experiment, the pressure drop, and fluidized bed height were measured at the corresponding time intervals.

4. RESULTS AND DISCUSSION
4.1 Mechanisms of Heavy Metal Binding in Algae

Several studies concluded that the major biosorption mechanism involving algae is an ion exchange reaction type between cations (light metals: Ca^{2+}, Mg^{2+}, Na^{+} and K^{+}) already bound to the algae and other metals present in the aqueous solution (**Naja and Volesky, 2006**). **Fig.3** describes the progression of a molecule of adsorbate from the bulk towards the site of ion exchange on algae (**Hamm et al., 2002**). There are two major determining factors for exchange biosorption: the first one is the strength of the charge on the ions (electronegativity), the other is the size of the adsorbate (atomic radius of metal ion). **Table 3** shows the atomic properties of Pb^{2+}, Cd^{2+}, Cu^{2+} and As^{3+} ions (**Wikipedia, 2012**). Algal biomass generally contains alkali and alkaline earth metals such as K^{+}, Na^{+}, Ca^{2+} and Mg^{2+} which are originally presented from fresh water. So that, when algal biomass reacts with the heavy metals bearing solution, the light metals released causing an increase in the pH of solution due to form of light metal alkalis. In addition, the release of these light metals caused the increase of electrical conductivity value (EC).

To find the pH and electrical conductivity variation along the biosorption process, four flasks of 250 ml were filled with 100 ml at pH value=4 of four metal solution (50 ppm) and 1 g of dried algae. The flasks were then placed on a shaker and agitated continuously for 4 h at 200 rpm. The pH and EC were measured at different time intervals during the agitation process. **Fig. 4 and 5** show the increase in the pH and electrical conductivity values with time. In this case, the cations of light metals were being eluted from the algal biomass during the experiments, while the heavy metals were being sorbed onto the biomass. **Fig.6** shows the amount of light metals released due to biosorption of these heavy metals onto algal biomass.

4.2 Minimum Fluidization Velocity

The minimum fluidization velocity (U_{mf}) was determined experimentally by measuring the pressure drop through the bed of algal particles. Two particle sizes were used in this study ranging from 0.4-0.6 mm and 0.6-1 mm diameter. The column was partially filled with particles of known mass and then vigorously agitated with water in order to arrange particles and break down any internal structure. After that the bed left to settle down, and then the flow rate increased incrementally from 0 to 100 l/h using a rotameter. At each flow rate increment, the pressure drop was recorded using manometer. **Fig.7** shows the pressure drops across the bed against the superficial fluid velocity in logarithmic scale. The graph is used to read the minimum fluidization velocity (U_{mf}), as well as to show the pressure drop rises linearly below minimum fluidization in the packed bed region and then plateaus above minimum fluidization. The U_{mf} can be read from the sharp change in the pressure drop over the fixed bed region. **Table 4** shows the minimum fluidization velocity, plateau pressure drop (ΔP) and fluidized bed height (h_{mf}) of two different size particles that used in biosorption process.

4.3 Bed Expansion

It is important to be able to establish the relationship between the superficial liquid velocity (U) and the bed voidage (ε) (**Ngian and Martin, 1980**).
The bed voidage can be found experimentally by subtracting the volume of the particles (V_p) from the total volume of the fluidized bed (V_b). Hence, the voidage of the fluidized bed is:

$$\varepsilon = \frac{V_{\varepsilon}}{V_b} = \frac{V_b - V_p}{V_b} = 1 - \frac{V_p}{V_b} = 1 - \frac{m_p}{\rho_p V_b} = 1 - \frac{m_p}{\rho_p . A . H} \quad (10)$$

where V is void volume, m_p is the mass of particles (kg), A is the cross sectional area of the bed (m^2), H is the bed height (m).

4.4 Mass Transfer Coefficient

Several authors proposed generalized correlation to predict the mass transfer coefficient. **Park et al., (1999)** concluded the following correlation obtained from experimental data of fluidized bed reactor:

$$\frac{Sh.\varepsilon^{0.5}}{Sc^{1/3}} = 0.62 \, Re_p + 0.6 \quad (11)$$

The diffusivity of each metal can be calculated from the following equation:

$$D_m = 2.74 * 10^{-9}(M_w)^{-1/3} \quad \ldots\ldots (12)$$

where M_w is the molecular weight of metal.

The calculated mass transfer coefficient values at fluid velocity $1.1U_{mf}$ were $2.975*10^{-5}$, $4.53*10^{-5}$, $4.02*10^{-5}$, and $4.887*10^{-5}$ m/s for Pb^{2+}, Cd^{2+}, Cu^{2+} and As^{3+} respectively. In case of fluid velocity equal to $1.5U_{mf}$, values of mass transfer coefficient were $4.86*10^{-5}$, $5.506*10^{-5}$, $5.31*10^{-5}$ and $5.887*10^{-5}$ mm/s respectively.

4.5 Breakthrough Curves

The breakthrough curves for each metal are obtained by plotting C/C_o versus time for Pb^{2+}, Cd^{2+}, Cu^{2+} and As^{3+} respectively. The experimental and predicted breakthrough curves are presented in **Figures (8 to 11)** at different operating conditions. The shape and sharpness of the breakthrough curve for a given adsorbent mainly depend on such factors: equilibrium adsorption isotherm, mass transfer rate, and hydrodynamic factors (such as bed height and contact time) (**Wang et al., 2011**). Different operating conditions were carried out, i.e., changing static bed height, fluid superficial velocity and particle diameter. The biosorption experiments were operated for each metal at static bed heights corresponded to the 50, 100 and 150 g for each particle (sizes 0.4-0.6 and 0.6-1 mm). The fluidizing velocities used in adsorption tests were equal to $1.1U_{mf}$ and $1.5U_{mf}$ mm/s.

The effect of varying the bed height of algal biomass on the biosorption process was investigated in **Fig. 8** for $U=1.1U_{mf}$, $C_o=50$ ppm, $d_p=0.4-0.6$ mm and bed weight 50, 100 and 150 g (corresponding to static bed heights 2.5, 5 and 7.5 cm). It can be seen in these Figures with increasing the weight of particles biomass the time at which an effluent concentration reached equilibrium increased, this is due to large contact time occurred between metal solution and particles at high bed height, smaller bed heights will be saturated in less time. Also, an increase in the bed depth will increase the surface area or adsorption site which improves the adsorption process.

The fluid velocity is a major parameter in the design of adsorption column due to its effect on the contact time between the particles and metal solution. **Fig. 9** shows the breakthrough curves that obtained for different fluid velocity ($U=1.1U_{mf}$, $U=1.5U_{mf}$) at bed height=7.5 cm and $C_o=50$ ppm are presented in. It can be seen that steeper curves occurred for all metals i.e increasing fluid velocity the breakthrough point appeared earlier, this is due to high fluid velocity of the metal in the solution leaves the bed before equilibrium occurs due to the reduction in the contact time. As well as, at low flow rate the metal molecules will have a sufficient contact time to occupy the spaces within the particles. The effect of particle diameter was investigated for four metal solutions at constant flow rate and bed height. **Fig. 10** shows the breakthrough curves at different particle sizes of 0.5 and 0.8 mm. It can be seen that an increase in particle size causes a decrease of the breakthrough time and makes the breakthrough curves much steeper, which would be anticipated with the decreasing the surface locations of ion exchange between the metals and particles.

In addition, the biosorption of each metal was investigated in quaternary system to find the effect of one metal ion on the other. **Fig. 11** shows the experimental and predicted breakthrough curves for the quaternary system. Comparison among the four metals shows that the time for reaching breakpoint ($C/C_o=0.1$) was 12, 10, 6 and 3 min. for Pb^{2+}, As^{3+}, Cu^{2+}, and Cd^{2+} respectively. This is due to higher affinity of algal biomass toward this metal for Pb than others. Also, due to competition effect occurs the weakest pollutant had a much steeper trend in its breakthrough curves. Additionally, It can be concluded that the adsorption capacity order for the quaternary system onto algal biomass are: Pb>As>Cu>Cd. Pb^{2+} demonstrated higher biosorption compared with others, this can be attributed to high electronagativty of this metal ion.

5. CONCLUSION

The present study evaluated the removal of Pb^{2+}, Cd^{2+}, Cu^{2+} and As^{3+} from wastewater using algal biomass as adsorbent material in fluidized bed reactor. The breakthrough curves were plotted for

each metal, Pb^{2+} showed the largest breakthrough time compared with others, while the Cd^{2+} had the lowest value. This can be attributed to the largest electronegativity value compared with others.

In fluidized bed system, an increase in the bed depth of algal biomass will increase the breakthrough time. An increase in the bed depth will increase surface area of adsorption. Increasing the solution flow rate decreased the breakthrough time due to the decrease in the contact time between the adsorbate and the adsorbent, as well as, at low flow rate the metal ions will have a sufficient contact time to occupy the spaces within the particles. Also, it was found that an increase in particle size caused a decrease of the breakpoint time due to surface area of large particles is lower than small particles.

ACKNOWLEDGMENT

REFERENCES

Al-Hassany, J.S., 2003, "A Study of the Ecology and Diversity of Epiphytic Algae on Some Aquatic Plants in Al-Hawizah Marshes, Southern Iraq", M.Sc. Dissertation, College of Science for Women, University of Baghdad.

APHA (American Public Health Association), 2005. Standard Method for the Examination of Water and Wastwater. 21st. ed. American Public Health Association.

Ali, A.H., 2011, "Performance of Adsorption/ Biosorption for Removal of Organic and Inorganic Pollutants", Ph.D. Thesis, University of Baghdad, College of Engineering.

Brady, J.M., Tobin, J.M., Roux. J., 1999. Continuous fixed bed biosorption of Cu^{2+} ions: application of a simple two parameters

mathematical model. Chem. Tech. and Biotech., 74, 71-77.

Crist, R.H., Martin, J.R., Carr, D., Waston, J.R., Clarke, H.J., Crist, D.R., 1994. Interaction of metals and protons with algae. Environ. Sci. Technol. 28, 1859-1866.

Cui, H., Grace, J.R., 2007. Fluidization of biomass particles: A review of experimental multiphase flow aspects, Chemical. Eng. Sci 62,45-55.

Davis, A., Volesky, B., Mucci, A., 2003. A review of the biochemisty of heavy metals biosorption by brown algae. Water Research 37, 4311-4330.

Diniz, V., Weber, M.E., Volesky, B., Naja, G., 2008. Column biosorption of lanthanum and europium by sargassum. Water Research 47, 363-371.

Figueria, M.M., Volesky, B., Ciminelli, V.S.T., Roddlick, F.A., 2000. Biosorption of metals in brown seaweed biomass. Water Research 34, 196-204.

Fu, Y., Liu, D., 2007. Novel experimental phenomena of fine-particle fluidized bed. Experimental Thermal and Fluid Science 32, 341-344.

Gin, K.Y., Tang, Y., Aziz, M.A., 2002. Derivation and Application of a new Model for Heavy Metal Biosorption by Algae. Water Research 36, 1313-1323.

Hamm, L.L., Hang, T., McCab, D.J., King, W.D., "Preliminary ion exchange modelling for removal of cesium from Hanford waste using hydrous crystalline silicotitanate material", Westinghouse Savannah River Company: WSRC-TR-2001-00400. pdf internet source, 2002, 17 May 2012, <http://sti.srs.gov/fulltext/tr2001400/t r2001400.pdf>.

Kassim, T., "The phytoplankton in Iraqi aquatic habitats", pdf internet source, 2007, 15 May 2012. <http://www.estis.net/includes/file.asp ?site=envmissan&file=23DD79EE-6DDD-45F4-8A4E-DB77E591 BA75>.

Knaebel, K., 1999. The basic of adsorber design. Chemical Engineering. 92-101.

Kratochvil, D., 1997. A study of the Metal Biosorption Process Utilizing Sargassum Seaweed Biomass, Ph.D Thesis, McGill University, Department of Chemical Engineering.

Melcakova, I., Ruzovic, T., 2010, "Biosorption of Zink from Aqueous Solution Using Algae and Plant Biomass", Nova Biotechnologica, 10(1), 33-43.

Naja, G., Volesky, B., 2006. Behavior of mass transfer zone in a biosorption column. Environ. Sci. Technol. 40(12), 3996-4003.

Ngian, K.F., Martin, W.R., 1980. Bed expansion characteristics of liquid fluidized particles with attached microbial growth, Biotechnol. and Bioeng. 22, 1843-1856.

Park, Y.G., Cho, S.Y., Kim, S.J., Lee, G.B., 1999 Kim B.H., Park S.J., Mass transfer in semi-fluidized and fluidized ion-exchange beds. Envi. Eng. Res 4(2), 71-80.

Rathinam, A., Maharshi, B, Janardhanan, S.K, Jonnalagadda, R.R, Nair, B.U., 2010, "Biosorption of cadmium metal ion from simulated wastewaters using Hypnea valentiae biomass: A kinetic and thermodynamic study", Biores. Technol., 101, 1466–1470.

Richardson, J.F., Harker, J.H., Bachurst, J.R., 2002," Coulson and Richardson's CHEMICAL ENGINEERING, Particle Technology and Separation Processes", Vol.(2), 5th Edition, Butterworth-Heinemann.

Ridha, M.J., 2011, "Competitive Biosorption of Heavy Metals Using Expanded Granular Sludge Bed Reactor", Ph.D. Thesis, University of Baghdad, College of Engineering.

Romera, E., Gonzalez, F., Ballester, A., Blazquez, M.J., 2006. Biosorption with algae: statistical review. Crit. Rev. Biotechnol. 26, 223-235.

Romera, E., Gonzalez, F., Ballester, A., Blazquez, M.J., 2007. Comparative study of heavy metals using different types of algae. Bioresource Tech. 98, 3344-3353.

Sulaymon, A.H., Ebrahim, S.E., Abdullah, S.M., Al-Musawi, T., 2010. Removal of Lead, Cadmium, and Mercury Ions Using Biosorption. Desalination and Water Treatment 24,344-352.

Sunduqgee, R.H., "Marine algae", Asharq Al-Awsat newspaper. No: 9977, 23 March 2006. <http://www.numumultimedia.com/por tfolio/asharq-al-awsat-website/>.

Wang, J., Chen, C., 2009, "Biosorbents for heavy metals removal and their future", Biotechnol. Advances, 27, 195-226.

Wang, D., McLaughlin, E., Pfeffer, R., Lin, Y.S., 2011. Aqueous phase adsorption of toluene in a packed and fluidized bed of hydropholic aerogels. Chemical Engineering168, 1201-1208.

Wikipedia, "The Free Encyclopedia", Internet Resource, 4 June 2012 <http://en.wikipedia.org/wiki/periodic_table#>.

Williams, C.J., Aderhol, D., Edyvean, R.G.J., 1998. Comparison between biosorbents for the removal of metal ions from aqueous solutions. Water Research 32, 216-224.

NOMENCLATURE

a	Specific surface area (m^2/m^3)	m_p	Mass of particles (g)
A	Cross sectional area of the bed (m^2)	Mw	Molecular weight (g/mole)
C_i	Initial heavy metal conc. (mg/l)	ΔP	Pressure drop in fluidized bed (pa)
C^*	Equilibrium heavy metal conc. (mg/l)	q_M	Adsorption amount of metal ions (mg/kg)
C	Conc. of heavy metal at any time (mg/l)	Sc	Schmidt number , $\mu/\rho.D$
d_p	Particle diameter (mm)	Sh	Sherwood number, $K_L.d/D$
D_m	Diffusivity coefficient (mm^2/s)	t	Time (min)
H	Bed height (cm)	U	Superficial velocity (mm/s)
h_{mf}	Fluidized bed height (cm)	U_{mf}	Minimum fluidization velocity (mm/s)
L	Total bed height (cm)	V	Volume of solution (l)
		z	Bed height (cm)

GREEK SYMBOLS

ρ_L	Density of liquid (kg/m^3)	μ_L	Viscosity of liquid (kg/m.s)
ρ_P	Real density of particles (kg/m^3)	ε	Bed voidage

Table 1. Division, genus, species and weighting percentage of collected algae

Division	Genus and Species	Percentage	
		June 2011	September 2011
Cyanophyta	Oscillatoria princeps	88 %	91 %
Chlorophyta	Spirogyra aequinoctialis	5 %	3 %
Cyanophyta	Oscillatoria subbrevis	2 %	2 %
Cyanophyta	Oscillatoria formosa	3 %	1 %
Chlorophyta	Mougeta sp	1 %	2 %
others	---	1 %	1 %

Table 2. Particles properties of algal biomass

Particle diameter (mm)	0.4-0.6	0.6-1
Bulk density (kg/m^3)	474	400
Real density (kg/m^3)	1120	1120
Surface area (m^2/g)	1.88	1.65
Particle porosity (--)	0.713	0.77
Bed Voidage ε(--)	0.577	0.642

Table 3. The atomic properties of Pb^{2+}, Cd^{2+}, Cu^{2+} and As^{3+} ions (Wikipedia, 2012)

Metal	Atomic Radius (pm)[*]	Electronegativity (Pauling scale)[**]
Pb^{2+}	175	2.33
Cd^{2+}	151	1.69
Cu^{2+}	128	1.9
As^{3+}	119	2.18
Sequence	Pb>Cd>Cu>As	Pb>As>Cu>Cd

[*] pico meter $=10^{-12}$ m.

[**] Pauling Scale: A dimensionless quantity, on a relative scale running from around 0.7 to 3.98 (Hydrogen was chosen as the reference, its electronegativity was fixed first at 2.1, later revised to 2.20).

Table 4. U_{mf}, ΔP and h_{mf} of two different size particles

Particle size (mm)	Mass (g)	Static height (cm)	U_{mf} (mm/s)	ΔP (pa)	h_{mf} (cm)
0.4-0.6	50	2.5	2.27	56.3	5
	100	5	2.27	80.1	10
	150	7.5	2.27	112	15
0.6-1	50	3	3.64	66.1	6
	100	6	3.64	103.3	12
	150	9	3.64	124.8	18

Fig.1 A model of a fluidized bed reactor (Park et al., 1999)

A: Metal solution tank   B: Pump
C: Flow meter   D: Distributer
E: Column reactor   F: Manometer

Fig.2 Schematic diagram of fluidization experimental setup
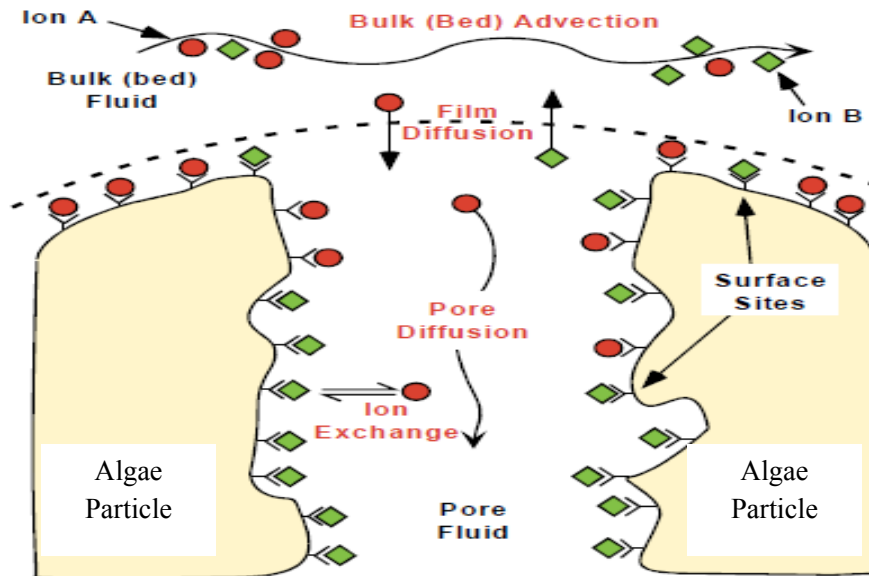
Fig. 3 Graphical representation of various mass transport mechanisms due to ion exchange between A and B ions in algae (Hamm et al., 2002)
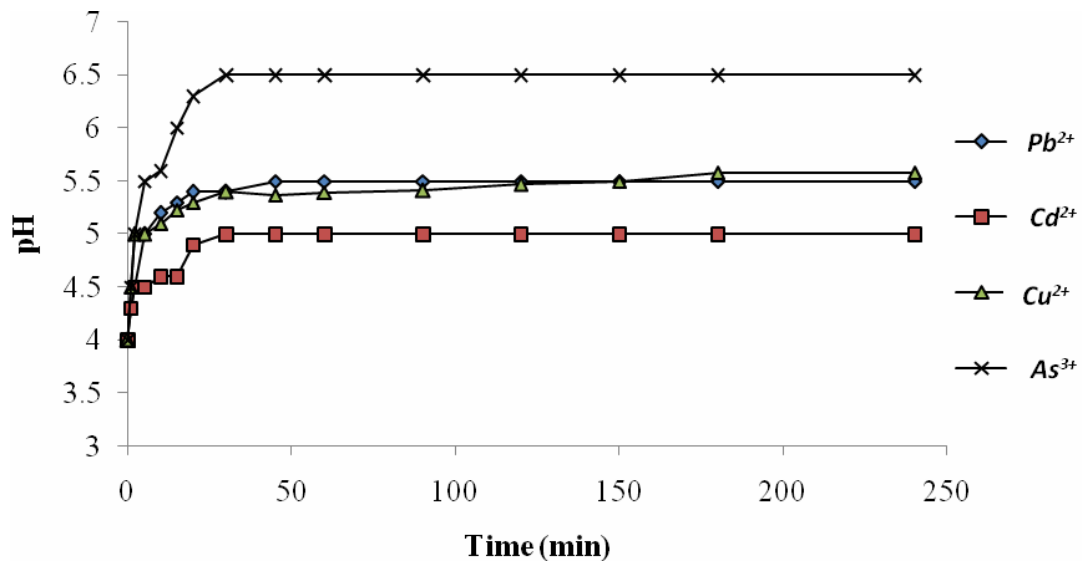
Fig.4 pH evolution as a function of time of Pb^{+2}, Cd^{+2}, Cu^{+2} and As^{+3} ions biosorption, C_o=50 ppm, contact time 4 h and 200 rpm

479
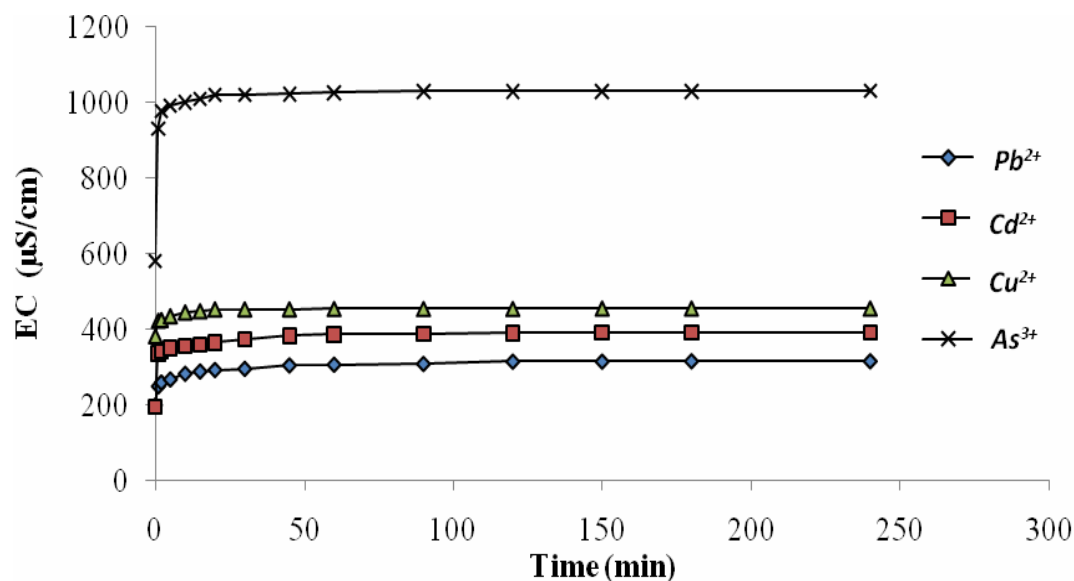
Fig. 5 EC evolution as a function of time of Pb^{+2}, Cd^{+2}, Cu^{+2} and As^{+3} ions biosorption, C$_o$=50 ppm, contact time 4 h and 200rpm
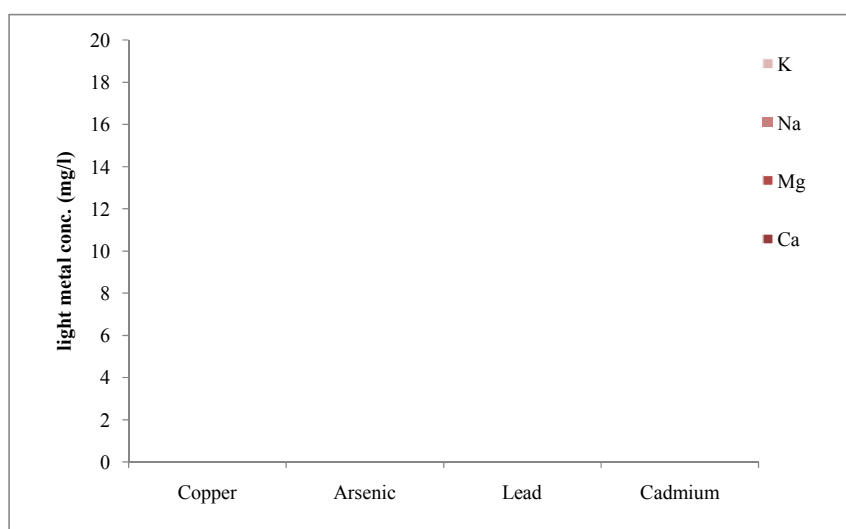
Fig.6 Amounts of light metals released due to heavy metal biosorption, C$_o$=50 ppm, contact time 4 h. and 200rpm
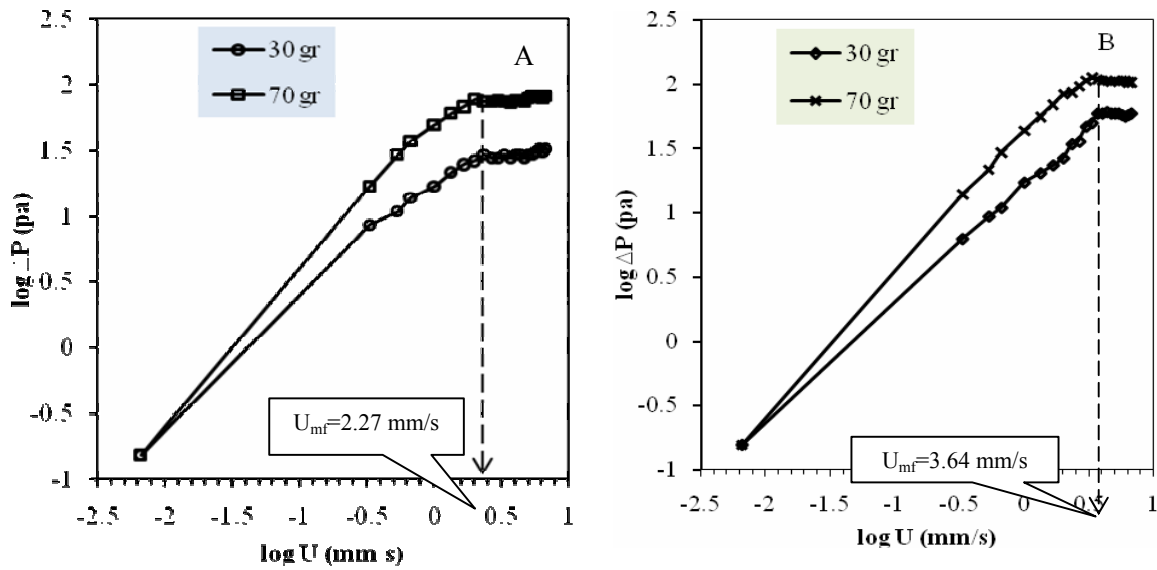
Fig.7 Pressure drop vs. superficial fluid velocity in algal bed, A: 0.4-0.6 mm and B: 0.6-1 mm diameter
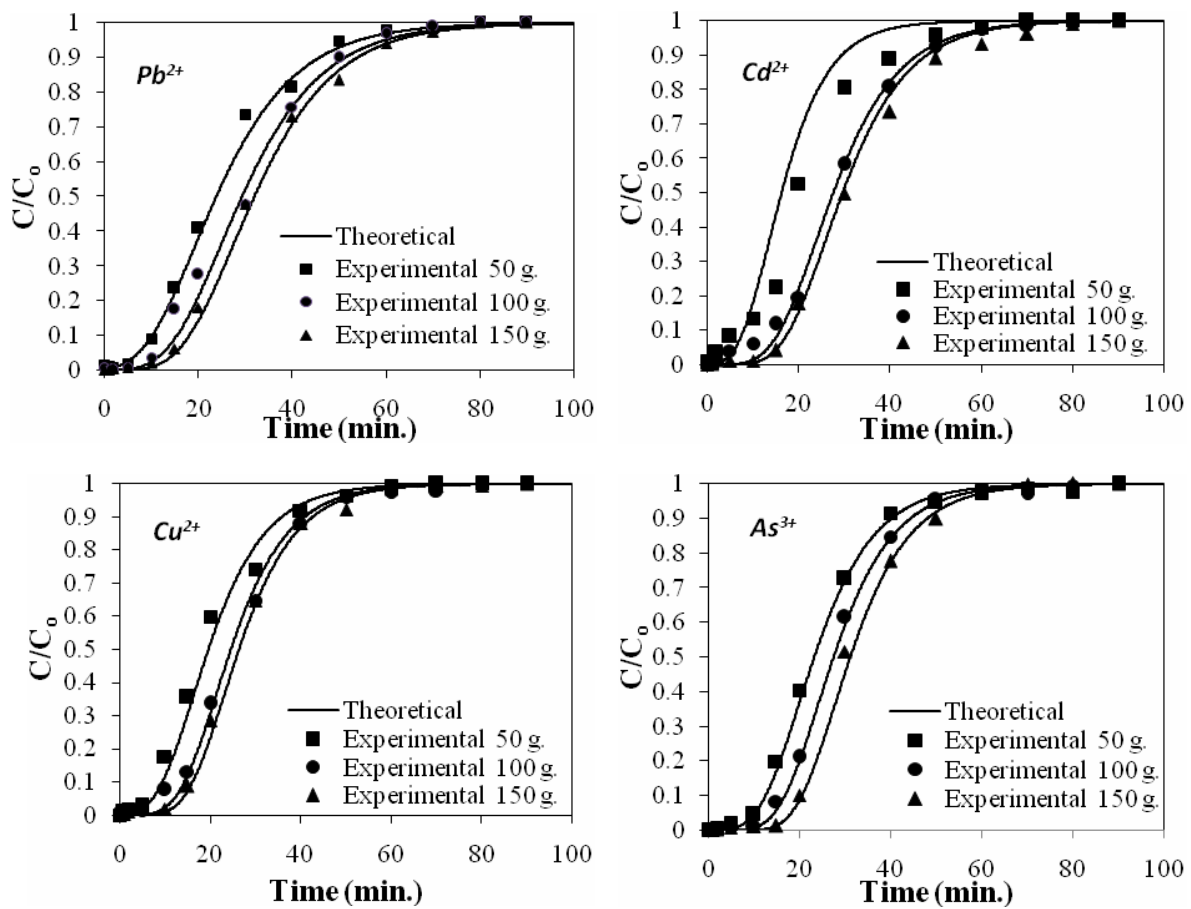
Fig.8. Experimental and theoretical breakthrough curves at different bed weight, Co=50 ppm, pH=3, 25°C, d_p=0.5 mm and U=1.1U_{mf}.
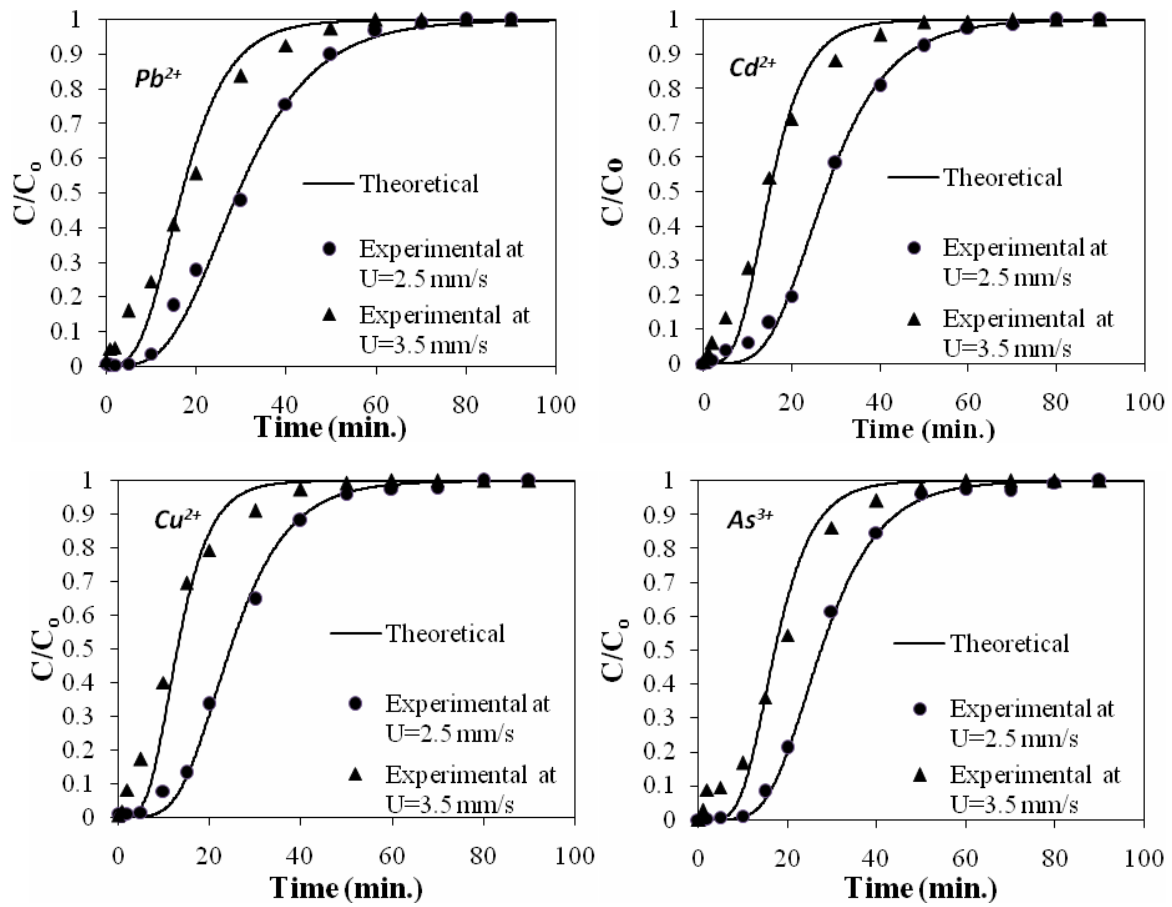
Fig.9. Experimental and theoretical breakthrough curves at 100 g algal biomass, Co=50 ppm, pH=4, 25°C, dp=0.5 mm, U=2.5 and 3.5 mm/s
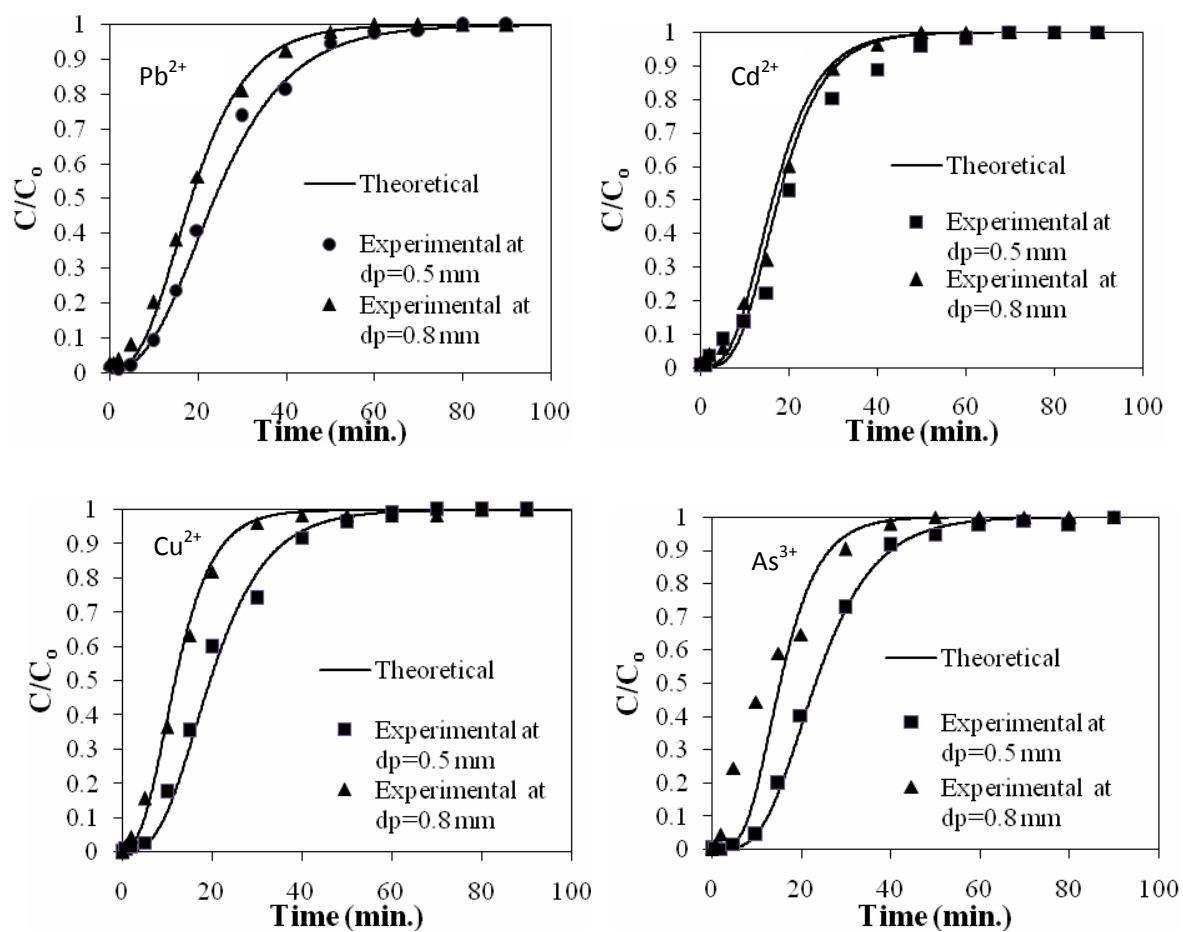
Fig.10. Experimental and theoretical breakthrough curves of 50 g, C_o=50 ppm, pH=4, 25°C, U=2.5 mm/s, d_p=0.5 and 0.8 mm
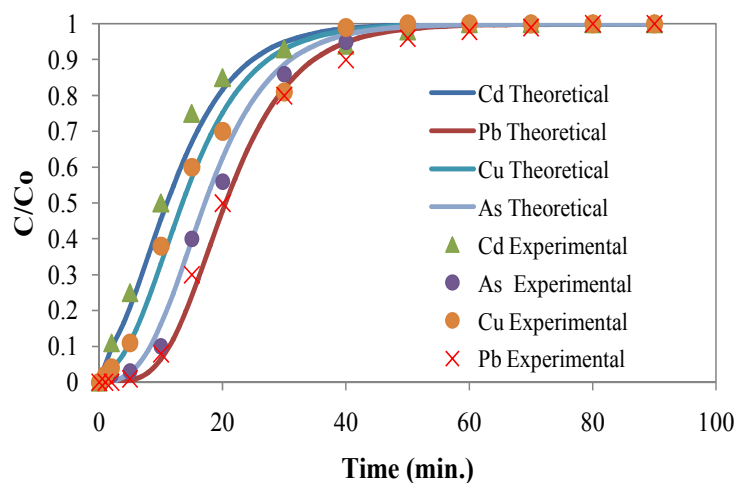
Fig.11. The experimental and predicted breakthrough curves for biosorption of quaternary system , pH=4, C_o=50 ppm, w=150 g

Numerical Study of Solar Chimney with Absorber at Different Locations

Asst. Prof. Dr.Karima E. Amori **Asst. Lect. Khawla Naeem Hmood**
Univ. of Baghdad/ Mech. Eng. Dept. , Aljaderiya - Baghdad-Iraq
drkarimaa@yahoo.com   nh.khawla@yahoo.com

ABSTRACT:
Heat transfer process and fluid flow in a solar chimney used for natural ventilation are investigated numerically in the present work. Solar chimney was tested by selecting different positions of absorber namely: at the back side, front side, and at the middle of the air gap. CFD analysis based on finite volume method is used to predict the thermal performance, and air flow in two dimensional solar chimney under unsteady state condition, to identify the effect of different parameters such as solar radiation. Results show that a solar chimney with absorber at the middle of the air gap gives better ventilation performance. A comparison between the numerical and previous experimental results shows fair agreement.

Key Words: solar chimney, CFD, buoyancy; natural ventilation; free cooling

دراسة نظرية لمدخنة شمسية لمواقع مختلفة للسطح الماص

أ.م.د. كريمة أسماعيل عموري   م.م. خولة نعيم حمود
جامعة بغداد- كلية الهندسة ــ قسم الميكانيك

الخلاصه

تم إجراء درسة عددية لعملية انتقال الحرارة وجريان المائع في المدخنة الشمسية. اختبرت المدخنة الشمسية بأختيار مواقع مختلفة للسطح الماص وتحديدا" بوضع السطح الماص على الجانب الخلفي ، الجانب الأمامي ، وفي منتصف فجوة الهواء. تم استخدام تحليل ديناميك الموائع الحسابية وبأعتماد طريقة الحجوم المحددة لتحديد الأداء الحراري وجريان الهواء في مدخنة شمسية ببعدين ولظروف غير مستقرة لبيان تأثير عوامل مختلفة مثل الأشعاع الشمسي. بينت النتائج ان المدخنة الشمسية بسطح ماص في منتصف الفجوة الهوائية يؤدي افضل تهوية . بينت المقارنة بين النتائج الحالية والنتائج التجريبية السابقة توافقا مقبولا".

الكلمات الرئيسية: مدخنة شمسية ، ديناميك الموائع الحسابية ، الطفو ، التهوية الطبيعية ، التبريد الغير مكلف.

Asst. Prof. Dr.Karima E. Amori
Asst. Lect. Khawla Naeem Hmood

Numerical Study of Solar Chimney with Absorber at Different Locations

INTRODUCTION

A solar chimney (or thermal chimney) is a way for improving the natural ventilation of buildings by using convection of air heated by passive solar energy. Passive solar design refers to the use of the sun's energy for heating and cooling of living spaces. Operable windows, thermal mass and solar chimneys are common elements found in passive design. **Bouchair and Fitzgerald (1988)** conducted a theoretical study of the heat stored in solar chimney using a finite difference technique. They showed that the amount of the heat collected is strongly dependent upon its azimuth. **Bansal et al.(1989)** used a mathematical model to calculate the performance of a wind tower system integrated with a solar chimney. The work aimed to predict the results based on the proposed energy balance equation of the solar chimney and air flow rate equations. The study also confirmed that the thermal performance of the solar chimney was comparatively higher for lower incident winds. The result showed that the solar chimney can increase the mass flow rate of induced air by up to 50% for the case of high incident solar radiation and low wind speeds. The solar chimney integrated with a wind tower was able to generate airflow up to 1.4 kg/s which doubles that of a single wind tower producing only up to 0.75 kg/s. The author concluded that the effect of the solar system is more significant than that of the wind tower and combining both systems will enhance the ventilation rates by increasing the mass flow rate of induced air. **Awbi and Gan(1992)** compared the analytical and simulated solution for Trombe wall and solar chimney. Air speed and temperature results showed that airflow within the solar chimney ducts was not symmetrical due to air entering at right angle to the duct. **Ong(2003)** proposed a simple mathematical model of a solar chimney. The physical model is similar to that of the Trombe wall. The equations were solved using a matrix-inversion solution procedure. The thermal performance of the solar chimney as determined from the glass,

wall and air temperatures, air mass flow rate and instantaneous heat collection efficiency of the chimney are presented. Satisfactory correlation was obtained with experimental data from other investigators. Later, **Ong and Chow (2003)** proposed a mathematical model of a solar chimney to predict its performance under varying ambient and geometrical features. Steady state heat transfer equations were set up using a thermal resistance network and solved using matrix inversion. The effects of air gap and solar radiation intensity on the performance of different chimneys were investigated.

Chantawong et al. (2006) studied the thermal performance of Glazed Solar Chimney Walls (GSCW) under the tropical climatic conditions of Thailand. A prototype of GSCW was integrated into southern wall of a small room of 2.8m³ volume . They found that GSCW is highly suitable for hot countries, it can reduce heat gain through glass walls into the house by developing air circulation, which can help improve the thermal comfort of residents too. The use of GSCW can also reduce the usage of fans due to induced ventilation. **Mathur et.al (2006)** investigated experimentally the effect of the ratio between height of absorber and air gap of a solar chimney used for room ventilation. They found that highest rate of ventilation induced with the help of solar energy was 5.6 air changes per hour in a room of (27 m^3), at solar radiation 700 W/m^2 incident on vertical surface with the height to air gap ratio of 2.83. **Jia et.al. (2007)** presented a mathematical model for simulating air flow within solar channel of the insulated Trombe solar wall system. They discretized and solved mass, momentum and energy conservation equations using the finite difference method. They carried out experimental study of solar chimney to validate the proposed mathematical model. The differences between the predicted and measured results of airflow rate were less than 3%. **Harris and Helwig (2007)** studied numerically the design of a solar chimney to induce ventilation in building. CFD modeling was used to assess the impacts of inclination

angle, double glazing and low-emissivity finishes on the induced ventilation rate. A solar chimney south facing chimney of dimensions (3m) height, (0.1-0.3m) cavity width, and (1m) cavity breadth, at an inclination angle of 67.5^o from the horizontal for the location chosen (lat. 52^oon 15th July), gives 11% greater efficiency than the vertical chimney, and a 10 % higher efficiency was obtained by using a low – emissivity wall surface. **Lee and Strand(2009)** used numerical simulation and found that: (1) chimney height, solar absorptance and solar transmittance turned out to have more influences on natural ventilation improvement than air gap width. **Kaiser and Zamora (2009)** have studied numerically the laminar and turbulent flow induced by natural convection in channels. Numerical results of the average Nusselt number and the non- dimensional induced mass-flow rate have been obtained for values of Rayleigh number varying from 10^5 to 10^{12} for symmetrical and isothermal heating. **Gan(2010)** used CFD to simulate the natural ventilation of buildings using two different sizes of computational domain for different heat fluxes and wall heat distribution. He found that utilizing computational domain larger than the physical size gives accurate prediction of the flow rate and heat transfer in ventilated buildings with large openings, particularly with multiple inlets and outlets as demonstrated with two examples for natural ventilation of buildings. **Rahimi and Bayat (2011)** investigated a buoyancy induced air flow within a vertical pipe experimentally. The flow rate was a function of the pipe height, surrounding temperature and mean temperature of air inside the pipe. They found that the pressure losses at the inlet and outlet of the pipe along with that of the main pipe are compensated by the buoyancy pressure. The flow rate increases as the length of the pipe is increased and its variation becomes negligible for extremely large length of pipe. For a constant length of the pipe, the maximum of flow rate occurs where the mean temperature of the flow is

one and a half times greater than the surroundings temperature.

Tan and Wong (2012) constructed a solar chimney system to enhance the air ventilation within the interior spaces using a series of solar assisted ducts that linked the lower floor classrooms and upper floor hall in a zero energy building (three story building) in Singapore. Results showed that the solar chimney system is operating well in the hot and humid tropics, including cooler days. The interconnecting thermal stack experienced in the hall, can induce an average air speed of 1.5 m/s and 0.4 m/s within the solar chimney and level 1 classroom respectively.

The objective of the present work is to investigate numerically the thermo-fluid phenomena takes place in a full scale solar chimney under Iraq environmental condition testing different positions of the absorber (at front side, back side, and at the middle of the air gap) which is up to date is rarely studied.

MATHEMATICAL MODEL

A mathematical model of the natural buoyancy-driven fluid flow and heat transfer in the chimney shown in Figure(1) have been adopted. The following assumptions have been used to simplify the governing equations:

1- Transient incompressible 2-D air flow in the chimney (no variations are considered along the width).

2-Conduction heat transfer along the absorber wall and the glass cover is neglected

3- Radiation heat transfer is neglected.

4- Constant thermo-physical properties of the working fluid.

5- Air density is dependent of temperature.

6- Dissipation Function is neglected.

Governing Equations

The governing differential equations of the natural convection in the solar chimney may be written in Cartesian coordinates as: (**Versteeg and Lasekea 1995**)

Continuity equation:

Asst. Prof. Dr.Karima E. Amori
Asst. Lect. Khawla Naeem Hmood

Numerical Study of Solar Chimney with
Absorber at Different Locations

$$\frac{\partial \rho}{\partial t} + \frac{\partial}{\partial x}(\rho u) + \frac{\partial}{\partial y}(\rho v) = 0 \qquad (1)$$

X-momentum equation:

$$\frac{\partial}{\partial t}(\rho u) + \frac{\partial}{\partial x}(\rho u u) + \frac{\partial}{\partial y}(\rho v u) =$$
$$-\frac{\partial P}{\partial x} + \frac{\partial}{\partial x}(\mu \frac{\partial u}{\partial x}) + \frac{\partial}{\partial y}(\mu \frac{\partial u}{\partial y}) \qquad (2)$$
$$- \rho g(T - T_\infty) \sin \theta$$

Y-momentum equation:

$$\frac{\partial}{\partial t}(\rho v) + \frac{\partial}{\partial x}(\rho u v) + \frac{\partial}{\partial y}(\rho v v) =$$
$$-\frac{\partial P}{\partial y} + \frac{\partial}{\partial x}(\mu \frac{\partial v}{\partial x}) + \frac{\partial}{\partial y}(\mu \frac{\partial v}{\partial y}) \qquad (3)$$
$$- \rho g(T - T_\infty) \cos \theta$$

Energy equation:

$$\frac{\partial}{\partial t}(\rho T) + \frac{\partial}{\partial x}(\rho u T) + \frac{\partial}{\partial Y}(\rho v T) =$$
$$\frac{\partial}{\partial x}\left(\Gamma \frac{\partial T}{\partial x}\right) + \frac{\partial}{\partial y}\left(\Gamma \frac{\partial T}{\partial y}\right) \qquad (4)$$

where:

$$\Gamma = \frac{\mu}{pr}$$

x, y Cartesian-coordinate of the system.

ρ & μ are air density (kg.m^{-3}) and dynamic viscosity (kg/m.s) respectively
For (Ra > 10^9) k-ε turbulence model is used, and μ, Γ are replaced by their effective values μ_{eff} which can be defined as sum of the eddy viscosity μ_t and fluid dynamic viscosity μ (**Andonikos et al.2007**). The turbulent kinetic energy and the dissipation rate can be defined using the following equations:

$$\frac{\partial}{\partial t}(\rho k) + \frac{\partial}{\partial x}(\rho u k) + \frac{\partial}{\partial y}(\rho v k) =$$
$$\frac{\partial}{\partial x}\left(\Gamma_k \frac{\partial k}{\partial x}\right) + \frac{\partial}{\partial y}\left(\Gamma_k \frac{\partial k}{\partial y}\right) + S_k \qquad (5)$$

where

$$\Gamma_k = \mu_{eff} / \delta_k \qquad (6)$$
$$S_k = G - C_D \rho \varepsilon \qquad (7)$$
$$\mu_t = \rho C_\mu k^2 / \varepsilon \qquad (8)$$

$$\frac{\partial}{\partial t}(\rho \varepsilon) + \frac{\partial}{\partial x}(\rho u \varepsilon) + \frac{\partial}{\partial y}(\rho v \varepsilon) =$$
$$\frac{\partial}{\partial x}\left(\Gamma_\varepsilon \frac{\partial \varepsilon}{\partial x}\right) + \frac{\partial}{\partial y}\left(\Gamma_\varepsilon \frac{\partial \varepsilon}{\partial y}\right) + C_1 \frac{\varepsilon}{k}G - C_2 \rho \frac{\varepsilon^2}{k} \qquad (9)$$

where

$$G = \mu_t \left(2\left[\left(\frac{\partial u}{\partial x}\right)^2 + \left(\frac{\partial v}{\partial y}\right)^2 \right] + \left(\frac{\partial u}{\partial y} + \frac{\partial v}{\partial x}\right)^2 \right)$$

$$\Gamma_\varepsilon = \mu_{eff} / \delta_\varepsilon$$

The turbulent constants ($C_\mu, C_D, C_1, C_2, \delta_k$, and δ_ε) are given in table (1)

Boundary and Initial Conditions

The air velocity boundary conditions at inlet of the chimney are: (**Mossowi 2001**)

$$\mathbf{u(x,0) = 0} \quad ; \quad \mathbf{v(x,0) = v_{in}} \qquad (10)$$

While the inlet air temperature is:
$$\mathbf{T(x,0) = T_\infty}$$

The outlet boundary conditions can be written as: (**Kasayapanand 2007**)

$$\left.\frac{\partial u}{\partial y}\right|_L = \left.\frac{\partial v}{\partial y}\right|_L = 0$$
$$\left.\frac{\partial T}{\partial y}\right|_L = 0 \quad ; \quad P(x, L) = P_\infty \qquad (11)$$

No slip boundary conditions are adopted on solid boundaries

$$u(0, y) = v(0, y) = 0$$
$$u(w, y) = v(w, y) = 0 \qquad (12)$$

The glass cover and absorber are subjected to the following thermal boundary conditions:

$$\frac{\partial T}{\partial x}(0, y) = \alpha_g I \quad ; \quad \frac{\partial T}{\partial x}(w, y) = \tau \alpha I$$

respectively, where α_g is glass absorbtivity.
The turbulent kinetic energy and the dissipation rate at the inlet of the chimney are: (**Mosi and Clayton 1980**)

$$k(x,0) = k_{in} = C_k v_{in}^2$$
$$\varepsilon(x,0) = \varepsilon_{in} = C_\mu k_{in}^{3/2} / (0.5 D_h C_\varepsilon) \qquad (13)$$

where D_h is the hydraulic diameter.

while at the outlet (**Taylor et al. 1984**):

$$\frac{\partial k}{\partial x}\bigg|_{y=L}=\frac{\partial \varepsilon}{\partial x}\bigg|_{y=L}=0 \qquad (14)$$

The boundary conditions for turbulent model (when $Ra > 10^9$ (**Patankar 1980**) are:

$$k(0,y)=\frac{\partial \varepsilon}{\partial y}\bigg|_{y=0}=0$$

$$k(w,y)=\frac{\partial \varepsilon}{\partial y}\bigg|_{y=L}=0 \qquad (15)$$

The following initial conditions used through the numerical solution can be written as:

$$T=T_\infty \quad ; \quad P = P_\infty$$
$$u = v =0 \quad (x,y,t=0) \qquad (16)$$

The above governing equations together with the boundary and initial conditions have been solved numerically using SIMPLE algorithm with segregated unsteady-state solver embodied in Fluent commercial software. The material and thermophysical properties needed are presented in table (2).

Figure (1) shows the different views for the investigated solar chimneys. The main parts of the solar chimney are the absorber wall, 2.25m height (ductile steel plate of 0.001m thickness), and the glass cover of (0.004m) thickness.

Air flow rate through the channel is calculated such that:

$$Q_{vent}=v_{avg}*A \qquad (17)$$

where:

v_{avg} is the average velocity at the exit cross section of the chimney (m/s)

A is the outlet cross section area of the chimney (0.1455 m^2)

Q_{vent} is the flow rate of the hot air (m^3/s).

The weather data such as (ambient temperature, solar radiation and wind speed) was adopted for Al-Kufa city located at (44.34° longitude East) and (32° latitude North) (**Mohammed 2010**) on 20th July

2010. The hourly average air velocity (V_{avg}) at chimneys outlet is calculated as:

$$V_{avg}=\frac{1}{W}\int_0^W V dx \qquad (18)$$

where:

W=thickness of air gap (m)

Air Change per Hour (ACH) refers to the amount of air ventilated and replaced by fresh air. This parameter can be calculated as:-

$$ACH = \frac{Q_{vent} \times 3600}{V} \qquad (19)$$

where V is the volume of a room taken as $(3 \times 4 \times 3)$ m^3

The thermal efficiency of the solar chimney is calculated as:

$$\eta=\frac{\rho\, Q_{vent}\ Cp(T_{out}-T_{in})}{I\times L\times b} \qquad (20)$$

where:

η thermal efficiency

Cp air specific heat (J/kg K)

I incident solar energy (W/m^2).

L absorber height = 2.25m

b chimney's width =0.97m

Numerical Approach

The Navier–Stokes equations simultaneously with the continuity governing equations and energy equations together with the boundary and initial conditions have been solved numerically using SIMPLE algorithm with segregated unsteady-state solver embodied in Fluent commercial software.

RESULTS AND DISCUSSION

Testing the performance of the solar chimney was performed at ambient conditions on 20th July 2010 in Al-Najaf city (32.° lat north). Numerical experiments have been conducted on vertical solar chimney with absorber at the front side, at the back side , and at the middle of the air gap.

The hourly distribution of solar radiation (I) and ambient temperature (T_∞) are displayed in Figure(2). These values are

Asst. Prof. Dr.Karima E. Amori
Asst. Lect. Khawla Naeem Hmood

Numerical Study of Solar Chimney with Absorber at Different Locations

adopted as input data to the simulation code. The maximum incident solar radiation and ambient temperature were (945 W/m^2 and 47.7 ^{o}C) respectively.

The predicted absorber average temperature was compared with the measured values published by **Mohammed (2010)** as shown in Fig.(3). The minimum and maximum deviations were (0.44% and 18.83%) respectively.

Figure(4) shows the variation of hourly absorber temperature and glass cover temperature at five different levels (T1 to T5) along chimneys height which are given in table (4). These temperatures are changing along with the intensity of solar radiation. The highest maximum absorber temperature was (94.5 ^{o}C at 12:00 PM), while the glass cover temperature was (59.4 ^{o}C at 12:00 PM).

Figure (5) illustrate a comparison of absorber temperature between cases I and II. Higher absorber temperature is reported for case I since the absorber is back insulated, while air is in contact with the two faces of absorber for case II. The same results are obtained in Fig.(6).

Figure(7) shows the variation of hourly air average temperature at different heights along the chimney for case I. The maximum air temperature recorded is (77°C). The maximum air temperature reported was (60°C) for case II as shown in Fig. (8), while for case III it was (53°C) for air gap between glass cover and absorber, and (54.5^{o}C) for air gap behind the absorber as depicted in Fig.(9).

A considerable change in air velocity of induced ventilation during day hours is shown in Fig.(10). The distribution of air velocity across the air gap for case III is presented in Fig.(11). The maximum air velocity is indicated near the absorber (before and after the absorber). Figure (12) reported higher values of air change per hour for case III compared with cases I and II, while its thermal efficiency was the lowest as shown in Fig.(13).

CONCLUSIONS

The effect of different locations of the absorber at thermal and air velocity inside a solar chimney used for induce natural ventilation has been studied numerically. The following conclusions can be extracted;

1) The position of absorber affects the performance of the chimney. Solar chimney with absorber at middle of air gap has the best thermal performance.
2) The thermal performance of the solar chimney is decreased when absorber is located at front side. Quantitatively the maximum air temperature reached at chimneys' outlet was (77°C) for absorber at back side while it was (60 ^{o}C) when absorber at front side.
3) The highest air change per hour was obtained for solar chimney with absorber at the middle of air during day hours.
4) The highest thermal efficiency was indicated for solar chimney with absorber at the back side during day hours.

REFERENCES

Al Mossowi A.N., Turbulent developing flow and heat transfer in a porous square duct, MSc. Thesis, Mechanical and Construction Department, University of Technology, Baghdad, Iraq 2001, (written in Arabic)

Andronikos E.F., Dionysios M., Evngellos B., Michalis GR.V., Maria K.K., Stamatis A.M., Study of natural convection phenomena inside a wall solar chimney with one wall adiabatic and one wall under a heat flux, Applied thermal engineering 27 (2007) 2266-2275.

Awbi H.B., Gan G., Simulation of solar-induced ventilation, Renewable Energy Technology and the Environment 4 (1992) 2016–2030.

Bansal NK, Mathur R. Solar chimney for enhanced stack ventilation. Build Environ 28 (1989) 373–7.

Bassiouny R., Korah N.S.A., Effect of solar chimney inclination angle on space flow pattern and ventilation rate, Energy and Buildings 41 (2009) 190-196.

Bouchair A., Fitzgerald D., The optimum azimuth for a solar chimney in hot climates, Energy and Building 12 (1988) 135-140.

Chantawong P., Hirunlabh J., Zeghmati B., Khedari J., Teekasap S., Win M.M., Investigation on thermal performance of glazed solar chimney walls, Solar Energy, 80 (2006) 288-297.

Eckert E., Jackson T.W., Analysis of turbulent free convection boundary layer on flat plate, (Report 1015, (1950) supersedes NACA TN 2207).

Gan G., Simulation of buoyancy-driven natural ventilation of buildings-impact of computational domain, Energy and Building 42 (2010) 1290-1300.

Harris D.J., Helwig N., Solar chimney and building ventilation, Applied Energy 84 (2007) 135–146.

Jia H., Li J., Duanmu X., Li Y., Sun Y., Study on the air movement character in solar wall system, College of architecture and civil engineering, Beijing university of technology, (2007), Beijing, 100022 Building simulation.

Kaiser A.S, Zamora B., Optimum wall-to-wall spacing in solar chimney shaped channels in natural convection by numerical investigation, Applied thermal Eng. 29 (2009) 762–769.

Kasayapanand N., Enhanced heat transfer in inclined solar chimneys by electro-hydrodynamic technique, School of Energy, Environment, and Materials 1 (2007) 0960-1481.
Lee K.H., Strand .K., Enhancement of natural ventilation in buildings using a

thermal chimney, Energy and Buildings 41 (2009) 615–621.

Mathur J., Bansal N.K, Mathur S., Anupma J.M., Experimental investigations on solar chimney for room ventilation, Solar Energy 80 (2006) 927–35.

Mohammed S.W., Experimental and numerical studies of solar chimney for natural ventilation in Iraq, MSc. thesis, Mechanical Eng. dept. , college of Eng., University of Baghdad, 2010.

Morsi Y.S., Clayton B. R., Determination of principal characteristics of turbulent swirling flow along annuli, Int. J. Heat and Fluid Flow 7 (1980) 208-222.

Ong K.S., A mathematical model of a solar chimney. Renewable Energy 28 (2003) 1047–60.

Ong K.S., Chow C.C., Performance of a solar chimney. Solar Energy 74 (2003) 1–17.

Patankar S.V., Numerical heat transfer and fluid flow, McGraw Hill, 1980, New York.

Rahimi M., Bayat M.M., An experimental study of naturally driven heated air flow in a vertical pipe, Energy and Buildings 43 (2011) 126-129.

Tan A.Y.K., Wong N.H., Natural ventilation performance of classroom with solar chimney system, Energy and Buildings 53 (2012) 19–27.

Taylor, Rance J., Medwell J.O., Turbulent flow and heat transfer in rotating ducts-preliminary results, Numerical methods for non-linear problems, Pincridge Press Swansea, U.K., 2 (1984) 839-847.

Versteeg H.K., Lasekera W. Mala, An introduction to computational fluid dynamics. The Finite Volume Method, 1st Pub., (1995) Long Man Group Ltd.

Asst. Prof. Dr.Karima E. Amori
Asst. Lect. Khawla Naeem Hmood

Numerical Study of Solar Chimney with
Absorber at Different Locations

Table (1): Values of Constants Used in
the $(k-\varepsilon)$ Model (**Eckert and Jackson 1950**)

C_μ	C_D	C_1	C_2	δ_k	δ_ε
0.09	1.00	1.44	1.92	1.0	1.3

Table (2): Physical Properties Of Used Materials
(Ong and Chow2003, Mohammed2010)

material	ρ kg/m^3	Cp J/kg.^{o}C	k_t W/m.^{o}C	Emissivity ε_t	absorptivity α	transmisivity τ
Absorber (ductile steel)	7850	500	0.345	0.95	0.95	0
Cover (comm. Glass)	2470	750	1.0	0.9	0.06	0.84
Air	1.1614 - 3.53E-3(T-300)	1007 - 4E-3(T-300)	(263+0.74(T-300)E-4	**(Bassiouny and Korah 2009)**		

Table (3): Computed Average Outlet Velocity Results (V$_{wind}$=1 m/s)

Time (hr)	I solar glass	T amb	V_{out} Case I	V_{out} Case II	V_{out} Case III
10	824	41.2	1.204	1.136	1.274
11	927	43.4	1.242	1.171	1.365
12	945	45.3	1.244	1.172	1.466
13	921	46.8	1.228	1.156	1.331
14	838	47.3	1.199	1.119	1.313
15	673	47.6	1.155	1.0720	1.198
16	484	47.7	1.121	1.0723	1.145
17	275	47.5	1.117	1.031	1.133

Table (4): Locations of indicated temperatures

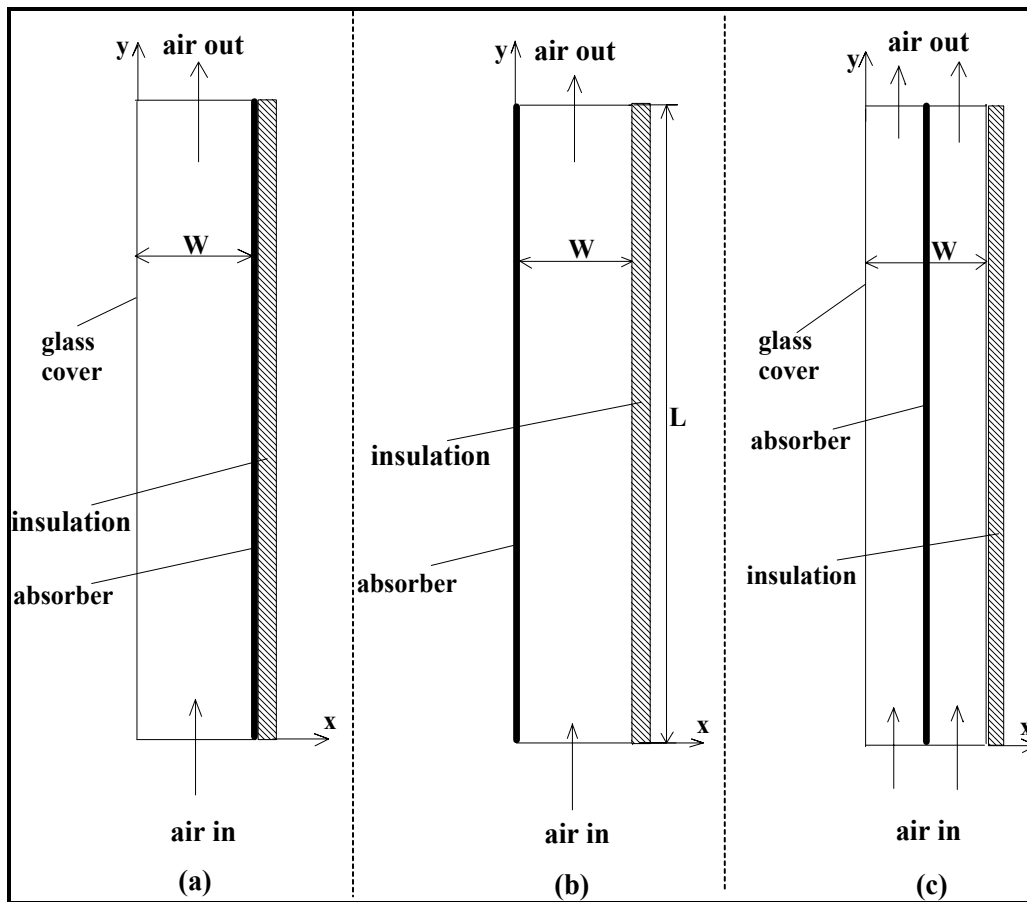| symbol	T1	T2	T3	T4	T5
Distance from inlet y= (mm)	260	755	1250	1745	2240

Fig.(1): Schematic Diagram of the Cases Studied of Solar Chimney. a) absorbe at back side, b) absorber at front side, c) absorber at the middle of air gap.
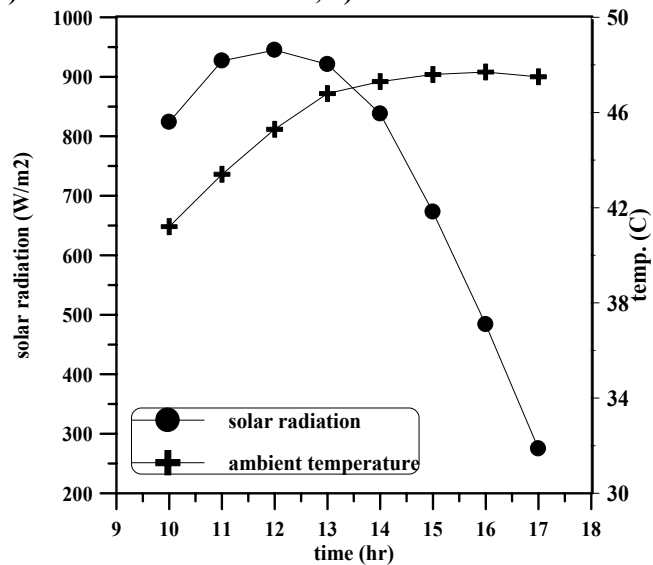

Fig.(2): Variation of Measured Ambient Conditions on 20th July 2010.
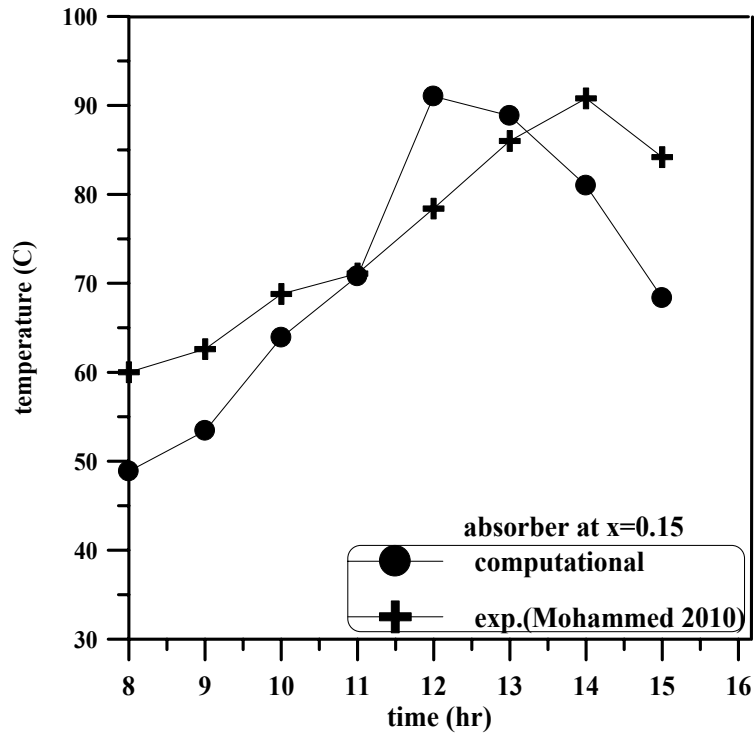
493

Asst. Prof. Dr.Karima E. Amori
Asst. Lect. Khawla Naeem Hmood

Numerical Study of Solar Chimney with Absorber at Different Locations

Fig.(3): Hourly Variation of Absorber Average Temperature. Comparison between the Computed results and Experimental results (Mohammed 2010)
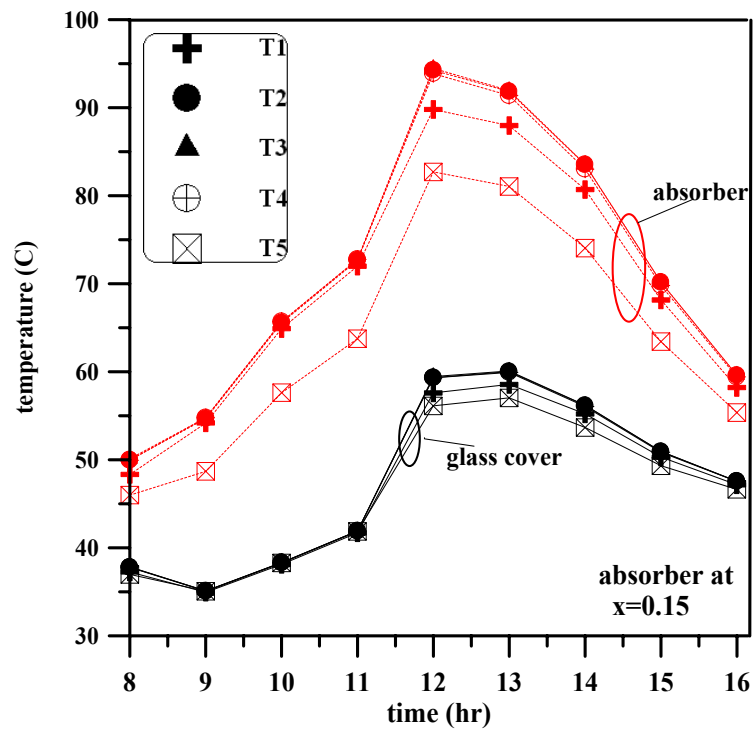
Fig. (4): Hourly Temperature distribution Case I

494
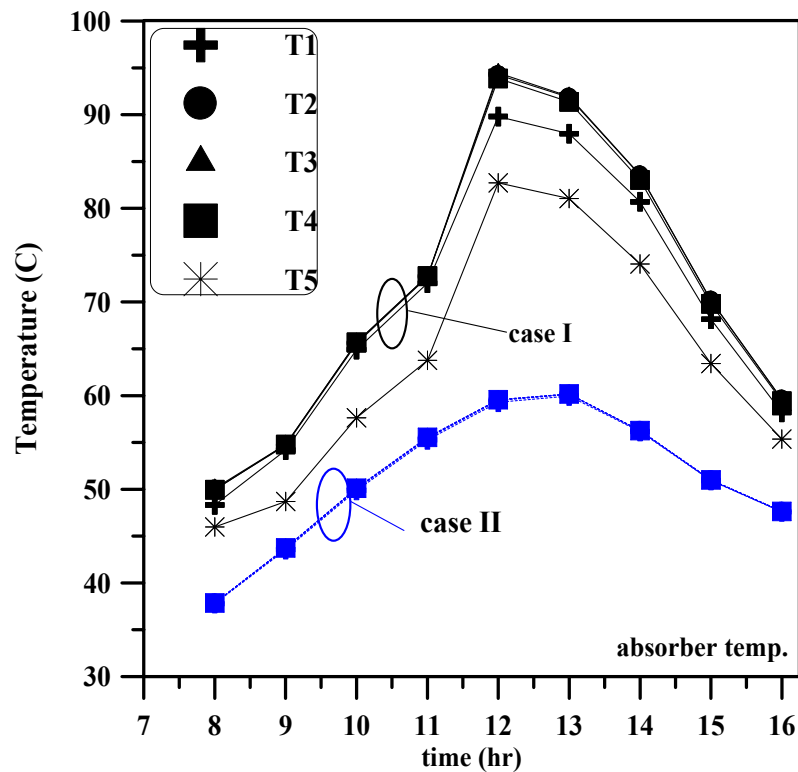
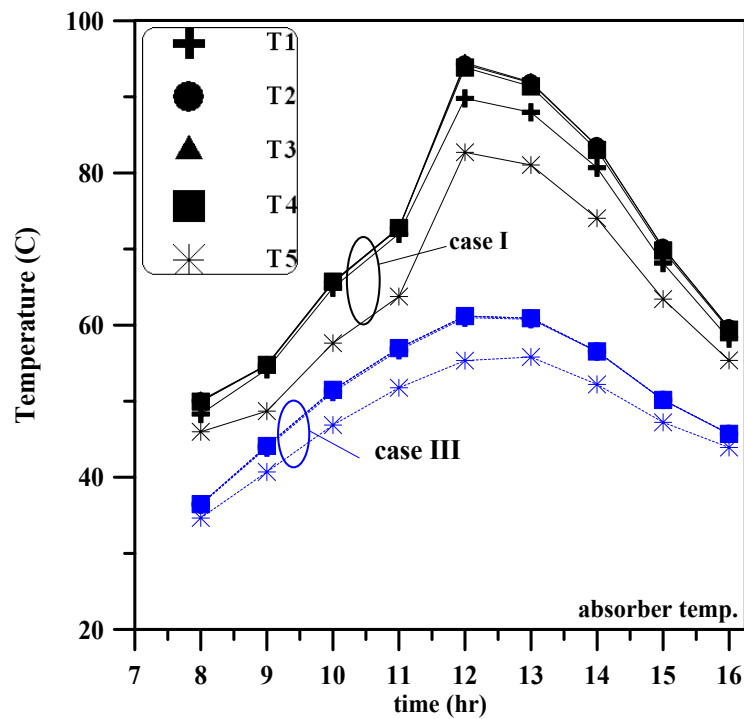**Fig. (5): Comparison of Hourly Temperature Distribution between Case I and Case II**

Fig.(6): Comparison of Hourly Temperature Distribution of the absorber between Case I and Case III
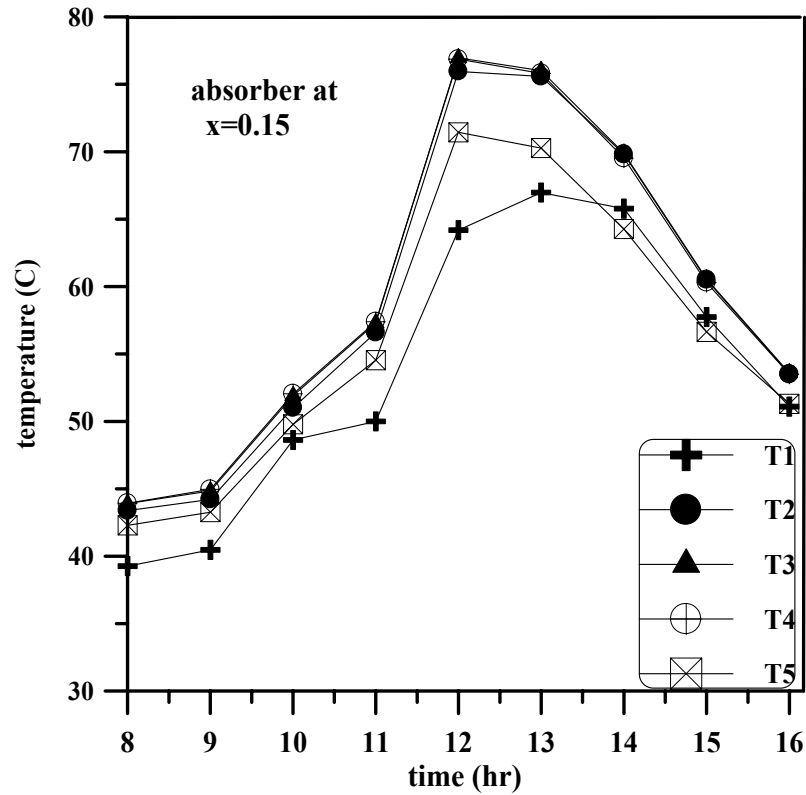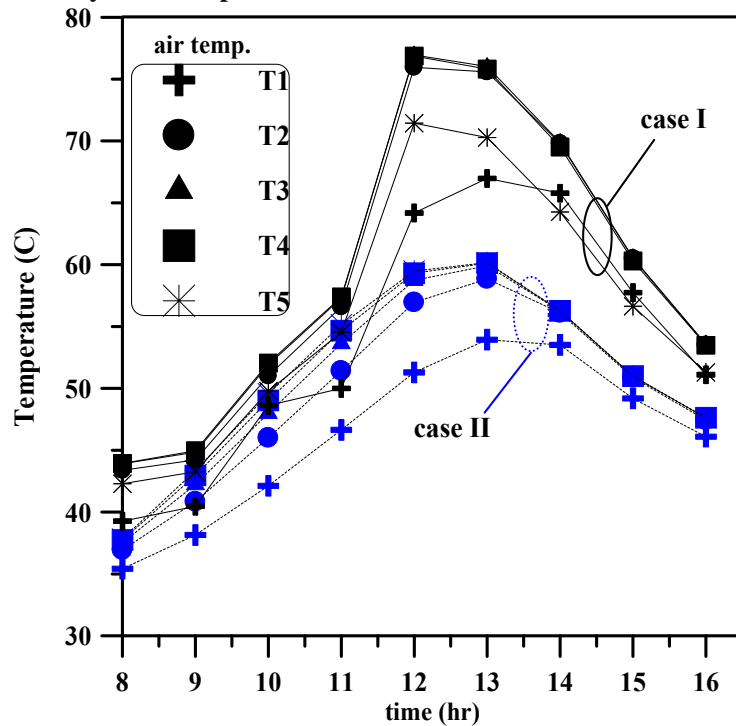
Asst. Prof. Dr.Karima E. Amori
Asst. Lect. Khawla Naeem Hmood

Numerical Study of Solar Chimney with
Absorber at Different Locations

Fig.(7): Hourly air Temperature distribution inside the chimney Case I

Fig.(8): Comparison of Hourly Air Temperature Distribution
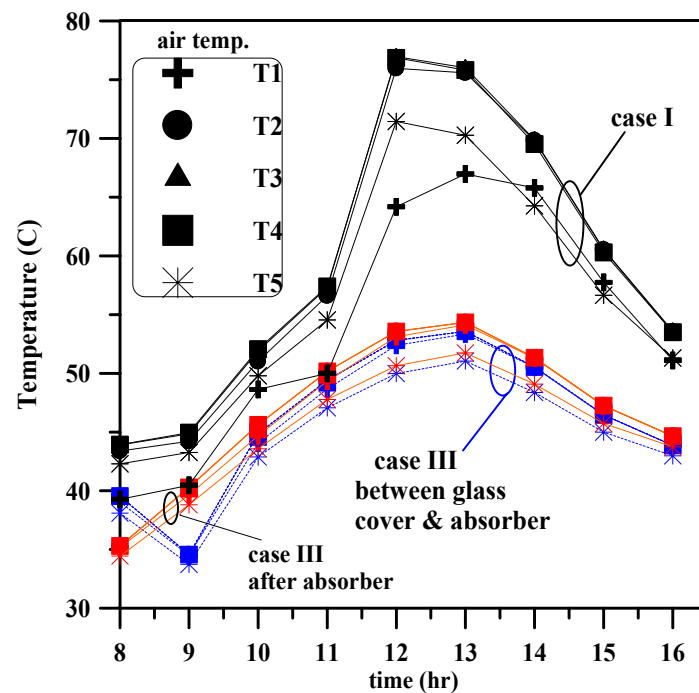**between Case I and Case II**

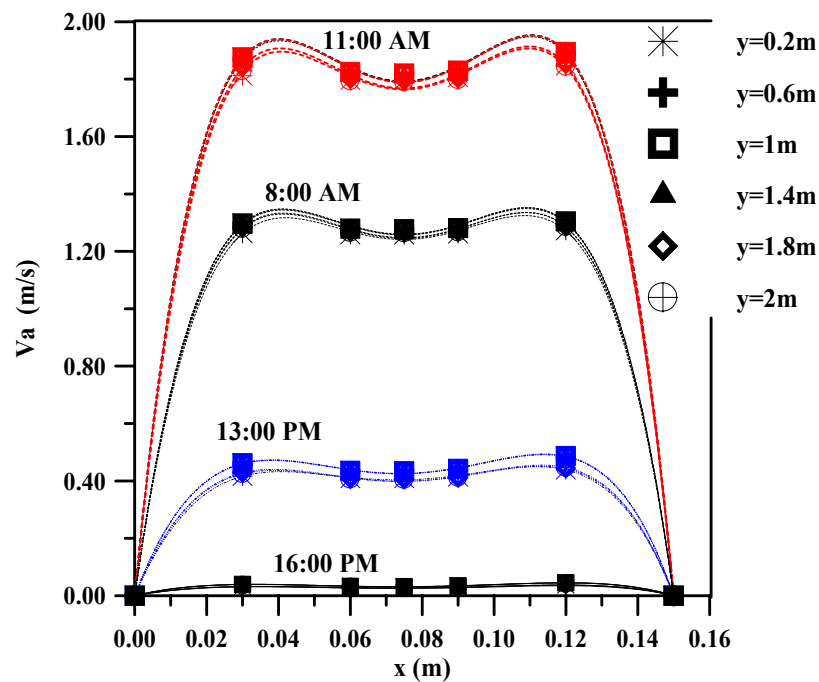**Fig. (9): Comparison of Hourly Air Temperature Distribution
between Case I and Case III**

Fig.(10): History of Velocity distribution across the gap of solar chimney for case I
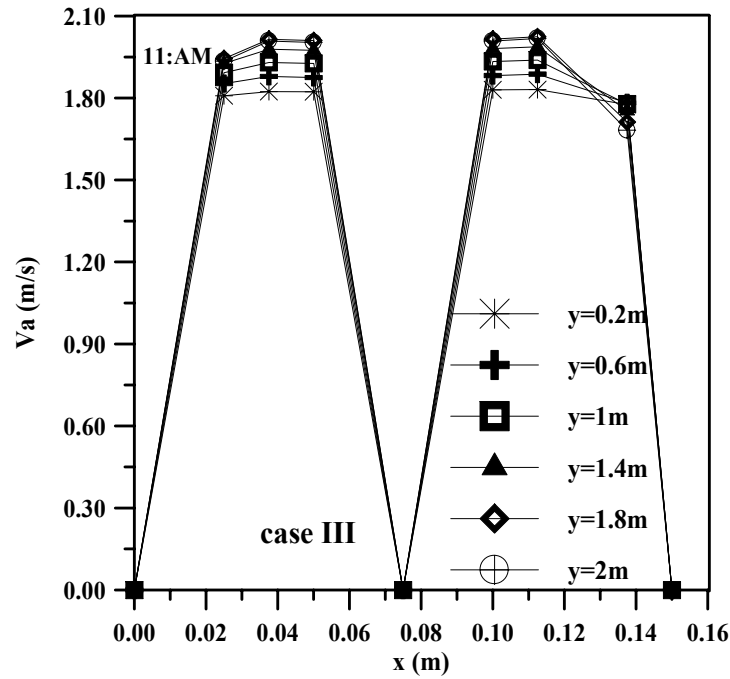
Asst. Prof. Dr.Karima E. Amori
Asst. Lect. Khawla Naeem Hmood

Numerical Study of Solar Chimney with
Absorber at Different Locations

Fig.(11): History of Velocity distribution across the gap of solar chimney for case III
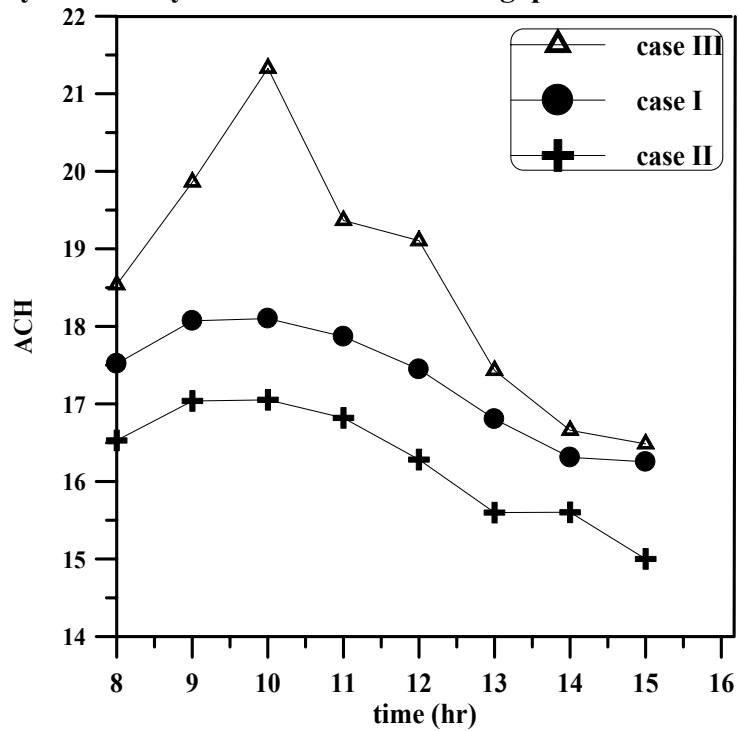

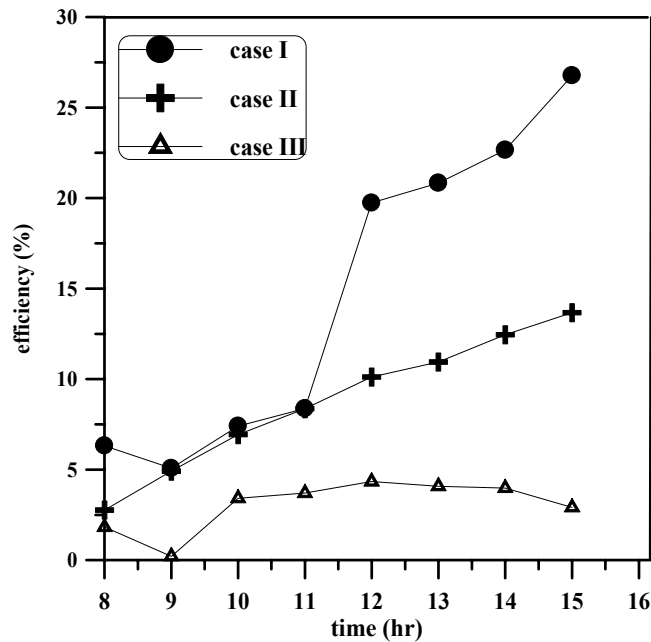**Fig.(12): History of Air Change per Hour of solar chimney**

498

Fig.(13): History of solar chimneys efficiency.

Nomenclature

Latin Symbols			
A	surface area (m^2)	Q_{vent}	Air discharge (m^3/s)
D_h	Hydraulic diameter (m)	t	time (s)
C_P	Specific heat (J/kg. K)	T∞	Ambient temperature (K)
g	gravitational acceleration(m/s^2) kinetic energy generation by shear (J)	$T_{i,m}$	Air inlet temperature (K)
h	heat transfer coefficient (W/m^2.K)	$T_{o,m}$	Air out temperature (K)
I	solar radiation (W/m^2)	T	Temperature (K)
k_t	thermal conductivity (W/m.K)	u, v	Velocity components in the x, y direction (m/s)
k	turbulent kinetic energy (m^2/s^2)	V	Volume (m^3)
L	chimney's height (m)	w	air gap (m)
P	pressure (Pa)	x,y	Cartesian coordinate (m)
Pr	Prandtl No.		
Greek Symbols			
α	absorptivity	μ_t	turbulent viscosity (N.s/m^2)
β	volume coefficient of expansion (1/K)	μ_{eff}	effective kinematics viscosity (N.s/m^2)
ε_t	emissivity	ρ	air density (kg/m^3).
ε	rate of dissipation of kinetic energy (m^2/s^2)	τ	transmisivity
η	thermal efficiency	μ	dynamic viscosity (N.s/m^2)

A Simulation of Core Displacement Experiments for the Determination of the Relative Permeability

أستخدام نمذجة تجارب الازاحة خلال النماذج المكمنية لحساب النفاذية النسبية

أحمد خليل جابر

Ahmed Khalil Jaber, SPE, Senior Reservoir Engineer**,** Ministry of Oil, Reservoir and Fields Development Directorate, Southern Department Studies, Baghdad, Iraq, E-mail: ahmedkhalil1974@yahoo.com

ABCTRACT

  Computations of the relative permeability curves were made through their representation by two functions for wetting and nonwetting phases. Each function contains one parameter that controls the shape of the relative permeability curves. The values of these parameters are chosen to minimize an objective function, that is represented as a weighted sum of the squared differences between experimentally measured data and the corresponding data calculated by a mathematical model simulating the experiment. These data comprise the pressure drop across core samples and the recovery response of the displacing phase. Two mathematical models are constructed in this study to simulate incompressible, one-dimensional, two-phase flow. The first model describes the imbibition process and the other describes the drainage process.

  The values of the relative permeability parameters are calculated by employing Rosenbrock optimization procedure. The reliability of this procedure has been confirmed by applying it to four displacement cases. The optimum values of the relative permeability parameters, which reflect the final shape of the relative permeability curves, are achieved at the minimum value of the objective function. All the above processes are be embodied in relative permeability package RPP which is constructed in this study using FORTRAN language.

INTRODUCTION

  Relative permeability curves are important for many reservoir engineering calculations. Frequently, the relative permeability curves are constructed on the basis of laboratory displacement experiments. They are not measured directly, but instead are inferred from flow data measured during the displacement experiments through the use of some interpretive methods. The dynamic fluid-displacement experiments data of core samples are often used in the calculation of the relative permeability curves.

  There are two approaches for interpreting unsteady - state core flood data to obtain relative permeability estimates. Johnson – Bossler – Naumann (JBN) (1959), and Jones – Roszelle (1978) methods are explicit interpretive methods, were the relative permeability values are computed directly from coreflood data. However, these methods have two primary limitations. First, their applications are limited to situations described by the Buckley - Leverett model and then extended by Welge (1952) and thus are not appropriate for low-flow rate experiments for which the effects of capillary pressure are significant. Second, these methods require numerical or graphical differentiation of experimental data(Blair and weinaug,1969). A second approach(Archer and Wong,1973),

called implicit interpretive approach, was developed to overstep the limitations that are associated with the explicit approach .

In the implicit methods, the relative permeability curves are computed by representing them by two functions, each of which contains certain coefficient that controls the shape accuracy of the relative permeability curves. Relative permeability curves are adjusted until the values computed with a mathematical simulation of the laboratory experiment. Match in same sense the measured data(Kerig and Watson,1987, Sigmund and McCafery,1997.Archer and Wong (1973) used a reservoir simulator to model laboratory tests. The relative permeability curves are adjusted by trail-and-error procedure until calculated oil recovery and relative injectivity curves match those obtained from the laboratory displacement tests.

Sigmund and McCaffery (1979) suggested that the determination of relative permeability curves be executed by representing it with two functions, each of which contains one coefficient. The values of these coefficients are calculated for different rocks by employing nonlinear-least-squares optimization procedure.

In this study, estimation of relative permeability curves from two-phase displacement experiments are considered. This is achieved through preparing a package RPP by which relative permeability curves may be determined. Employing numerical techniques solves the mathematical models, which are used to develop the package. The implicit method is used for this purpose.

MATHEMATICAL FORMULATION

The relative permeability curves are to be computed by assuming a function of two parameters, then use is made of optimization technique to calculate the optimum value that fulfill a preassigned conditions.

To estimate relative permeabilities with a parameter estimation approach, an objective function is constructed as a weighted sum of squared differences between the measured and the calculated data from a mathematical model of coreflood experiment. The objective function may be determined from :

$$J = \left[\vec{Y} - \vec{F}(\vec{\beta}) \right]^T W \left[\vec{Y} - \vec{F}(\vec{\beta}) \right] \quad ...(1)$$

where,

J : is the objective function to be minimized;

$\vec{F}(\vec{\beta})$: is the (NPx 1) vector of the unknown parameters;

$\vec{Y}$: is the (N x 1) vector of the observed (measured) data;

W : a (NxN) weighting matrix;

N : total number of data point;

NP: number of parameters; and

T : transpose operation.

The above form of the objective function is adopted by numerous workers(Batycky et al.,1981,Tao and Watson,1984).

For a typical displacement experiment, the measured data consists of the pressure drop a cross the core sample, ΔP^{obs}, and the cumulative volume of displacing phase recovery response, E_R^{obs}

Two mathematical models have been considered; one for imbibition process and the other for drainage process. The quantities, ΔP^{cal} ,and E_R^{cal} may be obtained by solving these models.

FUNCTIONAL REPRESENTATION OF THE RELATIVE PERMEABILITY CURVES

The relative permeability curves for both wetting and nonwetting phases may be written as follow:

$$k_{rnw} = k_{rnwe} \left[\frac{(1 - Se)^{Enw} + b_1(1 - Se)}{1 + b_1} \right] \quad ....(2b)$$

$$Se = \frac{S_w - S_{w\,min}}{S_{w\,max} - S_{w\,min}} \quad ....(2c)$$

in which;

where, a1, b1 are constants .

The values of the constants a1, and b1 were suggested to be 0.01 for computational purpose to linearize the relative permeability

curves as these curves approach zero; but which otherwise do not influence the shapes of curves.

The functional relationships between relative permeabilities and saturation defined by Eqs.2 with their two adjustable saturation exponents, and the values used for the constants a1 and b1 appeared to describe adequately the flow characteristics of the porous media that were studied Sigmund and McCaffery (1979).

Capillary pressure effects are expressed in

$$P_c = P_{cb}\left[\frac{1}{S_{pc}^{(1/\lambda)}} - 1\right] \dots\dots\dots\dots(3a)$$

terms of the following equation[3]:
in which,

$$S_{pc} = \frac{S_w - S_{wr}}{S_{wo} - S_{wr}} \dots\dots\dots\dots\dots(3b)$$

and

$$P_{cb} = \frac{\sigma}{\left(\frac{k}{\phi}\right)^{1/2}} \dots\dots\dots\dots\dots(3c)$$

Theoreatically, λ could have any positive value greater than zero(Brooks and Corey,1964); being small for media having a wide range of pore size and large for media with a relatively uniform pore size.

In the current project and based on Brooks and Corey study it is found that the values of the parameter range from 1.0 to 7.5 for different porous media. In this context an alternative approximation for the value of λ is made, that depends upon the degree of homogeneity for the estimation of λ.

The range of the parameter λ may be subdivided into four categories:
A-Very homogeneous porous media, $\lambda \geq 7.5$
B- Homogeneous porous media, $7.5 > \lambda \geq 5.0$
C- Non - homogeneous porous media, $5.0 > \lambda \geq 3.0$
D- Highly non homogeneous porous media, $3.0 > \lambda \geq 1.7$
Application of these approximations is found to give good results

The end points relative permeabilities

$$k_{rnwe} = \frac{Q_{wi}L\mu_{nw}}{kA(\Delta P_{nw})_{init.}} \dots\dots\dots (4a)$$

$$k_{rwe} = \frac{(\Delta p_{nw})_{init.}}{(\Delta p_{nw})_\infty}\frac{\mu_w}{\mu_{nw}}k_{rnwe} \dots\dots (4b)$$

$$k_{rwe} = \frac{Q_{nwi}\,L\,\mu_{nw}}{kA(\Delta P_{nw})_{init}} \dots\dots\dots\dots (5a)$$

$$k_{rnwe} = \frac{(\Delta P_{nw})_{init.}}{(\Delta P_{nw})_\infty}\frac{\mu_w}{\mu_{nw}}k_{rwe} \dots\dots (5b)$$

k_{rwe} and k_{rnwe} are calculated using Darcy's Law as follow:
1- In the case of imbition.
2- In the case of drainage.
Where,
$(\Delta P_{nw})_{init.}$: is the initial pressure drop;
$(\Delta P_{nw})_\infty$: is the final pressure drop;
Q_{wi} : flow rate of the injected wetting

$$q_{nwi} = \frac{Q_{nwi}}{A\Delta x} \dots\dots\dots\dots\dots(11a)$$

$$q_{wi} = \frac{Q_{wi}}{A\Delta x} \dots\dots\dots\dots\dots(11b)$$

phase;
and Q_{nwi} : flow rate of the injected nonwetting phase.

The values of k_{rwe} and k_{rnwe} are considered as constants in the model calculations.
The values of the relative permeability parameters Ew and Enw which written in Eqs.2 are chosen to minimize Eq.1, by employing Rosenbrock optimization procedure.

IMBIBITION AND DRAINAGE MODELS

The flow equations for unsteady state displacement of incompressible, one-dimensional, two phases fluid flow (which include capillary pressure and ignore gravity effects) may be expressed as(Azaz and Settari,1979,Nolen and Berry,1979,Peaceman,1977).

$$\frac{k}{\mu_w}\frac{\partial}{\partial x}\left[krw\frac{\partial P_w}{\partial x}\right]=\phi\frac{\partial S_w}{\partial t}+q_{wi} \quad\text{...........(6)}$$

$$\frac{k}{\mu_{nw}}\frac{\partial}{\partial x}\left[krw\frac{\partial P_{nw}}{\partial x}\right]=\phi\frac{\partial S_{nw}}{\partial t}+q_{nwi} \quad\text{... (7)}$$

$$P_c = P_{nw} - P_w \qquad\qquad\text{...................... (8)}$$

$$S_w + S_{nw} = 1.0 \qquad\qquad\text{...................... (9)}$$

$$\frac{\partial S_w}{\partial t}+\frac{\partial S_{nw}}{\partial t}=0 \qquad\text{...................... (10)}$$

where,

The derivation of above equations was given by Dake (1978). To solve these equations, the finite difference form of these equations has been used in the imbibition and drainage simulator.

The methods of solution were used for treating the nonlinear terms of Eqs. 6, 7, and 8 are:

1- One - point upstream transmissibility weighting;

2- Fully implicit transmissibilities using chord slope method to estimate derivatives;

3-Newton's–Raphson's method to handle nonlinearities resulting from the use of capillary pressure.

The Boundary and initial conditions for Eqs.6 through 8 have been discussed by Aziz and Settari, and Sigmuned and McCaffery among others. The initial conditions are a uniform distribution of saturation S_{winit}, and pressure P_{winit}. The inlet flow condition at X=0 is constant flow rate for the wetting or

$$\frac{Q_{wo}}{Q_{nwo}}=0\,\text{for}\quad S_{winit}\langle S_w\langle S_{wo}\text{ .... (12a)}$$

nonwetting phases (Q_{wi} or Q_{nwi}) for t>0. The outlet boundary condition at X=L must follow Darcy's law, and at the same time allows the pressure for both fluids in the porous medium to be continuous with the pressure just outside the outlet. In the case of imbibition, Aziz and Settari[1] stated these conditions mathematically at the outlet as:

and

$$\frac{Q_{wo}}{Q_{nwo}}=\frac{\dfrac{k_{rw}}{\mu_w}\cdot\dfrac{\partial P_w}{\partial x}}{\dfrac{k_{rnw}}{\mu_{nw}}\cdot\dfrac{\partial P_{nw}}{\partial x}}\Bigg|_{x=L}\quad\text{for }S_w=S_{wo}\text{ .... (12b)}$$

where, Qwo, Qnwo are the flow rate of the produced wetting and nonwetting phases respectively.

Where the outlet breakthrough of the wetting phase occurs when the wetting phase saturation increases from its initial value S_{winit}, to the value S_{wo} corresponding to zero capillary pressure. In the case of drainage, S_{wo} remains constant until the value (1- S_{winit}) is

$$\Delta P_D = \frac{\Delta P_{nw}}{(\Delta P_{nw})_{init}}\,\text{X}100\text{......................(18)}$$

reached at
the outlet face, which represent the maximum nonwetting phase saturation. Thus, the outlet condition is:

$$\frac{Q_{wo}}{Q_{nwo}}=\frac{\dfrac{k_{rw}}{\mu_w}\dfrac{\partial P_w}{\partial x}}{\dfrac{k_{rnw}}{\mu_{nw}}\dfrac{\partial P_{nw}}{\partial x}}\Bigg|_{x=L}\quad\text{for }S_{nw}=(1-S_{winit})\text{.....(13)}$$

The above conditions embodied the frontal advance of fluid- flow concept, which was suggested by Buckly and Leverett (1942)

The curved sides of the simulated core sample are assigned no flow boundaries, as actually is treated in the simulator models of the laboratory tests.

A grid size of $\Delta x = L / 40$ was used in all simulations. The values of the time step (Δt) that were used are determined from the equation:

$$\Delta t = \frac{0.01\,\phi\,AL(S_{wmax}-S_{wmin})}{Q_{mi}}\text{ .... (14)}$$

Moreover, material balance error (MBE) check is made at the end of each iteration to confirm the validity of the model, MBE'S values obtained for wetting and nonwetting phases are:

1- For imbibition model

$$|MBEW-1|\langle\,5.0\times10^{-5}$$

and

$$|MBENW-1|\langle\,2.0\times10^{-4}$$

2- For drainage model

$$|MBEW - 1| \langle\ 6.0 \times 10^{-6}$$

$$and$$

$$|MBENW - 1| \langle\ 4.0 \times 10^{-6}$$

The above values confirm the validity of the imbibition and drainage models.

The flow chart of the relative permeability package RPP is given in Appendix.

EVALUATION OF THE RELATIVE PERMEABILITY PACKAGE(RPP)

The dimensionless cumulative injection Qi, the recovery response E_R, and the dimensionless pressure response ΔP_D for both the imbibition and drainage cases are required for comparison purpose. These may be calculated at the end of each time step from the following equations:

$$Q_i = \frac{tQ_{im}|_{x=0}}{\varphi AL(S_{w\,max} - S_{w\,min})} \times 100 \ \dots\dots \ (15)$$

Recovery response is define for imbibition as:

$$E_R = \left[\frac{S_{w,av} - S_{w\,min}}{S_{w\,max} - S_{w\,min}} \right] \times 100 \ \dots\dots\dots \ (16a)$$

and for drainage as:

$$E_R = \left[1 - \frac{S_{w,av} - S_{w\,min}}{S_{w\,max} - S_{w\,min}} \right] \times 100 \ \dots\dots \ (16b)$$

The dimensionless pressure response for both imbibition and drainage are calculated from the following equations:

$$\Delta P_D = \frac{P_{nw}(0,t) - P_{nw}(L,t)}{P_{nw}(0,0^+) - P_{nw}(L,0)} \times 100 \dots\dots\dots(17)$$

Four runs were made on example problems which were presented by Sigmund and McCafgfery (1979), and Batycky et al. (1981), to confirm the reliability of the Resenbrock optimization procedure for obtaining the parameters Ew and Enw rather than the least - squares fitting procedure, which was adopted by a number of workers in this field.(Watson et al.,1988,Yong and Watson,1991).

In all the four runs bad initial estimates were used for the parameters Ew and Enw to confirm the efficiency of the RPP in computing the optimum values of these parameters.

In the subsequent sections the four-displacement case are discussed. The first case is the imbibition displacement for Swan Hills core, (limestone core type). The second is the drainage displacement for Swan Hills core. The third case is the imbibition displacement for Rainbow core, (dolomite core type); and the fourth case is the imbibition displacement for core sample of Carig, 1971.

CASE1-IMBIBITION DISPLACEMENT FOR SWAN HILLS CORE

Initial estimates of the parameters, Ew and Enw and initial step size were introduced to the RPP, the RPP will give the optimum values of these parameters. The preceding descriptions are summarized in Table 2.

Core flood parameters for this case are given in Table 1. Fig.1 shows the observed dimensionless pressure drop ΔP_D, and recovery response E_R, data obtained from the experimental work, as functions of the dimensionless cumulative injection, Qi compared with simulator - calculated values which are obtained by using the Rosenbrock optimization procedure which is listed in Table 2 .The simulated values of Ew and Enw determined from the values are seen to match the experimental results remarkably excellent. The two parameters relative permeability curves characterized by the values of Ew and Enw which are given in Table 2 is shown in Fig.2, for both the imbibition and the drainage displacement (case 2).

The optimization constrains used in this case for the parameters Ew and Enw in the RPP are [0.1 ≤ Ew ≤8] and [1≤ Enw ≤10.5].

Table (1)-Core Flood Parameters

Parameters	CASE 1	CASE 2	CASE 3	CASE4
	Imbibition (Swan Hills Core)	Draina-ge (Rainb-ow Core)	Imbibitio-n (Rainbo-w Core)	Imbib-ition from Carig, 1971
S_{wmax}	0.727	0.727	0.608	0.625
S_{wmin}	0.265	0.199	0.192	0.476
S_{wr}	0.150	0.150	0.150	0.430
$\emptyset$	0.121	0.121	0.029	0.215
A, ft^2	0.086	0.086	0.065	0.021
L, ft	0.727	0.727	0.573	0.826
$Qi, ft^3/day$	0.105	0.105	0.080	0.010
$(\Delta P_{nw})_{init,}$ Psi	29	64.50	53.00	18.42
$(\Delta P_{nw})_{\infty,}$ Psi	65.0	26.50	48.70	
P_{cb}, Psi	4.0	33.40	About 0	0.984
k, md	10.10	10.10	4.070	476.0
$\mu_{w,}$ cp	1.050	1.050	1.050	0.888
$\mu_{nw,}$ cp	1.410	1.410	1.41	0.501
λ	3.10	3.10	2.10	3.00
No.of grids	40.0	40.0	40.0	40.0

CASE 2- DRAINAGE DISPLACEMENT FOR SWAN HILLS CORE

The coreflood parameters necessary for the calculation are given in Table1. Fig.3 shows the comparison between the observed dimensionless pressure drop and recovery response data with those calculated by the simulator approach at the optimum values of Ew and Enw were shown in Table2.

The simulated values are seen to match the experimental data reasonably well, with exception of the pressure at the end of the flood. These differences in the latter situation may be attributed to calculate the end - point relative permeability to the nonwetting pahase. The relative permeability curves as a function of wetting phase saturation is shown in Fig.2, where the comparison between drainage and imbibition values (case1), is made. The wide divergence between the relative permeability curves makes it mandatory to choose the correct one for predicting flooding behavior. Because the wetting and nonwetting phases relative permeability is history dependent, wetting phase flood performance should be predicted more accurately by unsteady-state.

The optimization constrained used in this case for the parameters Ew and Enw in the RPP are [$0.3 \leq$ Ew≤ 8] and [$1 \leq$ Enw ≤ 10.5], respectively.

CASE 3- IMBIBITION DISPLACEMENT FOR RAINBOW CORE

In this case the analysis of transient response curves for displacement of nonwetting by wetting phase in a heterogeneous, water-wet, Rainbow core is considered

Core-flood parameters for this case are given in Table1. Fig 4 shows a comparison between the computed dimension pressure drop and recovery response with the observed results using the values of Ew and Enw which are given in Table2; as determined by the Rosenbrock procedure. Initial estimates of Ew= 2.0 and Enw =3.5 which are bad relative to the initial estimates that were given by Sigmund and McCaffery (Ew = 0.5, Enw = 3.0) for least - squares procedure, were deliberately chosen to confirm the efficiency and superiority of the developed optimization procedure than that development by Sigmund and Mc Caffery.

The last procedure requires several preliminary simulator runs to make good initial guesses of the parameters Ew and Enw, which are necessary for the Gauss - Newton nonlinear least- squares that was a dopted by Sigmund and Mc Caffery.

The relative permeability curves characterized by the Ew and Enw given in Table2 are shown in Fig 5. The observed values are seen to be less than simulated values before breakthrough, this effect is due to the high degree of heterogeneity. Therefore, the application of the Johnson - Bossler - Naumann method to the data plotted in Fig.4 is impossible because of the high nonlinearity before breakthrough .

The concave shape presented for the wetting phase relative permeability in Fig.5 is a consequence of having only a single curvature presenting the relative permeability curves in Eqs. 2. This could be overcome by using a more general relationship between saturation and relative permeability or by employing a lower value of Swr in the simulator such as would be achieved experimentally with a high-rate drainage displacement.

Table(2)-Parameter-Estimation Results		
CASE-1	**Enw**	**Ew**
Initial guesses	2.5	1.9
Initial step sizes	0.005	0.001
Final optimum values	3.059	2.227
Number of the objective function evalution	36	
Remainder of the objective function	215.8	
CASE-2	**Enw**	**Ew**
Initial guesses	1.9	4.0
Initial step sizes	0.0008	0.05
Final optimum values	2.96	5.62
Number of the objective function evalution	40	
Remainder of the objective function	25.69	
CASE-3	**Enw**	**Ew**
Initial guesses	3.5	2.0
Initial step sizes	0.001	0.09
Final optimum values	2.96	0.48
Number of the objective function evalution	31	
Remainder of the objective function	510.4	
CASE-4	**Enw**	**Ew**
Initial guesses	4.0	1.0
Initial step sizes	0.1	0.01
Final optimum values	7.759	1.525
Number of the objective function evalution	10	
Remainder of the objective function	26.14	

CASE 4- IMBIBITION DISPLACEMENT FOR PROBLEM GIVEN BY BATYCKY ETAL. (1981)

In This case, the core properties data which were presented in Batycky et al. (1981) are considered.

By employing RPP conformable results of relative permeability curves have been obtained. Fig.6 illustrates the response curves for Ew = 1.525 and Enw = 7.759, the other core - flood parameters are given in Table1. The response curves of the results obtained

from RPP are seen to match the experimental data reasonably well with the exception of the pressure response before breakthrough. This problem was treated in RPP by using weighting factor. The choice of this weighting scheme partly reflects the spacing of data.

Fig.7 shows the relative permeability curves of this case. The initial guesses of the parameters Ew and Enw, and initial step sizes were presented in Table 2.

The constrained used in this case for the parameters Ew and Enw in the RPP are [0.1≤ Ew≤15] and [0.1 ≤Enw ≤15].

CONCLUSIONS

The following conclusions are drawn from this study

1- The RPP can be adopted in the two-phase relative permeability curves computations, for the unsteady-state data, with high reliability.

2- The parameter estimation approach, which adopted in this work, overcomes significant limitations of the classic calculation procedure of the Johnson - Bossler - Naumann method and related methods.

3- Rosenbrock optimization procedure that has been utilized in this study is more efficient than the Gauss-Newton.Nonlinear least squares technique that was used by Sigmund and Mc Caffery.

4- The application of the RPP give an occasion to calculate relative permeability curves for heterogeneous cores rather than the explicit methods, which applied for homogeneous cores only.

NOMENCLATURE

A = cross sectional area of the core sample, L^2

E_R = recovery efficiency, percent of movable fluid

recovery, dimensionless

E_{nw} = parameter in nonwetting phase relative perme-

ability expression, dimensionless

E_w = parameter in wetting phase relative permeability

Expression, dimensionless

k = absolute permeability, L^2

k_r = relative permeability, dimensionless

k_{rwe}= end-point relative permeability of wetting phase, dimensionless

k_{rnwe}=end-point relative permeability of nonwetting
        phase, dimensionless

L = length of the core sample, ft.

P_{cb} = capillary pressure scaling coefficient, m/L^2

P_c = capillary pressure, m/L^2

ΔP_D = dimensionless pressure drop across core

ΔP= transient pressure drop across core, m/L^2

P_{nw}= pressure in nonwetting phase, m/L^2

P_w= pressure in wetting phase, m/L^2

Q = flow rate, L^3/t

q = flow rate, $1/t$

Qi = dimensionless cumulative injection

R_D = dimensionless measure of viscous- to-capillary force ratio.

Se = saturation, normalized with respect to Sw_{min} and $Sw_{max.}$

S_{pc}= stauration, dimensionless normalized with respect to S_{wo} and S_{wr}

S_w = wetting - phase saturation, dimensioless.

S_{nw} = nonwetting - phase saturation, dimensionless

S_{wo}= wetting - phase saturation corresponding to zero capillary
        pressure, dimensionless

S_{winit}=initial wetting- phase saturation, dimensionless

S_{wmin}= is the minimum wetting phase saturation established by a
        drainage displacement, dimensionless

S_{wr} =irreducible wetting phase saturation, dimensionless

S_{wmax}= is the maximum wetting phase saturation established by an
        imbibition displacement, dimensionless

$S_{w,av}$ =average wetting phase saturation, dimensionless

t = time, t

Δt =time increment, t

x= distance, L

Δx = distance increment, L

ϕ = porosity, dimensionless

λ = measure of pore-size distribution, dimensionless

μ = viscosity, m/Lt

σ = interfacial tension, m/L^2

SUBSCRIPTS

nw =nonwetting phase

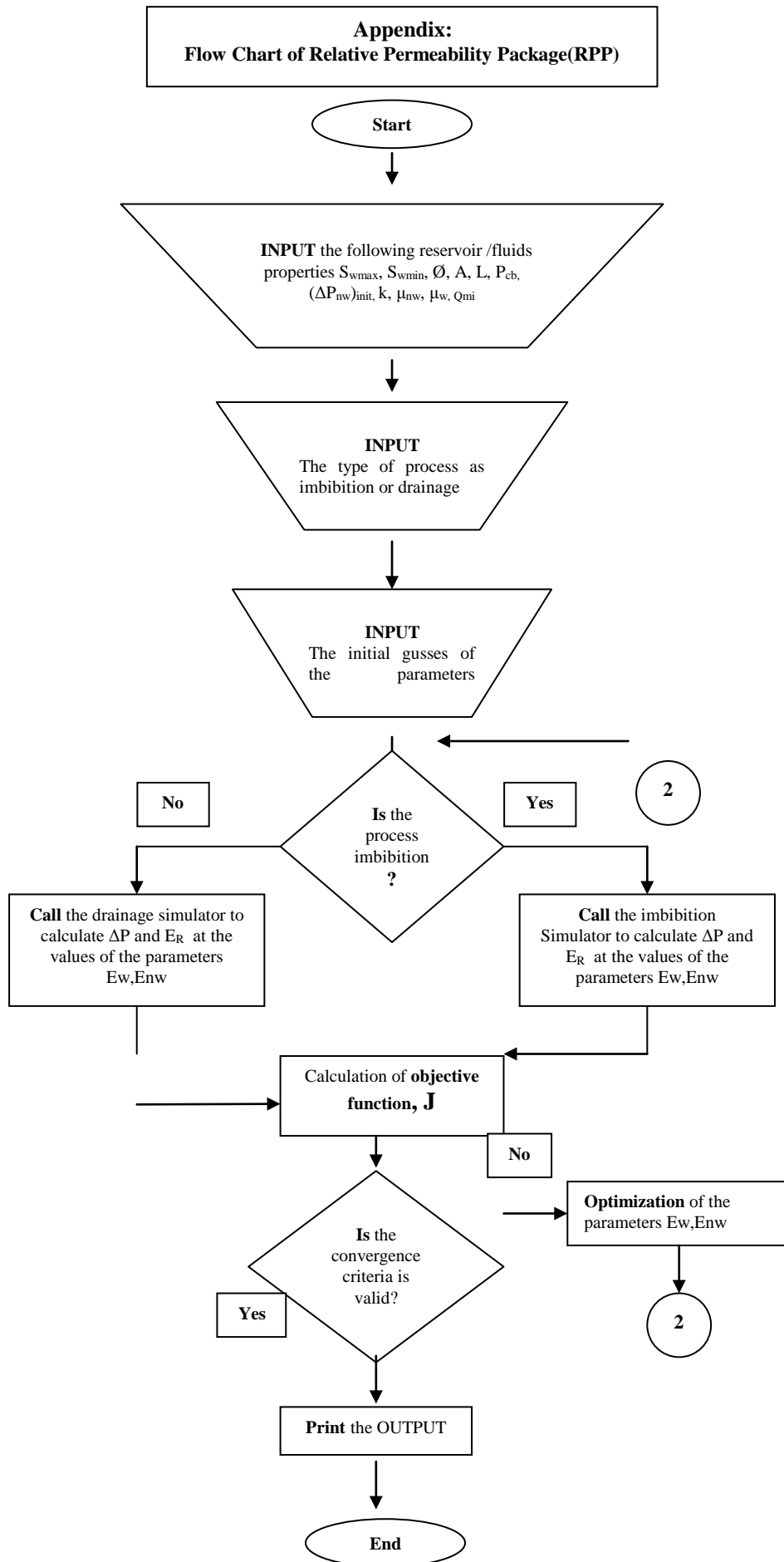m = wetting or nonwetting phase

w = wetting phase

SUPERSCRIPTS

cal.=calculated data value

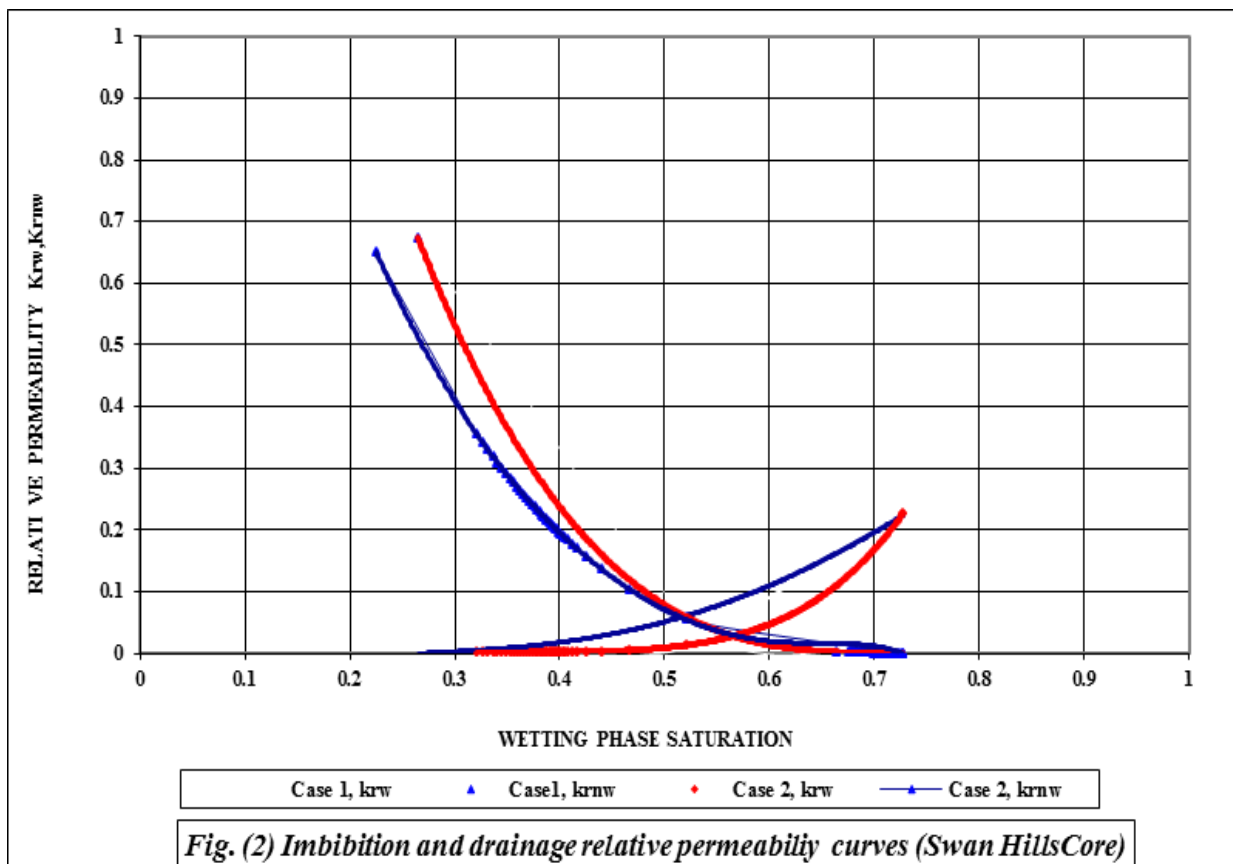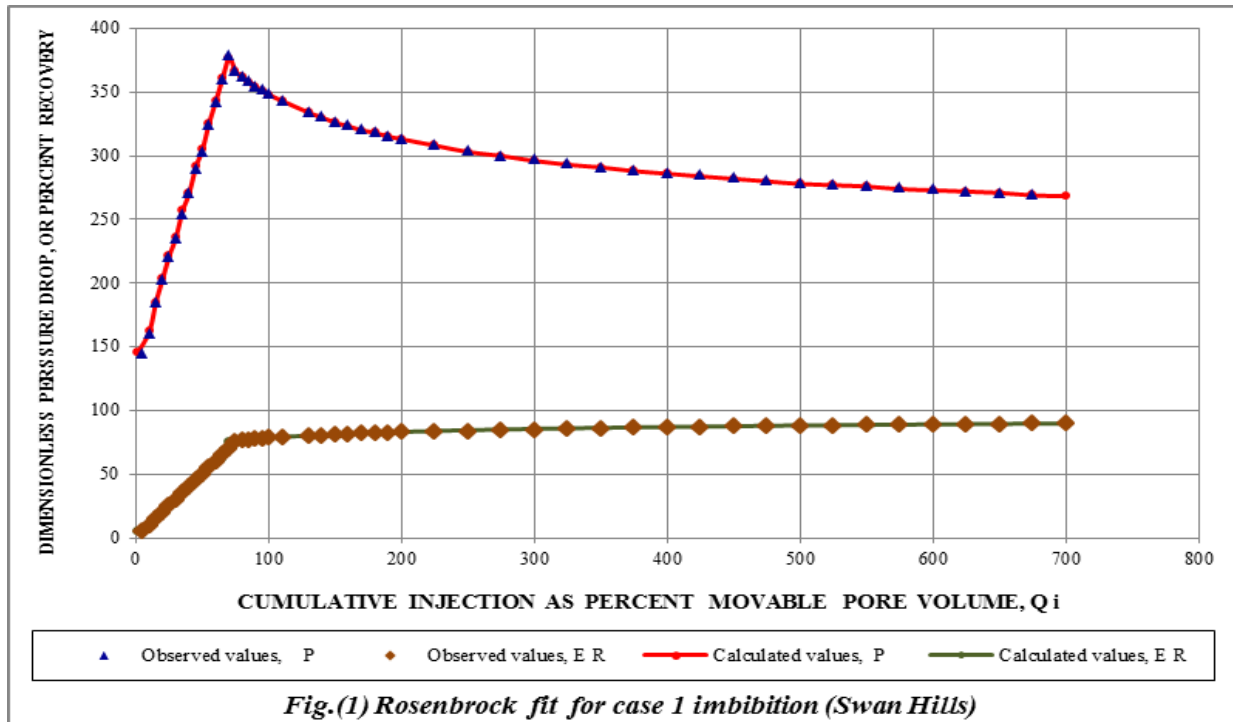obs.=observed or measured data value
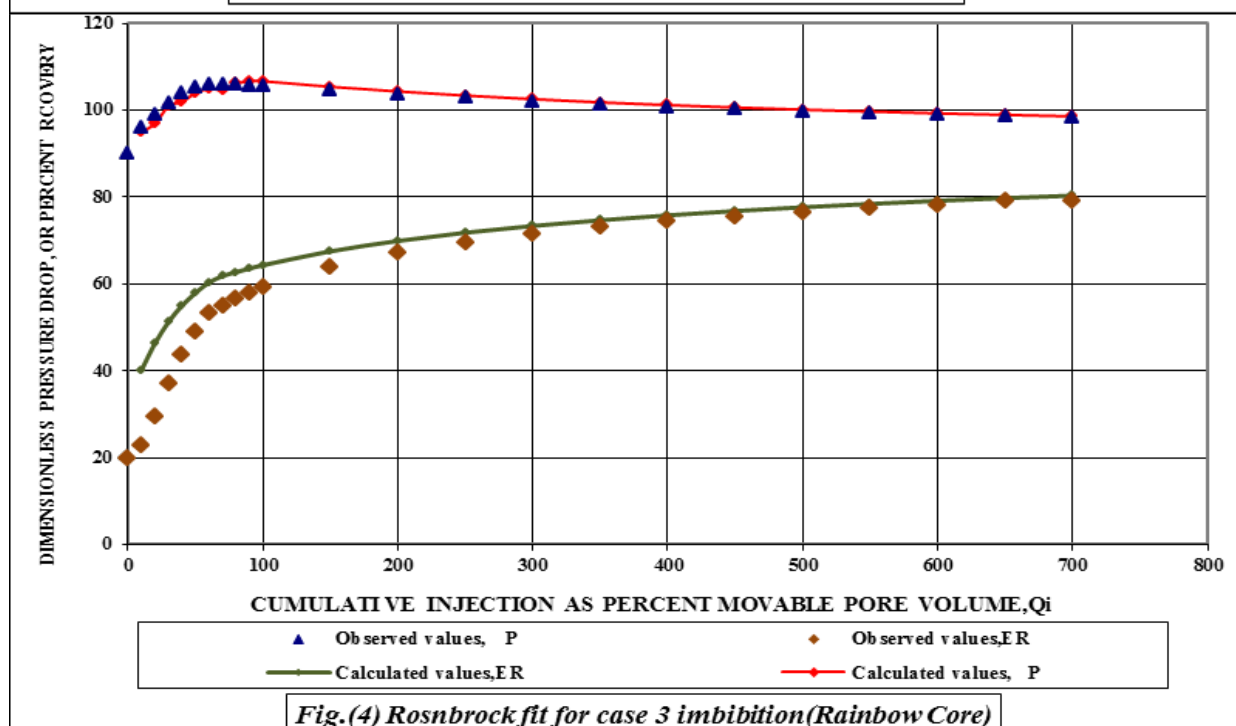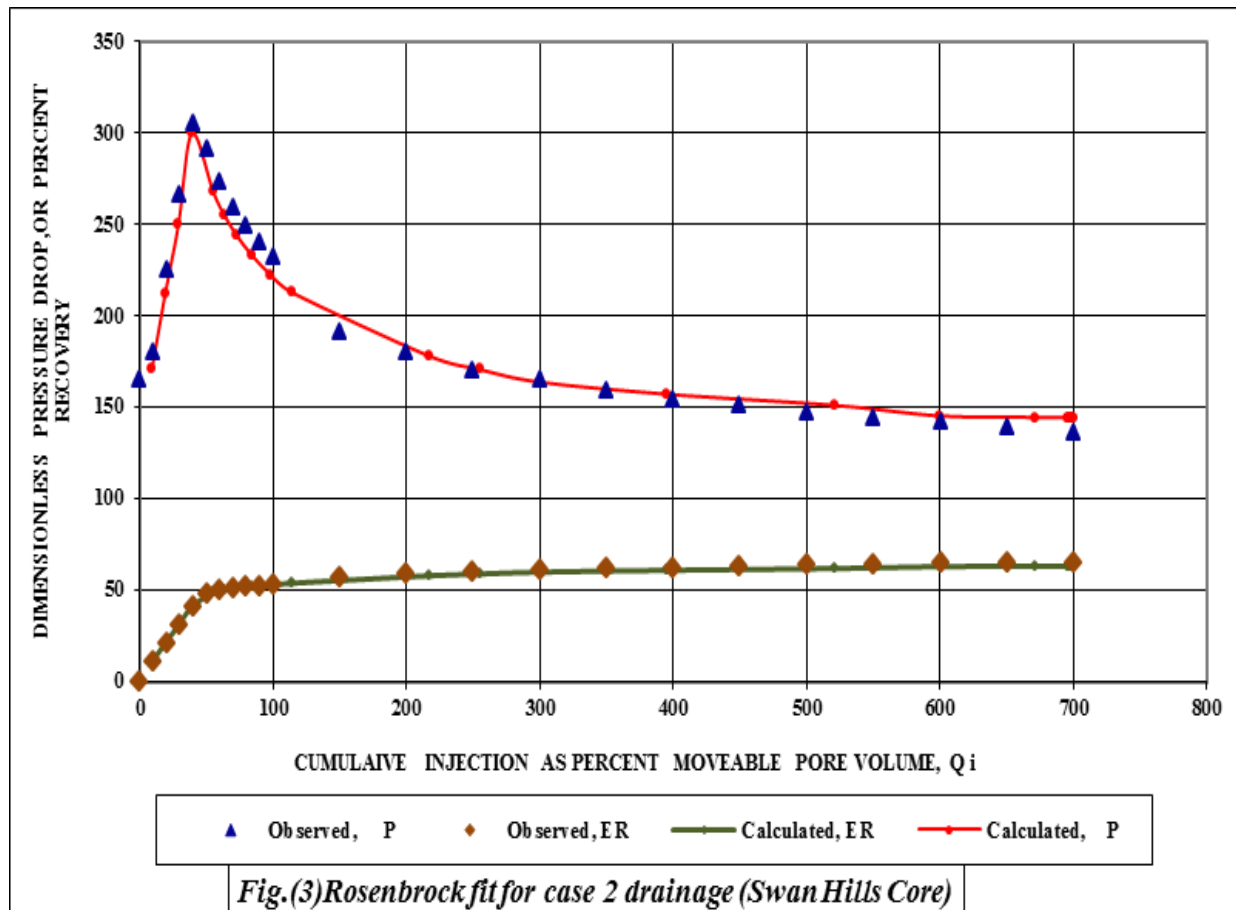
$\rightarrow$ = vector notation

REFERENCES

Aziz, K. and Settari, A. : Petroleum Reservoir Simulation. Applied Science Publishers LTD, London (1979).

Archer, J.S. and Wong, S.W.: "Use of a Reservoir Simulator to interpret Laboratory Water flood Data, "SPEJ (Dec. 1973), PP. 343-347

Brooks, R.H. and Corey, A.T.: "Hydranlic Properties of porous Media," Hydrology Papers, Colorado State U., Colorado Springs (March 1964) No.3.

Buckley, S.E. and Levertt, M.C.: "Mechanism of Fluid Displacement in Sands, "Trans., AIME (1942) 146, PP.107 -116.

Batycky, J.R. etal: "Interpreting Relative Permeability and Wettability From Unsteady - State Displacement Measurements,"SPEJ (June 1981), PP. 296-308.

Blair, P.M. and Weinaug, C.F.: "Solution of Two Phase Flow Problems using Implicit Difference Equations, "SPEJ (Dec. 1969), PP. 417-424.

Carig, F.F.Jr: The Reservoir Engineering Aspects of Waterflooding, Monograph Series, SPE of AIME, Dallas (1971) 3.

Dake, L.P.: Fundamentals of Reservoir Engineering, Elsevier Scientific Publishing Co., Amsterdam (1978).

Johnson, E.F., Bosseler, D.P. and Naumann, V.O.: " Calculation of Relative Permeability from Displacement Experiments," Trans, AIME (1959) 216, PP.370 - 372.
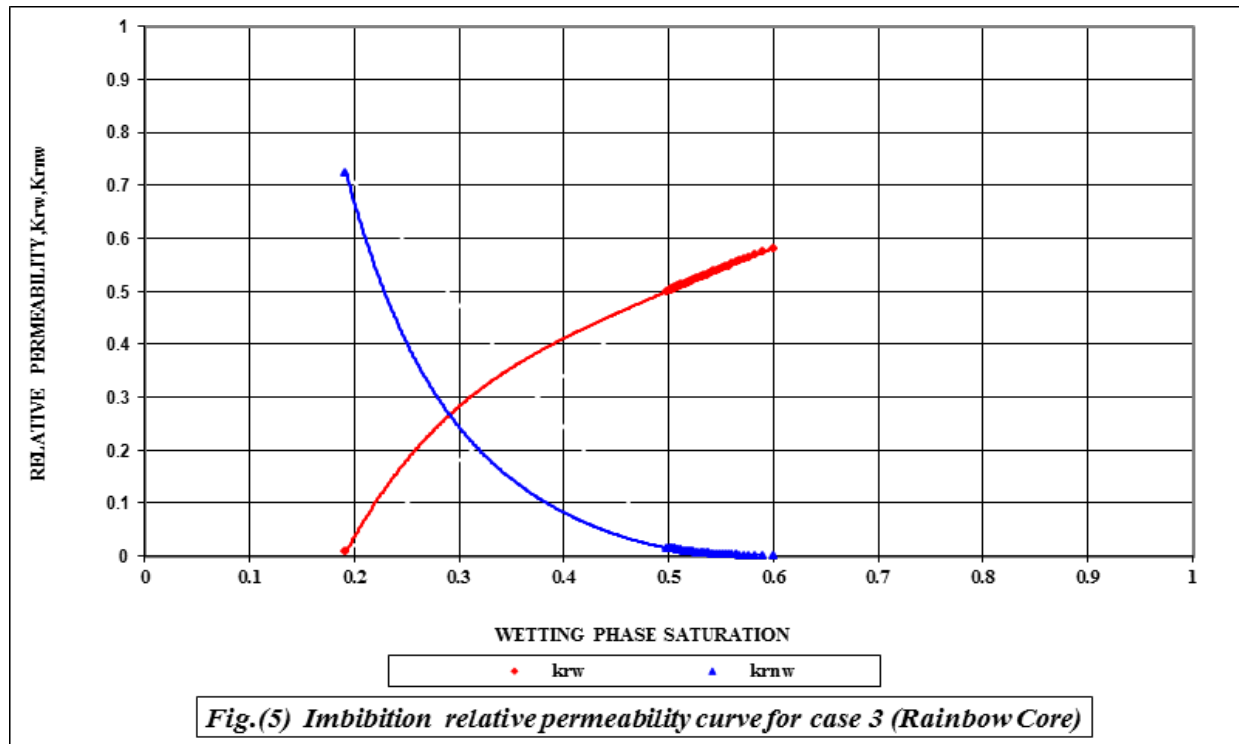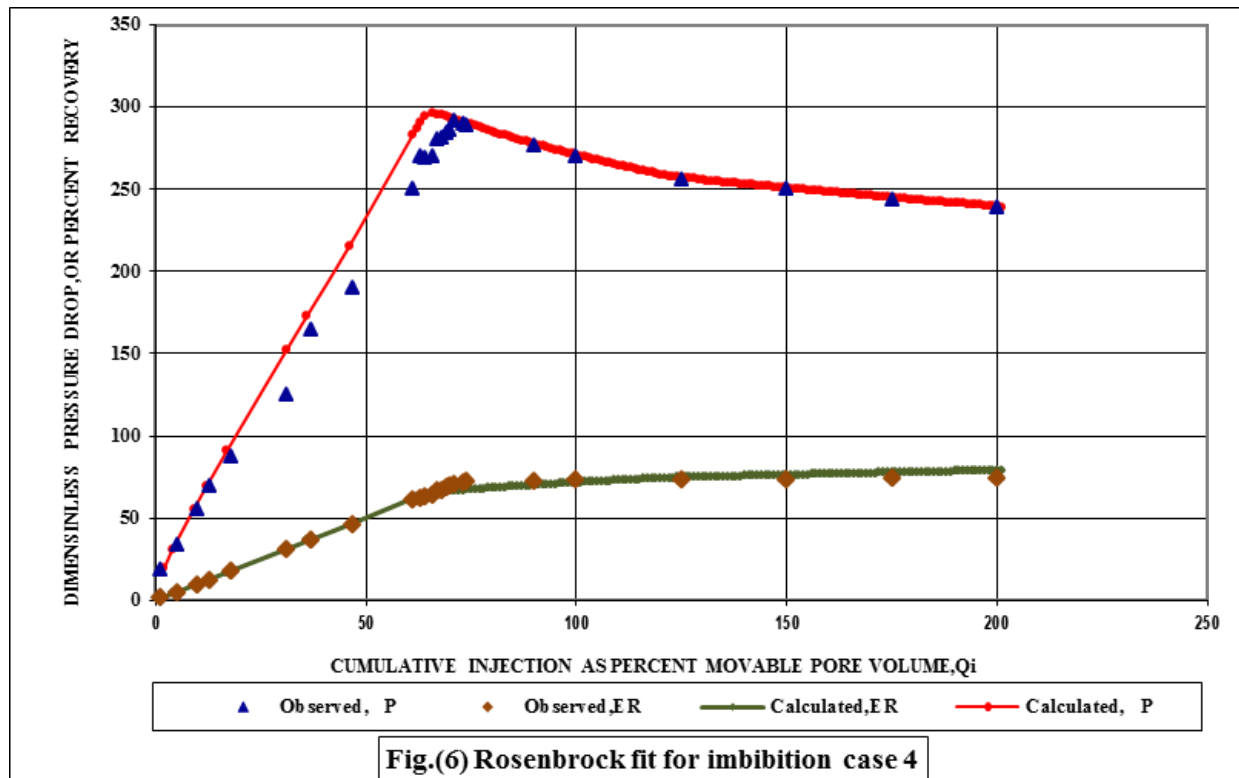
Jones, S.C. and Roszelle, W.O.: "Graphical Techniques for Determining Relative Permeability from Displacement Experiments," JPT (May 1978), PP.807-817.

Kerig, P.D. and Watson, A.T.: "A new Algorithm for Estimating Relative Permeability from Displacement Experiments," SPERE (Feb. 1987), PP.103-112.

Nolen, J.S. and Berry, D.W.:"Tests of the Stability and Time – Step Sensitivity of Semi-Implicit Reservoir Simulation Techniques," SPEJ (June 1972), PP. 253-266.

Peaceman, D.W.: Fundamentals of Numerical Reservoir Simulation. Elsevier Scientific Publishing Co., Amsterdam (1977).

Sigmund, P.M. and McCaffery, F.G.:"An Improved Un-steady State Procedure for Determining the Relative Permeability Characteristics of Heterogeneous Porous Media," SPEJ (Feb. 1979), PP. 15-28.

Tao, T.M. and Watson, A.T: "Accuracy of JBN Estimates of Relative Permeability: Part 1-Error Analysis," SPEJ (April 1984), PP. 209-214.

Toa, T.M. and Watson, A.T.: "Accuracy of JBN Estimates of Relative Permeability: Part 2- Algorithms, "SPEJ (April 1984), PP. 215- 224.

Welge, H.J.: "A Simplified Method for Computing Oil Recovery by Gas or Water Drive," Trans., AIME (1952) 195, PP.91-98.

Watson, A.T. et al: "A Regression - Based Method for Estimating Relative Permeabilities from Displacement Experiments," SPERE (Aug. 1988), PP. 953- 958.

Yang, P.H. and Watson, A.T.: " A Bayesion Methodology for Estimating Relative Permeability Curves," SPERE (May 1991), PP. 259- 265.

Appendix:
Flow Chart of Relative Permeability Package(RPP)

Start

INPUT the following reservoir /fluids properties S_{wmax}, S_{wmin}, $\emptyset$, A, L, P_{cb}, $(\Delta P_{nw})_{init}$, k, μ_{nw}, μ_{w}, Q_{mi}

INPUT
The type of process as imbibition or drainage

INPUT
The initial gusses of the   parameters

2

No   **Is** the process imbibition **?**   Yes

Call the drainage simulator to calculate ΔP and E_R at the values of the parameters Ew,Enw

Call the imbibition Simulator to calculate ΔP and E_R at the values of the parameters Ew,Enw

Calculation of **objective function, J**

No

Optimization of the parameters Ew,Enw

Is the convergence criteria is valid?

Yes

2

Print the OUTPUT

End

509

Fig.(1) Rosenbrock fit for case 1 imbibition (Swan Hills)

Fig. (2) Imbibition and drainage relative permeabiliy curves (Swan HillsCore)

Fig.(3)Rosenbrock fit for case 2 drainage (Swan Hills Core)

Fig.(4) Rosnbrock fit for case 3 imbibition(Rainbow Core)

Fig.(5) Imbibition relative permeability curve for case 3 (Rainbow Core)

Fig.(6) Rosenbrock fit for imbibition case 4

Comparison of the Combining Methods Used In Space Diversity

Ashwaq A. ALjanaby

Electronic and Communications Dept.

Baghdad University/Engineering Collage

ashwaq.aljanaby @yahoo.com

ABSTRACT

The basic concept of diversity; where two or more inputs at the receiver are used to get uncorrelated signals. The aim of this paper is an attempt to compare some possible combinations of diversity reception and MLSE detection techniques. Various diversity combining techniques can be distinguished: **Equal Gain Combining (EGC), Maximal Ratio Combining (MRC), Selection Combining and Selection Switching Combining (SS).**The simulation results shows that the **MRC** give better performance than the other types of combining (about 1 dB compare with **EGC** and 2.5~3 dB compare with **selection and selection switching combining**).

مقارنة لطرق الجمع المستخدمة مع نظام هوائي لمستقبل متنوع

اشواق عباس الجنابي

مدرس مساعد

كلية الهندسة / جامعة بغداد /قسم الالكترونيك والاتصالات

الخلاصة:

مبدأ الهوائي المتنوع هو إدخال إشارتين او اكثر الى المستقبل لتحصيل اشارات غير مرتبطة. الهدف من هذا البحث هو محاولة لمقارنة بعض طرق التجميع للاستقبال المتنوع مع تقنيات الكشف (MLSE) . انواع مختلفة من طرق التجميع ممكن ان تميز منها : الجمع المتساوي الربح، الجمع للنسبة الاعلى، الجمع الاختياري وجمع تحويل الاختيار. نتائج المحاكاة بينت بان طريقة الجمع للنسبة الاعلى تعطي اداءا افضل من باقي الانواع (حوالي 1dB مقارنة مع الجمع المتساوي الربح و dB 3~2.5 مقارنة مع الجمع الاختياري وجمع تحويل الاختيار).

1-INTRODUCTION:

IN a typical mobile radio environment, the communication between the cell site and mobile is established via many paths, very often without the direct one. This is because the direct path is obstructed by buildings and other obstacles. The resultant signal at the receiving antenna is characterized by deep frequency-selective fades with fading rates dependent on vehicle speed. An intersymbol interference resulting from the multipath propagation conditions arises, which for a global system for mobile communication (GSM)-like system, spans a few signaling intervals. In modern time division multiple-access (TDMA) digital mobile radio systems, data signals are transmitted in bursts of length equal to a few hundred bits, which include training sequence. In this case, a maximum-likelihood sequence-estimation (MLSE) receiver is preferred, but when exposed to deep fades (up to 40-dB notch depth), it can fail as well. Space diversity can improve its performance considerably. In this technique, several antennas, which are separated in space, are used in order to process a few versions of the received signal. When the antennas are spaced appropriately, the received signals can be considered as statistically independent. Therefore, there is a good chance that not all of them will fade at the same time.

Most of the papers devoted to diversity reception with equalization of signals transmitted on fading channels deal with linear or decision-feedback equalizers (P. Balaban and J. Salz, 1992 ,N. W. K. Lo, D. D. Falconer, and A. U. H. Sheikh, , 1991). Recently, MLSE diversity reception has been considered for digital mobile radio independently by a few authors (W.-H. Sheen and G. L. Stüber, 1991, P. Jung, B. Steiner, and Y. Ma, 1994, Q. Liu and Y. Wan, 1992, R. Krenz and K. Wesolowski, 1994). Sheen and Stüber derived the metrics and analyzed the performance of a receiver using a combined MLSE equalizer/decoder and diversity reception for multipath Rayleigh fading channels.They also derived a new upper bound on the bit error probability for such cases. In Jung and Steiner analyzed similar receivers deriving the metrics for the Viterbi algorithm (VA) realizing the optimum maximum-ratio combining of the diversity branch signals and its suboptimum combining versions such as equal-gain and selection combining. In the optimum case, the normalized metrics on the channel state trellis resulting from different diversity paths are weighted by the energy-per-bit to noise power density ratio characterizing the selected diversity path. In a similar receiver aimed particularly to GSM applications was considered. In [(Jung and Nasshan,1994) presented potential gains resulting from two-antenna diversity and coherent receiver for DCS 1800.In (Jung, 1995) demonstrated that the suboptimum detector applied jointly with diversity in a GSM-like mobile radio system performs similarly to the ML detector. Finally, one has to admit the original work of (Mogensen,1993) in which, due to the GSM system limitations, he proposed application of post detection soft-decision combining in the base station for an uplink and transmitter diversity, resulting in an intentional time spread used in the base station for a downlink. However, relatively less attention has been paid to the comparison of the optimum -diversity receivers employing the ML detector with other much simpler methods of combining the diversity branch signals when the ML detector is used.

2- DIVERSITY TECHNIQUES:

Diversity techniques can be used in wireless communications systems to improve the performance over a fading radio channel. Here receiver is provided with multiple copies of the same information signal which are transmitted over two or more real or virtual communication channels. Thus the basic idea of diversity is repetition or redundancy of information. In virtually all the applications, the diversity decisions are made by the receiver and are unknown to the transmitter (Vaughan, R. G., 1990, Neelam Srivastava, 2010).

Typically, the diversity receiver is used in the base station instead of the mobile station, because the cost of the diversity combiner can be high, especially if multiple receivers are necessary. Also, the power output of the mobile station is limited by the battery. Handset transmitters usually lower power than mobile mounted transmitters to preserve battery life and reduce radiation into the human body. The base station, however, can increase its power output or antenna height to improve the coverage to a mobile station.

There are several different kinds of diversity

techniques which are commonly employed in wireless communication systems :(Neelam Srivastava, 2010, Vijay K. Garg, 2007)

2.1 Space diversity

In Space diversity, there are multiple receiving antennas placed at different spatial locations, resulting in different (possibly independent) received signals.

2.2 Frequency diversity

The same information signal is transmitted on different carriers, the frequency separation between them being at least the coherence bandwidth.

2.3 Time diversity

The information signal is transmitted repeatedly in time at regularly intervals. The separation between the transmit times should be greater than the coherence time. The time interval depends on the fading rate, and increases with the decrease in the rate of fading.

2.4 Polarization diversity

Here, the electric and magnetic fields of the signal carrying the information are modified and many such signals are used to send the same information Thus orthogonal type of polarization is obtained. It enables detection of smaller radar cross-section (RCS) targets, and avoids the physical, mathematical, and engineering challenges of time of- arrival coherent combining.

2.5 Angle diversity

The scattering of signals from transmitter to receiver generates received signals from different directions that are uncorrelated with each other. Thus, two or more directional antennas can be pointed in different directions at the receiving site and provide signals for a combiner. This scheme may be applied at the base station or at the Mobile unit.

2.6 Path diversity

In code division multiple access (CDMA) systems, the use of direct sequence spread spectrum modulation allows the desired signal to be transmitted over a frequency bandwidth much larger than the channel coherence bandwidth. The spread spectrum signal can resolve in multipath signal components provided the path delays are separated by at least one chip period. A Rake receiver can separate the received signal components from different propagation paths by using code correlation and can then combine them constructively.

3- COMBINING METHODS FOR SPACE DIVERSITY:

The idea of diversity is to combine several copies of the transmitted signal, which undergo independent fading, to increase the overall received power. Different types of diversity call for different combining methods. The goal of a combiner is to improve the noise performance of the system. Here, we review several common diversity combining methods :(Mahrotra, A. ,1994,Neelam Srivastava, 2010,Vijay K. Garg, 2007)..

3.1 Selection Combiner

In this case, the diversity combiner selects the branch that instantaneously has the highest SNR (see Figure 1). We assume that the signal received by each diversity branch is statistically independent of the signals in other branches and is Rayleigh distributed with equal mean signal power P_o. The probability density function of the signal envelope, on branch i, is given as

$$P(r_i) = \frac{r_i}{P_o} e^{-r_i^2/(2P_o)} \qquad (1)$$

Where $2P_o$ = mean-square signal power per branch : $<r_i^2>$ and r_i^2 = instantaneous power in the ith branch.Assuming that the signal in each branch has the same mean, the probability that the SNR on any branch is less than or equal to any given value ζ_g is

$$P[\zeta_i \le \zeta_g] = \int_0^{\zeta_g} P(\zeta_i)d\zeta_i = 1 - e^{-(\zeta_g/\zeta_o)} \qquad (2)$$

Therefore, the probability that the SNRs in all branches are simultaneously less than or equal to ζ_g is given by:

$$P_{M(\zeta_g)} = P[\zeta_1,\zeta_2,...,\zeta_M \le \zeta_g] = \left[1 - e^{-(\zeta_g/\zeta_o)}\right]^M \qquad (3)$$

The probability that at least one branch will exceed the given SNR value of ζ_g is given by:

$$P(at\ least\ one\ branch \ge \zeta_g) = 1 - P_{M(\zeta_g)} \qquad (4)$$

The percentage of time the instantaneous output SNR ζ_M is below or equal to the given value, ζ_g is equal to P ($\zeta_M \le \zeta_g$).

3.2 Switched Combiner

The disadvantage with selection combining is that the combiner must be able to monitor all M branches simultaneously. This requires M independent receivers which are expensive and complicated; an alternative is to use switched combining. In this case only one receiver is needed, and it is only switched between branches when the SNR on the current branch is lower than some predefined threshold value ζ_g (see Figure 2). This is called a switch and stay combiner.

The performance of a switch combiner is less than that in selection combining, since unused branches may have SNRs higher than the current branch if the current SNR exceeds the threshold. The threshold therefore has to be carefully selected in relation to the mean power on each branch, which must also be estimated with sufficient accuracy.

3.3 Maximal Ratio Combiner

In maximal ratio combining, M signals are weighted proportionally to their signal- to-noise ratios and then summed (see Figure 3).

$$r_M = \sum_{i=1}^{M} a_i\, r_{i(t)} \qquad (5)$$

Where; a_i = weight of ith branch, M = number of branches. Since noise in each branch is weighted according to noise power,

$$\overline{n_j^2(t)} = \sum_{j=1}^{M}\sum_{i=1}^{M} a_i a_j\ \overline{n_{i(t)}n_{j(t)}} \qquad (6)$$

$$N_T = \sum_{i=1}^{M} a_i^2\ \overline{n_i^2(t)} = \sum_{i=1}^{M} a_i^2\, N_i \qquad (7)$$

Where: N_T = average noise power $\overline{n_i^2(t)} = 2N_i$, the SNR at the Output is given as:

$$\zeta_M = \frac{1}{2} \cdot \frac{\left|\sum_{i=1}^{M} a_i\, r_{i(t)}\right|^2}{\sum_{i=1}^{M} a_i^2\, N_i} \qquad (8)$$

We want to maximize ζ_M. This can be done using the Schwartz inequality.

$$\zeta_{Mmax} = \frac{1}{2} \cdot \sum_{i=1}^{M} \frac{r_i^2}{N_i}$$

$$= \sum_{i=1}^{M} \zeta_i \qquad (9)$$

Thus, the SNR at the combined output is

$$\overline{\zeta_{Mmax}} = \sum_{i=1}^{M} \overline{\zeta_i} = \sum_{i=1}^{M} \zeta_o = M\zeta_o \qquad (10)$$

3.4 Equal Gain Combiner

It is a co-phase combining that brings all phases to a common point and combines them. The combined signal is the sum of the instantaneous fading envelopes of the individual branches. **EGC** is similar to **MRC**, but there is no attempt to weight the signal before addition .Thus $a_i = 1$. The envelope of the output signal is given as:

$$r = \sum_{i=1}^{M} r_i(t) \qquad (11)$$

and mean output SNR is given as:

$$\overline{\zeta_M} = \frac{1}{2} \cdot \frac{\overline{|\sum_{i=1}^{M} r_i|^2}}{\sum_{i=1}^{M} \overline{N_i}} \qquad (12)$$

Assuming that mean noise in each branch is the same (i.e., N); and the resulting SNR is

$$\overline{\zeta_M} = \frac{1}{2NM} \cdot \overline{\left| \sum_{i=1}^{M} r_i \right|^2} = \frac{1}{2NM} \sum_{i,j=1}^{M} \overline{r_i r_j} \qquad (13)$$

4-COMPUTER SIMULATION AND RERSULTS:

Computer simulation test is carried out to compare the four combining methods for space diversity. The channel used in the test is the Rayleigh fading channel with 3 paths and Doppler frequency of 50 Hz.QPSK signal is transmitted through the channel and three branches (M=3) are used in the receiver. The received signals through these branches and the combining signal is obtained using the four combining methods.Figures 4,5,6 and 7 shows the received signals through three branches and the combining signals using EGC, MRC, Selection combining and Selection Switching combining respectively. It can be seen from figures 4 & 5 that the combined signal using EGC method has less fade than the combined signal using MRC.On other hand, the selection method and selection switching method give less performance then the EGC and MRC.

MLSE detection is used in the receiver; Figure (8) shows the performance of the four combining methods with three branches. It can be observed that the selection and the selection switching diversity combiner have the poorest performance and the maximal ratio the best. The performance of the equal gain diversity combiner is slightly lower than that of the maximal ratio combiner.

On other hand, the single branch (M=1) performance is compared with the three branches and it's clear that the performance of the three branches is better than the single braches. Table (1) shows the SNR required to have a BER of 10^{-4}.

5- CONCLUSION:

One can conclude from results that the space diversity enhance the performance of the detector (SNR improvement about 5 dB minimum). The other conclusion is that the use of the detector with maximal ratio combiner gives better performance than the other combining methods, while the detector with selection switching combiner give the worst performance compared with the other method but it still better than the non combined signal (receiver without diversity).

REFERENCES:
-Mahrotra, A. Cellular Radio Performance Engineering. Boston: Artech House, 1994.

- N. W. K. Lo, D. D. Falconer, and A. U. H. Sheikh, "Adaptive equalization and diversity combining for mobile radio using interpolated channel estimates," *IEEE Trans. Veh. Technol.*, vol. 40, no. 3, pp. 636–645, 1991.

- Neelam Srivastava .Diversity Schemes For Wireless Communication Short Review. Journal of The oretical and Applied Information Technology**,** Vol.15, No.2, pp.134-143, 2010.

- P. Balaban and J. Salz, "Optimum diversity combining and equalization in digital data transmission with applications to cellular mobile radio—Part I," *IEEE Trans. Commun.*, vol. 40, no. 5, pp. 885–894, 1992.

- P. Jung, B. Steiner, and Y. Ma, "Maximum-likelihood detector for coherent receiver antenna diversity," *Frequenz*, vol. 48, no. 3/4, pp.94–99, 1994.

- P. Jung and M. Nasshan, "Benefits of coherent receiver antenna diversity in DCS 1800 full speech transmission," in *Proc. IEEE PIMRC'94*, pp. 204–208.

- P. Jung, "Performance evaluation of a novel M-detector for coherent receiver antenna

diversity in a GSM type mobile radio systems," *IEEE*

J. Select. Areas Commun., vol. 13, no. 1, pp. 80–88, 1995.

- P. E. Mogensen, "GSM base station antenna diversity using soft-decision combining on up-link and delayed signal transmission on down-link," in *Proc. IEEE VTC'93*, pp. 611–616.

- Q. Liu and Y. Wan, "An adaptive MLSE receiver with dual diversity combining/selection," in *Proc. IEEE PIMRC'92*, pp. 245–249.

- R. Krenz and K. Wesolowski, "Comparison of several space diversity techniques for MLSE receivers in mobile communications," in *Proc. IEEE PIMRC'94*, pp. 740–744.

 - Vaughan, R. G. Polarization Diversity in Mobile Communications. IEEE Transactions Vehicular Technology, 39(3), 177-186, 1990. 316- 10 Antennas, Diversity, and Link Analysis.

-Vijay K. Garg Wireless Communications and Networking: Elsevier Inc, 2007.

- W.-H. Sheen and G. L. St¨uber, "MLSE equalization and decoding for multipath-fading channels," *IEEE Trans. Commun.*, vol. 39, no. 10, pp.1455–1464, 1991.
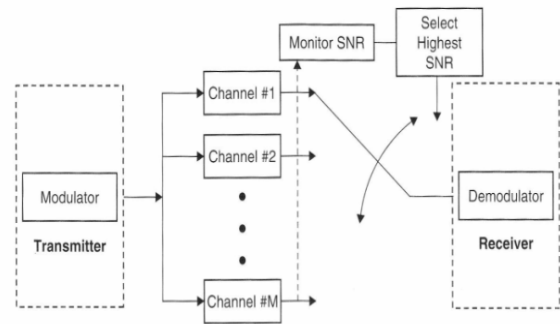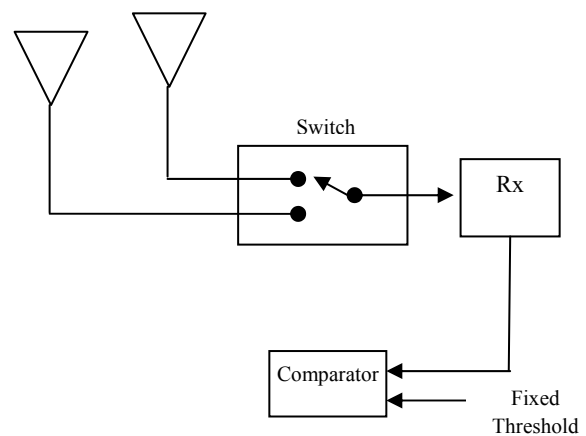

Figure (1) Diversity selection combiner

Figure (2) Diversity selection switching combiner

Table (1) SNR in dB required to achieve probability of error 10^{-4}
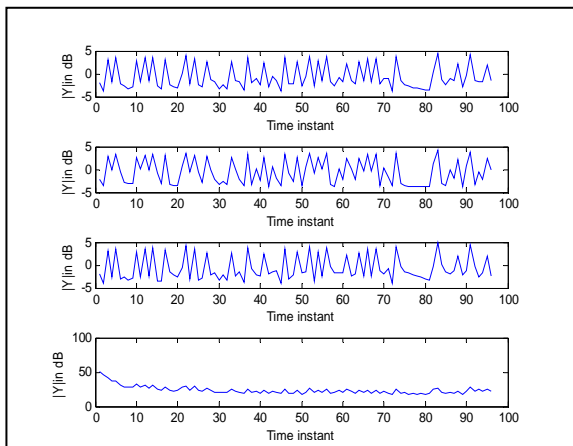
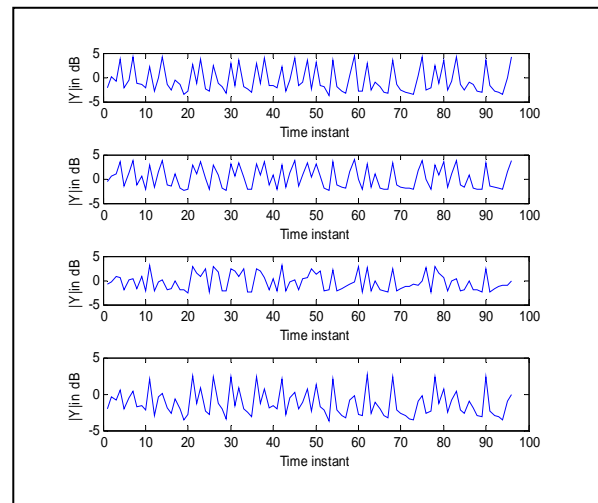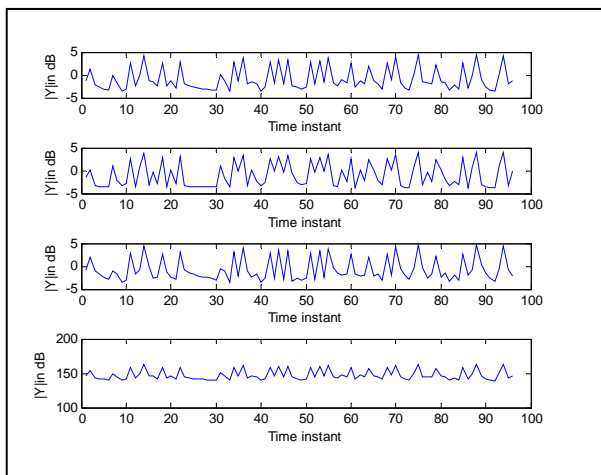| Combining Method	Without diversity (M=1)	EGC (M=3)	MRC (M=3)	Selection (M=3)	SS (M=3)
SNR in dB	25	17.5	16.5	19	20
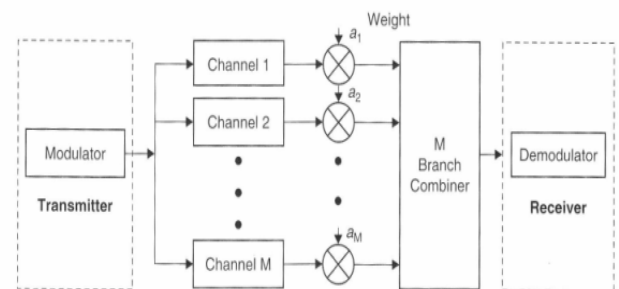
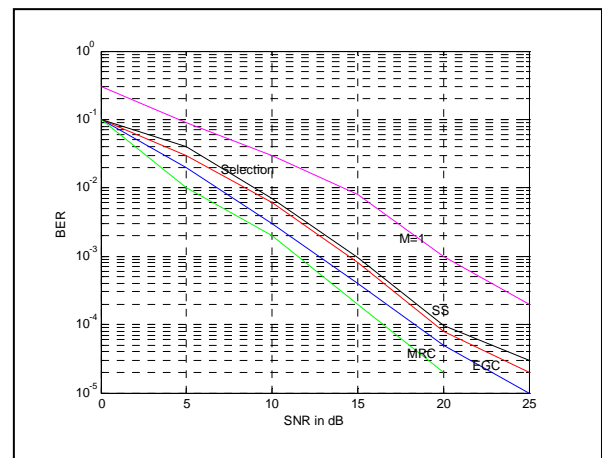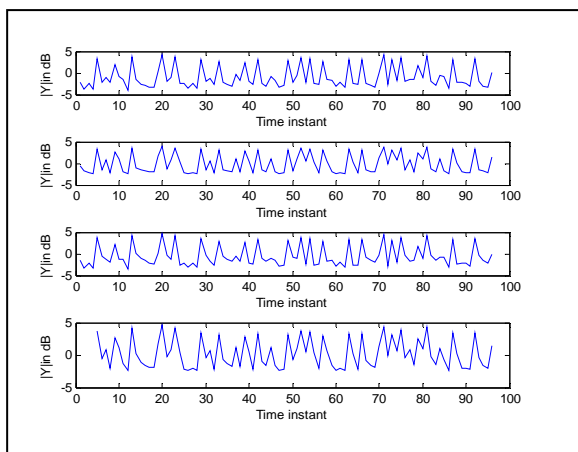**Figure (3)** Maximal ratio combining

Figure (4) Combining signals with EGC

Figure (5) Combining signals with MRC

Figure (6) Combining signals with Selection Method

Figure (7) Combining signals with Selection Switching method

Figure (8) Performance of the four combining schemes with M=3

The Effect of Tool Path Strategy on Twist Behavior In Single Point Incremental Sheet Metal Forming

Dr. Qasim Mohammed Doos Al-Attaby

kasim_daws@yahoo.com

Dr.Tahseen Fadhel Abaas

tfalani@yahoo.com

Aqeel Sabree Bedan

akeelsabree@yahoo.com

ABSTRACT:

In Incremental sheet metal forming process, one important step is to produce tool path, an accurate tool path is one of the main challenge of incremental sheet metal forming process. Various factors should be considered prior to generation of the tool path i.e. mechanical properties of sheet metal, the holding mechanism, tool speed, feed rate and tool size. In this work investigation studies have been carried out to find the different tool path strategies to control the twist effect in the final product manufactured by single point incremental sheet metal forming (SPIF), an adaptive tool path strategy was proposed and examined for several Aluminum conical models. The comparison of the proposed tool path with the conventional iso planar and helical tool paths shows that there is no effect of twisting in the final model when using adaptive tool path, while the twisting effect are clearly observed and measured in the final product when using both iso planar and helical tool path When forming 80 and 110mm depth conical cup.

The time of forming has been measured and its observed that in adaptive tool path the time of forming is less than 8.7 %from the helical tool path when forming conical cup with 50mm depth and less than of 8.91% when forming conical cup with 110mm depth.

Keywords: Single Point Incremental Forming (SPIF), Tool path Strategy, Twisting, forming time.

<div dir="rtl">

تأثير مسار العدة على سلوك الالتواء في التشكيل النقطي التزايدي للصفائح المعدنية

الخلاصة :

يعتبر استنتاج وتوليد مسار العدة في عملية التشكيل التزايدي خطوة مهمة يجب اخذها بنظر الاعتبار ويعتبر مسار العدة الامثل هو من التحديات التي تواجه هذا النوع من عمليات التشكيل حيث يجب مراعاة عدة عوامل مثل الخواص الميكانيكية للصفائح المعدنية المراد تشكيلها، طريقة تثبيت الشريحة المعدنية، سرعة دوران العدة ومعدل التغذية وحجم العدة (القطر ،الطول) لتحديد نوع مسار العدة الملائم للتشكيل.

تم في هذا البحث دراسة تاثير نوع مسار العدة على خاصية الالتواء الحاصلة بالمنتج بعد التشكيل وتطوير مسار عدة للحد من ظاهرة الالتواء ومقارنة مسار العدة المطور مع عدد من مسارات العدة الشائعة الاستخدام في تشكيل عدد من النماذج المختلفة. تبين النتائج المستحصلة من خلال هذا البحث بان الطريقة المطورة حدت بشكل كبير من ظاهرة الالتواء حيث لم يظهر اي التواء في تشكيل النماذج بعمق 50ملم في حين كانت نسبة الالتواء بسيطة جدا مقارنة مع المسارات الاخرى عند تشكيل النماذج للاعماق 80 و110ملم على التوالي. ومن ناحية اخرى فان زمن التشكيل باستخدام مسار العدة الطبقي اقل من زمن التشكيل عند استخدام مسار عدة الحلزوني وبنسبة مئوية تراوحت 8.7% عند تشكيل جزء مخروطي بعمق 50ملم الى8.91 % عند تشكيل جزء مخروطي بعمق 110ملم.

الكلمات الرئيسية: التشكيل النقطي التزايدي، تتراجية سار العدة، الالتواء، زمن التشكيل.

</div>

INTRODUCTION:

The Singe Point Incremental Forming (SPIF) is a new forming process used in sheet metal forming. Different steps of this process are shown in figure (1) (Rattanachan K. (2009)). Incremental displacements of the tool in various directions allow to form the sheet in order to

provide the required shape. The main advantages of SPIF are best formability of sheets - reducing costs when prototypes or batches have to be manufactured while the drawbacks manufacture's times longer sometimes poor geometry's respect and surface aspect. (Syed Asad Raza(2009)).

Tool path

Due to the elastic-plastic properties of the sheet metal, the tool path of a given shape will vary from the final shape as shown in Figure (2). This is obvious at the beginning of the process where there is evidence of both elastic and plastic deformation. The final shape of the formed part has been found to be dependent upon a number of factors including the tool-path, the material properties of the sheet metal, the tool material, tool speed and the tool feed rates. (Durante(2009)).

TOOL PATH STRATEGIES:

For positive geometry, the tool deform the sheet starting from the centre and moving towards the boundary, whereas for concave object geometry, both outer-to-inner and inner-to-outer paths can be used.
There are two main tool path strategies used in ISPF which are:(S. Dejardin(2010)).
 1- Iso-planar tool path
 2- Helical tool path
In Iso-planar tool path the tool deform the sheet metals from the center and moving towards the boundary then it progress to the final depth of forming in circular movement with out changing the feed direction , as illustrated in Figure (3).(Wang Ha(2001)).
In helical tool path strategy, the tool progressively deforms the blank with a

Spiral movement from the top going towards the maximum depth (direct forming, figure(4)).(Hu Zhu(2011)).
The twist effect can be clearly observed in the final product when using the above toolpath strategies, and to improve this an-adaptive tool path strategy have been developed for selected case studies.
In this work, an adaptive solution (to overcomes the twist effect) was proposed and tested, where the tool is progressively moved downwards up to the bottom of the object but it progress in circular movement and the feed direction was changed for each successive layer. An example of tool path generated is shown to figure (5).

CAD MODEL: (PROFILE-LAGRANGE+ TOOL PATH)

Starting from the CAD model of the symmetric object, the object profiles has been generated using one-dimension(1-D) Lagrange interpolation technique shown in figure (6), then the tool path was generated by dividing the total depth of the object to suitable number of layers to generate an acceptable side step towered the final depth of the forming.

The conical shape profile have been generated using 1-D Lagrange technique than the intermediate nodes have been generate to guide along toolpath. The 1-D Lagrange equation can be written as illustrated in equation (1&2).

$$f_n(x) = \sum_{i=0}^{n} L_i(x) f(x_i) \qquad (1)$$

Where n in $f_n(x)$ stands for the nth order polynomial that approximates the function $y = f(x)$ given at $n+1$ data points as $(x_0, y_0), (x_1, y_1), \ldots, (x_{n-1}, y_{n-1}), (x_n, y_n)$, and

$$L_i(x) = \prod_{\substack{j=0 \\ j \neq i}}^{n} \frac{x - x_j}{x_i - x_j} \qquad (2)$$

$L_i(x)$ is a weighting function that includes a product of $n-1$ terms with terms of $j=i$ omitted.(Tahseen (2011)).

An integration of tool path definition was created by Matlab and developed then the data have been transferred via "Ethernet" to the C-Tek vertical milling machine to control the tool.

EXPERIMENTAL WORK:

The material used to investigate the effects of the tool path is 1mm thick Aluminum alloy (Al 1050) for several models to determine the effect of the tool path on the twisting occurs in the final product. The properties and chemical composition of Al 1050 are as follows:-
- Ultimate strength (100- 110 MPa)
- yield strength (70 MPa).
- Total elongation during tensile test when using 70 mm initial gauge length is around 3-5%.

Forming limit diagram(FLD) shown in figure (7).

The technique utilized for obtaining the FLD involved electrochemical etching of a grid of circles with 2 mm initial diameter on the surface of the sheets before forming and measuring the major and minor axis of the ellipses that result from the plastic deformation of the circles during the formability tests. The values of strain were computed from (refer to the detail in figure (7)), where the symbol (R) represents the original radius of the circle and the symbols (a) and (b) denote the major and minor axis of the ellipse.(Maria(2011)).

$$\varepsilon_1 = \ln(\frac{a}{2R}) \qquad (3)$$

$$\varepsilon_2 = \ln(\frac{b}{2R}) \qquad (4)$$

The resulting FLD is plotted in figure (7) and was constructed by taking the principal strains (ε1, ε2) at failure from grid-elements placed just outside the neck (that is, adjacent to the region of intense localization) since they represent the condition of the uniformly thinned sheet just before necking occurs.

The intersection of the FLC with the major strain axis is found to occur at ε1=0.07 in fair agreement with the value of the strain hardening exponent of the stress–strain curve obtained by means of tensile tests,

$$\sigma = 140\varepsilon^{0.041} MPa \qquad (5)$$

MACHINE SET-UP:

The experimental work was implemented at university of technology using CNC milling machine (figure (8)), using machine speed 100 rpm and feed rate 750mm/min.

TOOL GEOMETRY:

The main tool geometries that used in SPIF are:-
1. Ball end tool.
2. Hemispherical tool.
3. Flat with round tool.

In this work we used a Ball end tool with diameter 12mm and length100mm, material of this tool is tool steel (X210) has HRC 58 (figure (9)), which is used in all the experimental to neglect the effect of the tool geometry on the twist behavior.

RESULTS AND DISCUSSION:

Nine conical shapes have been implemented (3x3). Test the effect of the tool path strategy on the twist behavior, 50 mm depth conical cup have been found with:
- Isoplaner
- Helical
- Adaptive

The same procedure has been repeated to form conical shapes with final depth of 80mm and 120mm as shown in figure (10).

The effect of the three tool path strategy on twisting was plotted in the figures (11, 12&13) as a relationship between twist angle value and forming depth.

The actual time of forming for the conical shapes of the three tool path strategies has been measured and plotted as a relation between forming depth and forming time as shown in figure (14).

CONCLUSIONS:

In this work, Al 1050 sheet were incremental sormed under different tool path strategies and their effects stradies, the following conclusions were drawn from the study:

1. there is no twisting in the final conical cup when using the adaptive tool path strategy while the twist effect can be observed for the same model when using both isoplaner and helical tool path.
2. as the following depth increased the twisting angle is increased, but still that the adaptive tool path strategy has the lowest effect on twisting.
3. both isoplaner and adaptive toolpaths strategy has the same forming time for the same model while the helical tool path has longest forming time that's mean the proposed adaptive tool path strategies has lowest effect on twisting and decrease the time of forming of 8.7% for all the models comparing with the helical strategy.

REFERENCES:

Hu Zhu, "Spiral tool-path generation with constant scallop height for sheet metal CNC incremental forming", Int J Adv Manuf Technol 54:911–919, 2011.

Maria B. Silva, "Failure mechanisms in single-point incremental forming of metals", Int J Adv Manuf Technol 56:893–903, 2011.

Durante M., "The influence of tool rotation on an incremental forming process", Journal of Materials Processing Technology 209, 4621–4626, 2009.

Rattanachan K., " Formability in Single Point Incremental Forming of Dome Geometry", AIJSTPME 2(4): 57-63, 2009.

Syed Asad Raza Gardezi, "TOOL PATH GENERATION IN SPIF, SINGLE POINT INCREMENTAL FORMING PROCESS", 2009.

Dejardin S., "Experimental investigations and numerical analysis for improving knowledge of incremental sheet forming process for sheet metal parts", Journal of Materials Processing Technology 210 363–36, 2010.

Tahseen F. Abbas, Aqeel S. Baden, "Statistical and Visual Analysis of Error In Interpolating Sculptured Surfaces",Eng.&Tech.Journal,Vol.29,No.12 ,2011

Wang Ha, "Optimization of Tool Trajectory for Incremental Sheet Forming Using Closed Loop Control", IEEE International Conference on Automation Science and Engineering, 2011.
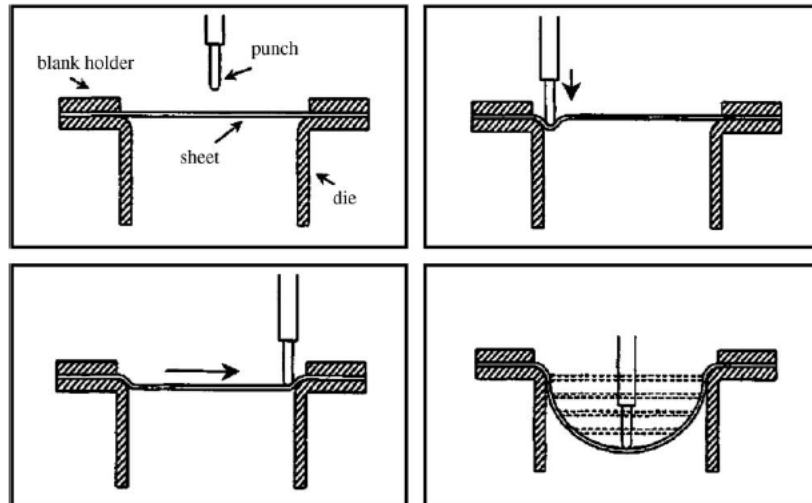
Figure (1) Principle of SPIF (Rattanachan K.2009).

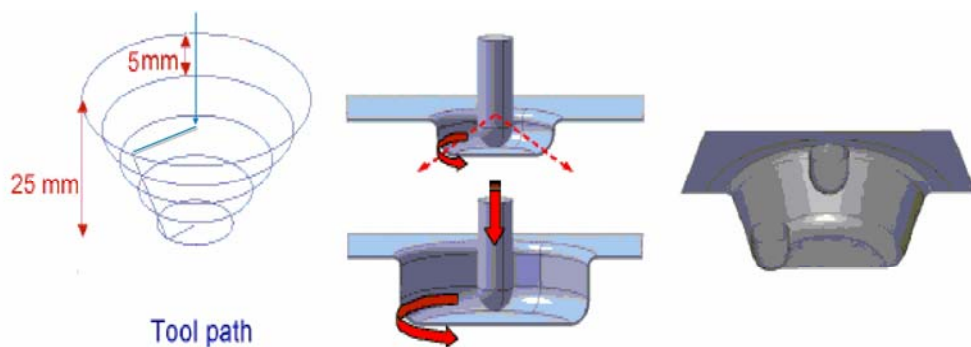**Figure (2) Tool path of forming process (Durante M.2009).**
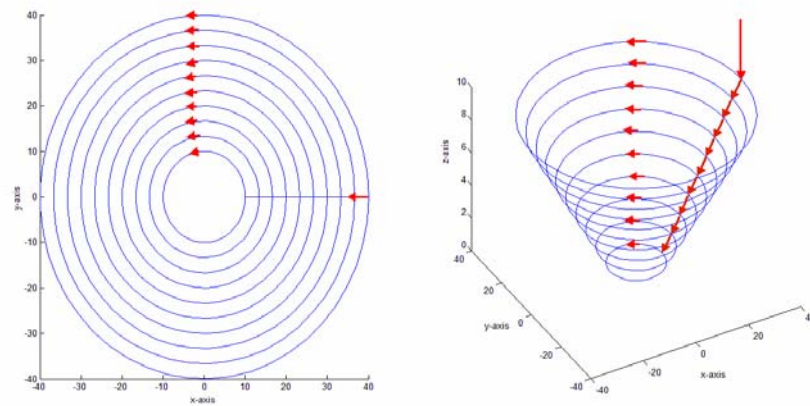
Figure (3) Isoplaner tool path.
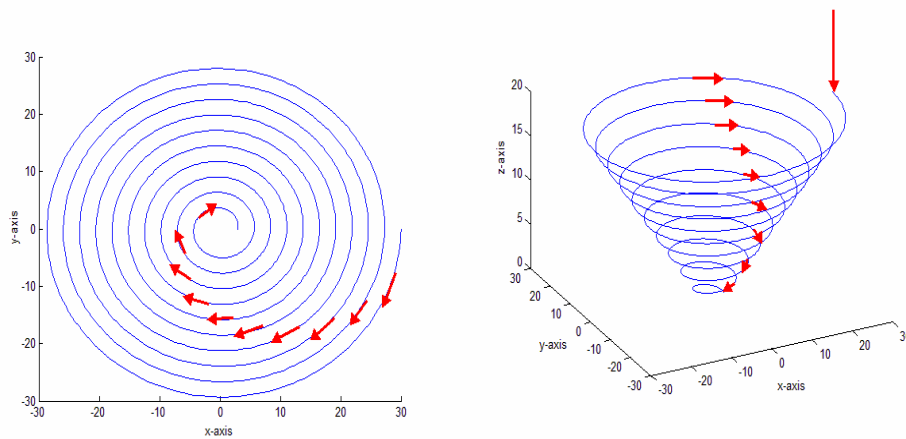
Figure (4) Helical tool path.
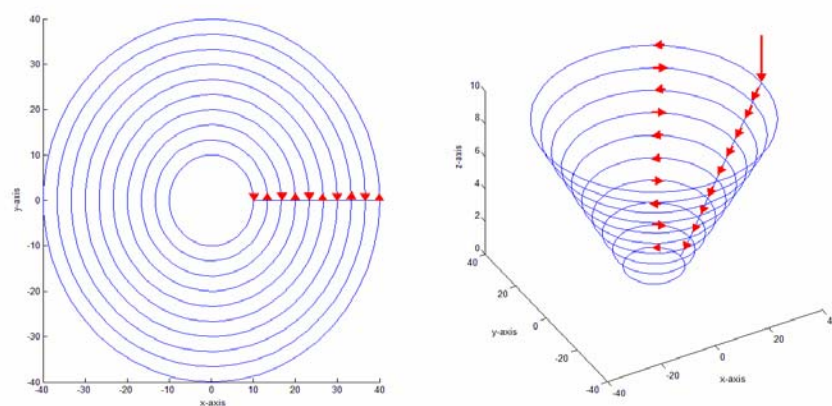
Figure (5) Adaptive tool path of present work.
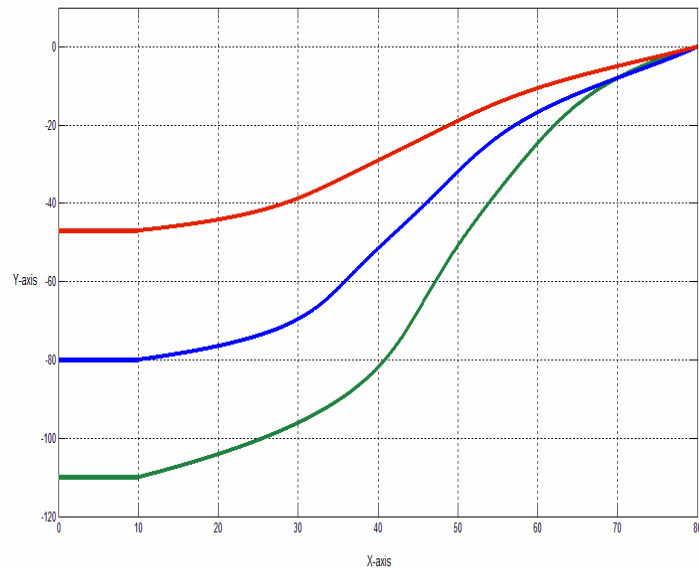
Figure (6) Conical cup profile using Lagrange method of 50, 80 &110mm depth.
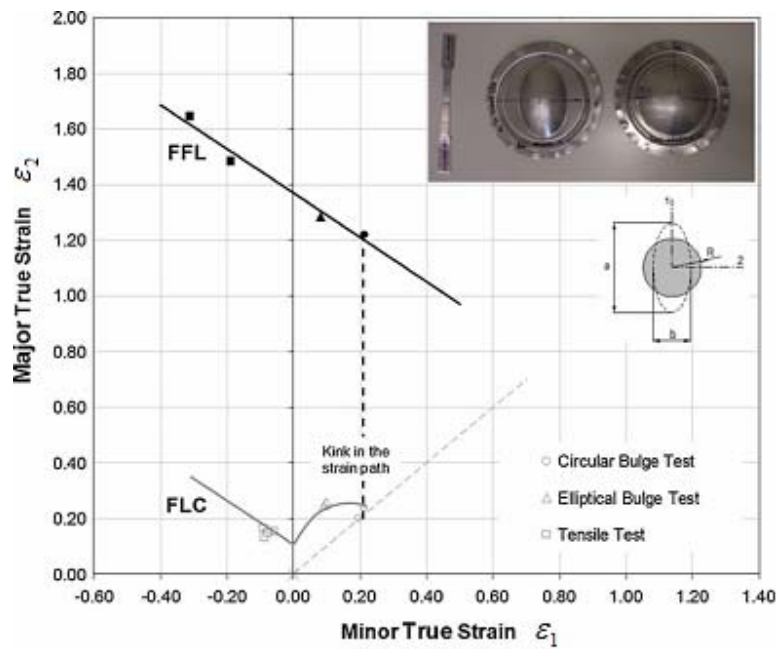
Figure (7) forming limit diagram of AL1050.
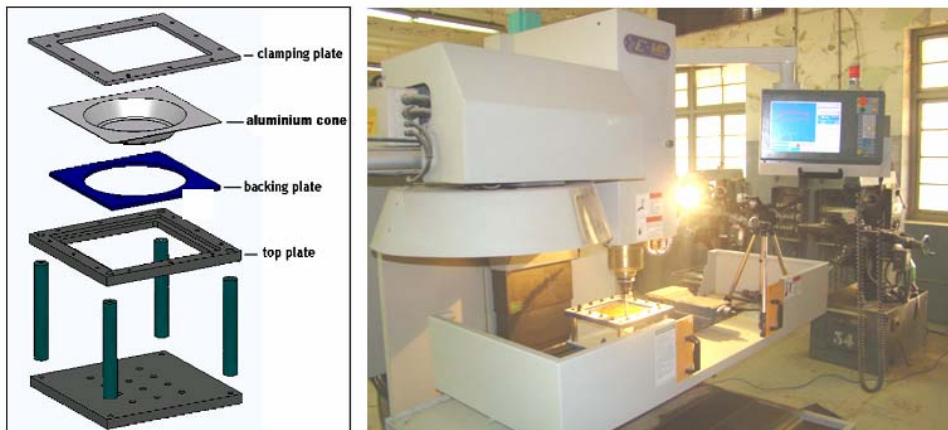
Figure (8) C-Tek vertical CNC milling machine
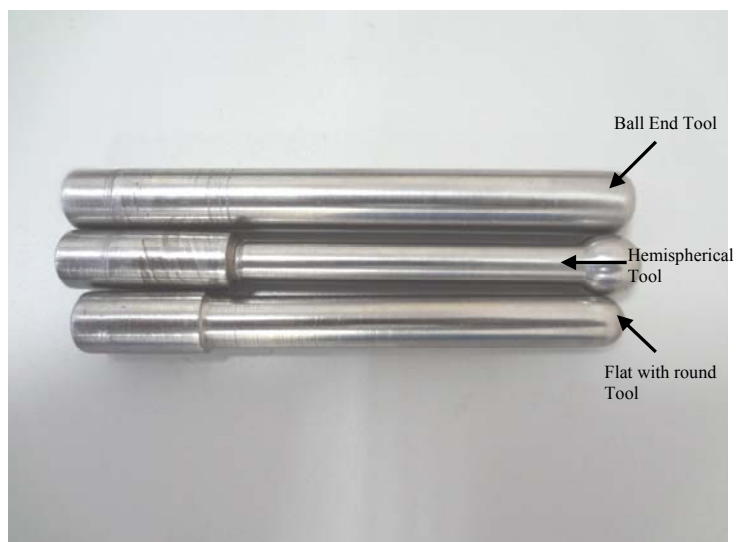
Figure (9) Tool geometry.
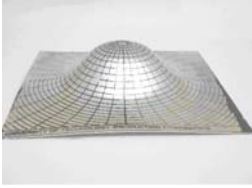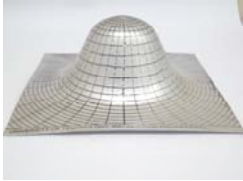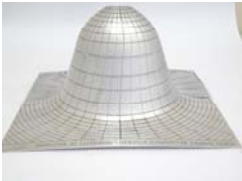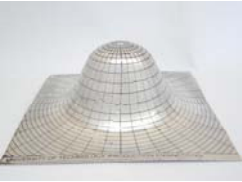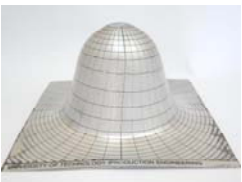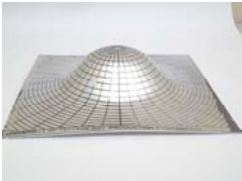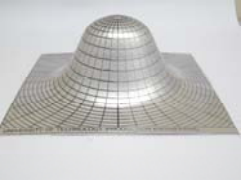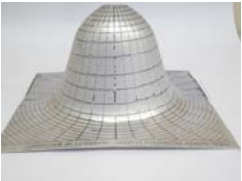
	Depth (50mm)	Depth (80mm)	Depth (110mm)
Isoplaner Toolpath			
	Actual forming time=55.5 min	Actual forming time=95.4 min	Actual forming time=134.9min
Helical Toolpath			
	Actual forming time=60.8 min	Actual forming time=104.7 min	Actual forming time=148.1min
Adaptive Toolpath			
	Actual forming time= time=55.5 min	Actual forming time= time=95.4 min	Actual forming time=134.9min
Maximum Forming angle	38.6^o	63°	71°

Figure (10) produced conical shapes.
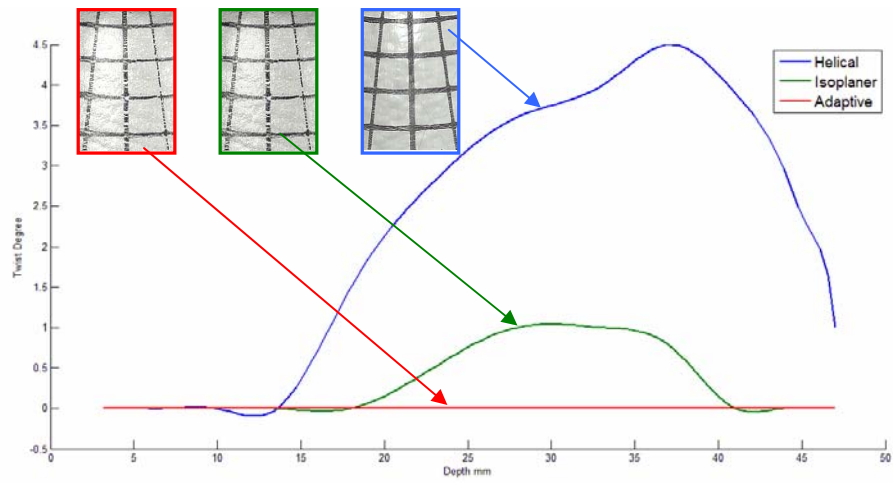
Figure (11) Relationship between twist angle value and forming depth equal to 50mm.
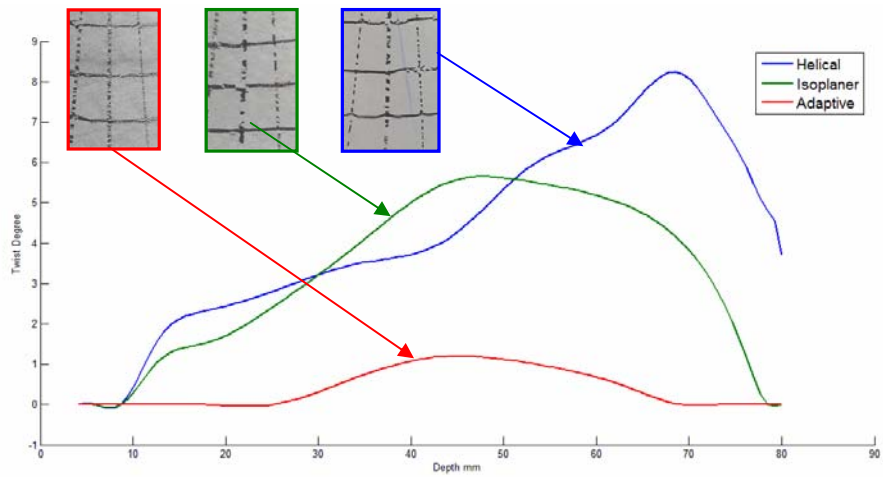
Figure (12) Relationship between twist angle value and forming depth equal to 80mm.

530
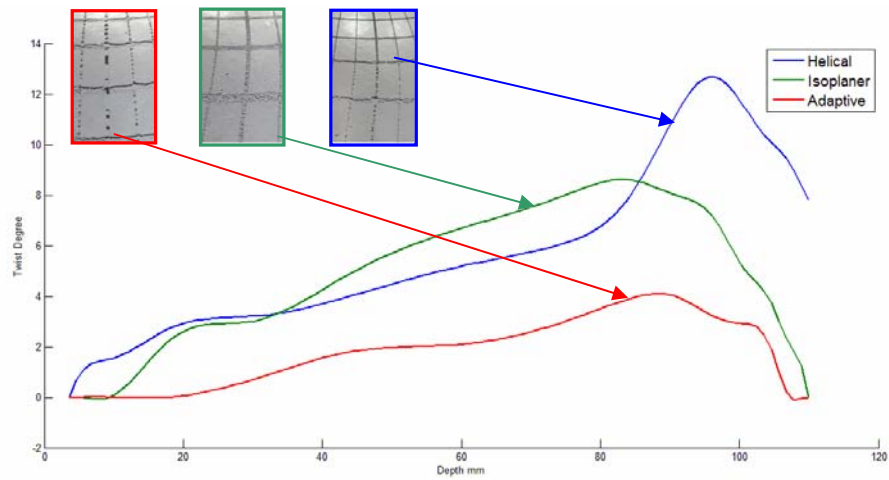
Figure (13) Relationship between twist angle value and forming depth equal to 110mm.
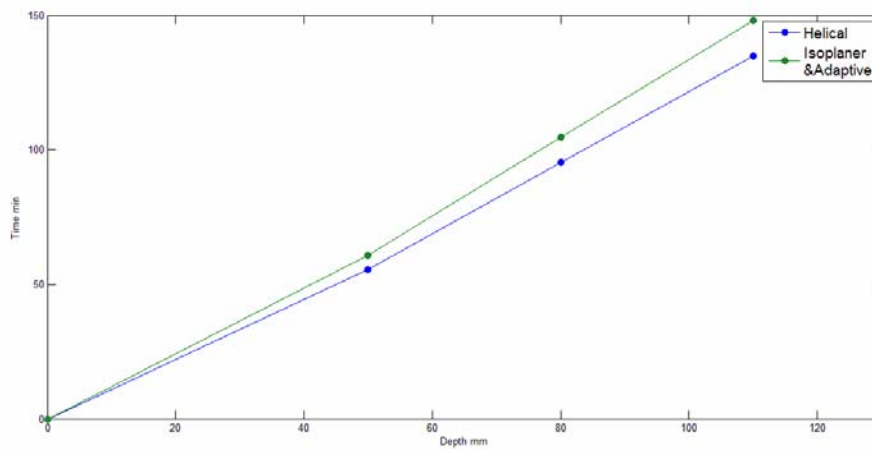
Figure (14) Relation between depth and forming time for the produced conical shapes.

تطوير مستوى جودة المنتج الجاهز(معجون الاسنان)
حالة تطبيقية في الشركة العامة للزيوت النباتية

سلمان حسين عمران
مدرس ـ قسم الميكانيك ـ معهد التكنولوجيا/ بغداد

:

.

-   (   )
. (ISO 9001–2008)

)

2011   (

(A, B, C, D)

(100, 50, 10, 1)

.

75   (   )

% (80-70)

.   1100 .

:

U

.

Development of Quality Rating Evaluation of Outgoing Product Case Study Applied at the General Company for Vegetable Oils

Salman Hussain Omran
Lecturer
Mechanical Dept. - Institute of Technology – Baghdad

ABSTRACT:

Research covers the uses the method of Quality Rating Evaluation to evaluate the quality of production through which a determination of product quality of its production in order to determine the amount of sales hence the profits for the company. The most important function is to satisfy consumer at reasonable prices. Methods were applied to the product (toothpaste) in the General Company for Vegetable Oil – Almaamoon Factory .

The company's has obtained ISO-certified (ISO 9001-2008). Random samples of final product intended for sale were collected from the store during months (February, April , June , October and December) for the year 2011 to determine the "quality rating " through the application of the method on the products at final stage , where selected. The properties that affect product quality and varieties of defects for each property (A, B, C , D) and give the points of on rejects .

The research concluded that the percentage of output quality for the product toothpaste (AMBER) weighing 75 g ranges between (70-80%) is within quality level which is good in condition and that the company's plan was effective and influential in the development of its products. In addition to the significant improvement in the level of quality and process productivity statistically controlled and the results were within the limits of the chart quality control .Also it was found that is was within Iraqi specification (1100)

Key Words: Quality rating system, Demerits per production unit, U – Chart, Quality, Control Chart for Attributes, Quality Audit.

:

(Grosby)   .

(   )

(Juran)   . [2]

. [3]   .

(Ishikawa)   :

:

Juran)   . [4]   –

. [5]   (and Gryna   )

(Besterfield)   2011

–

:   (ASQ)

.

. [7]   –

-:

)

Demerit Per Productio Unit (U

. QualityRating

.

(U – Chart)

1.   :

:

. [8]

.

. [9]

. [1]

(Deming)

.   (6

.

                                                           (7

[10]   .

_____:

)   :

(   )   –

(

[13]

$$n = a \sqrt{2N} \text{ ------} \quad (1)$$ [11] .

:[12   8]:   :

: n

)   : N

(

:   a: 0.6   2.6

[12 , 10]

(1   –

.

(2

.   .

(3

.

(Demerits)   :

(4

*   (A) :

.(100)

.   *   (B) :

(5

.   (50)

*   (C) :

.   (10)

*   (D) :

.

(1)   **(2)**

[14]

.

100					(A)
50					(B)
10					(C)
1					(D)

–	–	100	A
–	–	50	B
–	–	10	C
–	–	1	D

[13 , 12]   **(1)**

(3)   :(U)   –

.

: [12]   (9000)   .

(2)   = (U)

(2)

$$\overline{U} = \frac{\sum C}{\sum n} \quad ------- (4)$$

(3)

[16   15]

$$UCL = \overline{U} + 3\sqrt{\frac{\overline{U}}{n}} \quad --------(5)$$

$$LCL = \overline{U} - 3\sqrt{\frac{\overline{U}}{n}} \quad --------(6)$$

(%)	
	(U)
100	0.99-0
90	1.99 – 1
80	2.99 – 2
70	3.99 – 3
60	4.99 – 4
50	5.99 – 5
40	6.99 – 6
30	7.99 – 7
20	8.99 – 8
10	9.99 – 9

C :

n : .

U : /   .

$\overline{U}$:

.

UCL :

LCL :

%60

%100   (   )

.

(U   –

[17   12   8   6] –Chart)

(U)   (U)

Defects –   U – Chart

Per – Unit Chart

(U)   (U)

Center Line

(U)   .

(Upper   ($\overline{U}$)

.   (Lower   Control Limit)

: Center Limit)   Control Limit)

/

1970   .

:

) $$U = \frac{C}{n} \quad ------ (3)$$

)

(

.   :

الشكل (1)   (   )

(Abrasive)

[18]

1_   (   )

2_   (SLS)

3_   (SCMC)

4_   (   )

5_   (   )

6_   (   )

7_   (   )

(1)

:

1 –

2-

3-

:

(   )

(75)   (2)

–

:

(

)

(2011   (111)

)

(

.

الشكل (1)   (   )

(1)

(a)   (0.6)

.

(   ) 75

1.282 = 2011 –

1.282   =   1.282 x 1000   =   1282

1282

= (N)

(2.4)   (   )

534.2 =   X 32

(   )

17093 =

(1)

$$n = a\sqrt{2N}$$

a = 0.6

$$= 0.6\sqrt{2\times17093}$$

$$= 110.9 \approx 111$$

n = 111

(n)

(4)

(4)

(5)

					( )
					- 2011
144	115	130	73	111	
					(n)
28827	18400	23403	7360	17093	

0	**0**	**0**	**0**	**0**	**0**	**A**
22	**7**	**5**	**4**	**2**	**4**	**B**
67	**15**	**10**	**15**	**13**	**14**	**C**
20	**5**	**4**	**4**	**3**	**4**	**D**
119	**27**	**19**	**23**	**18**	**22**	

(
( )
(5)
(A , B , C , D)

.

. (1)

–

(5)   (1)
.

–

(U   )
(2)
(6)

(6)

D	**C**	**B**	**A**		**1**
1	**10**	**50**	**100**		**2**
4	**14**	**4**	**0**		**3**
4X1 = 4	**14X10 = 140**	**4X50 = 200**	**0X100 = 0**	**2X 3**	
4	**140**	**200**	**0**		
344					

قيمة المنتوج
الواحد (U) لشهر
شباط 2011

$$= \frac{\text{المجموع الكلي لدرجات العيوب}}{\text{عدد العينة التي تم فحصها (العينة المفحوصة)}}$$

$$= \frac{344}{111} = 3.09 \approx 3$$
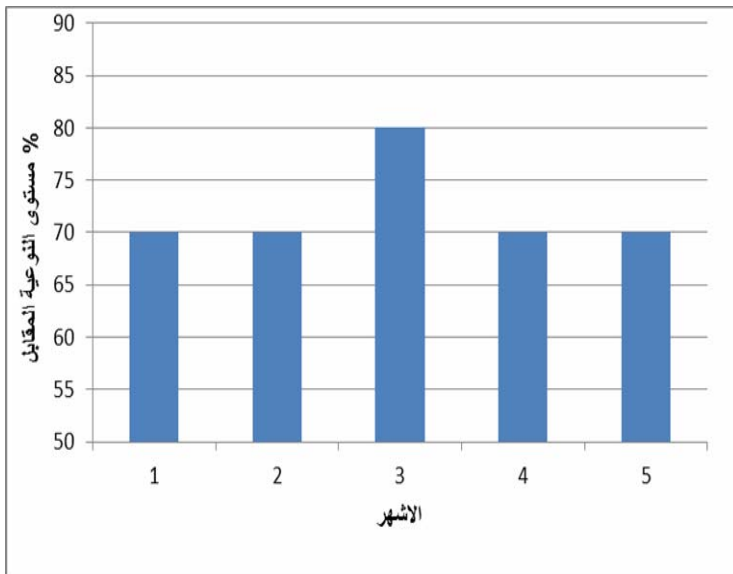
(6)   (2) .

(2)   (   )
%

-   (3)

(%)
(U)   3
70 %   (6) .
(7)

505	354	354	233	344
144	115	130	73	111 n
3.5	3	2.72	3	3 (U
70	70	80	70	70 %

-

(   )

(U –   –
(Chart
(U)
(9)   D, C, B,
A   (U)
CL , LCL)

(2)   (7) .

UCL , (.
(5 6 7)
– 2011 :
c = 22   (4)
n = 111   (8)

$$U = \frac{C}{n} = \frac{22}{111} = 0.198$$

$\sum C$ = 109   (8)
$\sum n$ = 573   (8)

$$\overline{U} = \frac{\sum C}{\sum n} = \frac{109}{543} = 0.200$$

$$UCL = \overline{U} + 3\sqrt{\frac{\overline{U}}{n}} \qquad = 0.2 + 3\sqrt{\frac{0.2}{111}} = 0.327$$

$$LCL = \overline{U} - 3\sqrt{\frac{\overline{U}}{n}} \qquad = 0.2 - 3\sqrt{\frac{0.2}{111}} = 0.073$$

(8)

(U)

	عدد المنتوجات المفحوصة n	عدد العيوب C	U (C/n)	UCL	LCL
شباط	111	22	0.198	0.327	0.073
نيسان	73	18	0.247	0.357	0.043
حزيران	130	23	0.177	0.318	0.082
ت 1	115	19	0.165	0.325	0.075
ك1	114	27	0.237	0.326	0.074
المجموع	543	109			

(8)

-

(3)

(3))

(U –

-:

1-

(70 – 80 %)

.

2- (5)

:

- (A)

.(100)

- B

(22)

1-

2-

3-

4-

.

(50)

70% - 80 % .

- (C)

(67) :

1- .

2- .

5- U- chart
.
-3
.
-4
.
-5
.
-6
.
-7
:
-1 (U) (C)

(%60))
(%100) (. (10)
(D) -
(20) :
-1
.
-2
.
-3
.
-4
.
-3

(U-chart)
-2 .
(3)
.
(U) .(3σ)
-3
.

. .
-4 -4
–
.
(U – -5 [19]
Chart)
( ) .
.

77

Majda Khalid ismail , 2006 , " Design a Computer Aided Quality Eating Out going products , Athesis submitted to the department of mechanical of Baghdad .

Juran .J.M,1974 , " Management of Quality Control ,3ed , copyright 860 united nation plaze , New York.

.   .

" 1994

. (120)

" 2000   .   .
            "

            .

N.S.Sreenivasan and V.Nayayana , 2005 , " Mahaging Quality Cancepts and Tasks " ,5th ed New Age International (P)Ltd .

            " 1985

        .   "

ISO-9004v, 1986 , " Quality Management and   Quality   Guieline ", International Organization for Standradization .

  " 1998

)
    14   –

                        "(
    .   –

  " 1990   .   .
  – "

-6

.

-7

.

:_____

" 2008   .
    /   –
            –

B.Janakiraman and R.K Gpal , 2008 , " Total Quality Management : Text and cases ", Prentice Hall of India Private Limited , New Delhi .

Vinay A.Kulkarni and Ananed .Bewoor , 2009 ,"Quality Control", Wiley India Put .Ltd , New Delhi .

Ishikawa, k . 1985 , " What is Total Quality Control ? The Japanese Way " , Prentice –Hall , London .U.K .

J.M Juran & Frank M.Gryna – 1980 , "Quality Planning and Analysis",From – Hill , INC . Development through Use , 2nd ,McGraw – Hill ,INC .

Dale H.Besterfield , 2009 , "Quality Control ", 8th ed –Prentice – Hill , New Jelsy

 2009   .   .
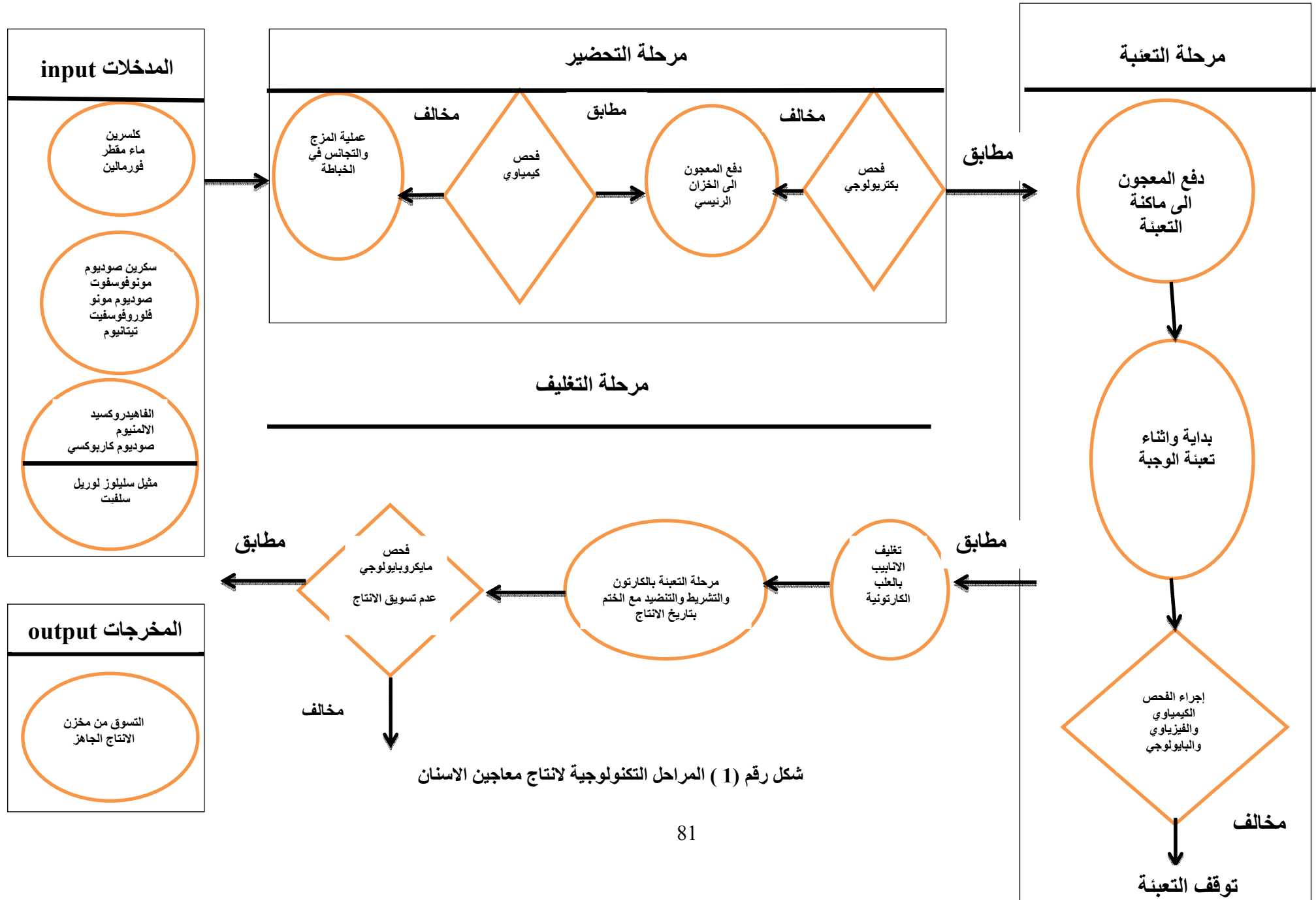   –   "   "

            –

    " 1989

                .

–

PR-WI-1-02

- 2000 .

[19] [1100]

–

(IQS : 1100 / 2010) .

(1)

D	C	B	A		
X	X				.1
X	X				.2
			X		.3
				( )	
		X	X	( )	.4
		X	X		.5
		X	X		.6
		X	X	( )	.7
		X	X		.8
		X	X		.9
			X	(PH)	.10
			X		.11
X	X				.12
X	X	X			.13
	X	X			.14
	X	X			.15
	X	X			.16
X	X			( )	.17

(2)

D	C	B	A	D	C	B	A	D	C	B	A	D	C	B	A	D	C	B	A		
	1				1																
D	C	B	A	D	C	B	A	D	C	B	A	D	C	B	A	D	C	B	A		
2	2	-	-	2	1	-	-	2	1	-	-	1	2	-	-	1	2	-	-		
1	3	-	-	1	2	-	-	-	3	-	-	1	1	-	-	2	3	-	-		
-	-	-	-	-	-	-	-	-	-	-	-	-	-	-	-	-	-	-	-		
-	-	-	-	-	-	-	-	-	-	-	-	-	-	-	-	-	-	-	-	)	
																				(	
-	-	-	-	-	-	-	-	-	-	-	-	-	-	-	-	-	-	-	-		
-	-	-	-	-	-	-	-	-	-	-	-	-	-	-	-	-	-	-	-		
-	-	-	-	-	-	-	-	-	-	-	-	-	-	-	-	-	-	-	-	( )	
-	-	-	-	-	-	-	-	-	-	-	-	-	-	-	-	-	-	-	-		
-	-	-	-	-	-	-	-	-	-	-	-	-	-	-	-	-	-	-	-		
-	-	-	-	-	-	-	-	-	-	-	-	-	-	-	-	-	-	-	-	(PH)	
-	-	2	-	-	-	1	-	-	-	1	-	-	-	1	-	-	-	1	-		
2	2	-	-	1	2		-	1	1	-	-	-	1	1	-	1	2	-	-		
-	1	2	-	-	1	1	-	1	2	-	-	-	-	2	-	-	2	-	-		
-	2	1	-	-	1	1	-	-	2	-	-	-	-	1	-	-	1	1	-		
-	2	-	-	-	1	-	-	-	2	-	-	-	-	2	-	-	2	-	-		
-	1	2	-	-	1	2	-	-	2	2	-	-	-	2	-	-	1	1	-		
-	2	-	-	-	1	-	-	-	2	1	-	-	-	2	-	-	1	1	-	)	
																				(	
5	15	7		4	10	5		4	15	4			3	13	2	4	14	4			

80

شكل رقم (1) المراحل التكنولوجية لانتاج معاجين الاسنان

ENGINEERING

College of Engineering **Baghdad University** **Baghdad**

List of Contents

English Section: **Page**